

STROJNIŠKI

VESTNIK 2

JOURNAL OF MECHANICAL ENGINEERING

strani - pages 71 - 144

ISSN 0039-2480 . Stroj V . STJVAX

cena 800 SIT

- 1.** Eksperimentalno določanje temperaturnega polja površine žarometa z uporabo uporovnih zaznaval
Measurement of the Surface-Temperature Field in a Fog Lamp Using Resistance-Based Temperature Detectors
- 2.** Vključitev numeričnih analiz v zgodnjih fazah konstrukcijskega postopka
Introducing Numerical Analyses in the Early Phases of the Design Process
- 3.** Trenutne smeri razvoja pri spajanju materialov v avtomobilski industriji
Current Development Trends for Material Joining in the Automotive Industry
- 4.** Numerično modeliranje hladilnega sistema na motorju z notranjim zgorevanjem
Numerical Modelling of an Engine-Cooling System
- 5.** Metoda robnih elementov v akustiki - primer ovrednotenja zvočnega polja enosmernega elektromotorja
The Boundary-Element Method in Acoustics - an Example of Evaluating the Sound Field of a DC Electric Motor
- 6.** Izboljšanje dinamične karakteristike tlačno polnjenega motorja z uporabo električnih podpornih naprav
Improving the Transient Response of a Turbocharged Diesel Engine by Using Electrical Assisting Systems



Vsebina

Contents

Strojniški vestnik - Journal of Mechanical Engineering
letnik - volume 50, (2004), številka - number 2

Razprave

- Wagner, A., Bajšić, I., Fajdiga, M.: Eksperimentalno določanje temperaturnega polja površine žarometa z uporabo uporovnih zaznaval 72
Bučar, T., Janežič, M., Pangeršič, P., Fajdiga, M.: Vključitev numeričnih analiz v zgodnjih fazah konstrukcijskega postopka 80
Tušek, J., Klobčar, D.: Trenutne smeri razvoja pri spajanju materialov v avtomobilski industriji 94
Mrakovčić, T., Medica, V., Škifić, N.: Numerično modeliranje hladilnega sistema na motorju z notranjim zgorevanjem 104
Furlan, M., Boltežar, M.: Metoda robnih elementov v akustiki – primer ovrednotenja zvočnega polja enosmernega elektromotorja 115
Katrašnik, T., Trenc, F., Medica, V., Rodman Oprešnik, S., Bizjan, F.: Izboljšanje dinamične karakteristike tlačno poljenjenega motorja z uporabo električnih podpornih naprav 129

Osebne vesti

Navodila avtorjem

Papers

- Wagner, A., Bajšić, I., Fajdiga, M.: Measurement of the Surface-Temperature Field in a Fog Lamp Using Resistance-Based Temperature Detectors 72
Bučar, T., Janežič, M., Pangeršič, P., Fajdiga, M.: Introducing Numerical Analyses in the Early Phases of the Design Process 80
Tušek, J., Klobčar, D.: Current Development Trends for Material Joining in the Automotive Industry 94
Mrakovčić, T., Medica, V., Škifić, N.: Numerical Modelling of an Engine-Cooling System 104
Furlan, M., Boltežar, M.: The Boundary-Element Method in Acoustics – an Example of Evaluating the Sound Field of a DC Electric Motor 115
Katrašnik, T., Trenc, F., Medica, V., Rodman Oprešnik, S., Bizjan, F.: Improving the Transient Response of a Turbocharged Diesel Engine by Using Electrical Assisting Systems 129

141 Personal Events

143 Instructions for Authors

Eksperimentalno določanje temperaturnega polja površine žarometa z uporabo uporavnih zaznaval

Measurement of the Surface-Temperature Field in a Fog Lamp Using Resistance-Based Temperature Detectors

Andrej Wagner · Ivan Bajšić · Matija Fajdiga

Sodobni žarometi so večinoma izdelani iz plastičnih mas, ki so sicer zelo primerne za izdelavo zahtevnih oblik, vendar so navadno temperaturno slabo obstojne. Posledice temperaturnih obremenitev so deformacije, ki imajo lahko vpliv na fotometrične lastnosti ter na odpornost žarometa na zunanje vplive.

V pričajočem prispevku smo za določen primer žarometa določili temperaturno polje na notranji in zunanji površini okrova žarometa ter temperaturo na delu parabole in senčniku. Merjenje temperatur je bilo izvedeno z uporabo uporavnih zaznaval iz platine. Rezultati meritve so omogočili določitev trirazsežnega temperaturnega polja okrova žarometa.

© 2004 Strojniški vestnik. Vse pravice pridržane.

(Ključne besede: žarometi avtomobilski, polja temperaturna, meritve temperature, metode eksperimentalne)

Modern headlamps are made from low-cost plastic materials that are very convenient for the design of these products. However, plastic materials are not suitable for use at high temperatures. The result can be deformations that result in problems with the photometric properties and with the sealing of the headlamp.

In order to predict the deformations the temperature was measured at significant points on the outer and inner parts of the headlamp housing, on the reflector and on the shield of the lamp. The measurements were made with a platinum-resistance temperature detector (RTD). The results of the measurements were then used in a finite element method (FEM) analysis to determine the deformations of the headlamp housing.

© 2004 Journal of Mechanical Engineering. All rights reserved.

(Keywords: vehicle headlamps, temperature fields, temperature measurements, experimental methods)

0 UVOD

Merjenje temperature na površini je zelo zahteven postopek, ker težko določimo pravi stik med zaznavalom in površino merjenca.

Za pregled porazdelitve temperature je zelo primerna toplotna kamera. Ta da trirazsežno porazdelitev temperature po žarometu, njena pomanjkljivost pa je, da je za določitev natančnih vrednosti potrebno dobro poznavanje emisijskih lastnosti površine merjenca. Podatki za emisijske lastnosti so zelo pomanjkljivi oziroma nedostopni.

Naša naloga je bila določiti temperaturo na delih žarometa, ki so se s prejšnjimi meritvami s pomočjo brezdotikalnega infrardečega inštrumenta za merjenje temperature pokazale kot kritične, ali pa so bile pomembne kot robni pogoji za kasnejšo

0 INTRODUCTION

Measuring the temperature of a surface is a demanding process, because it is very hard to determine the actual contact between the sensor and the surface being measured.

The thermal camera can give a very good overview of a temperature field. The camera also gives a good threedimensional view of temperature, but it also has a few drawbacks. If the emissive values of the surface are not known, the true value of the surface temperature cannot be determined, and the data for surface emissive values are often hard to get or are simply not available.

The aim of this work was to determine the temperatures on specific points of a lamp housing. The temperatures were determined with infrared measuring equipment and a thermal camera. The results from the measured points were taken as input data for subsequent

analizo z uporabo metode končnih elementov (MKE). Meritve s toplotno kamerjo in infrardečim termometrom so tudi pokazale, da je porazdelitev temperaturnega polja po različnih modelih meglenke podobna. Temperatura se po višini zmanjšuje linearno, prav tako se zmanjšuje linearno v globino žarometa. Pokaže se tudi skok temperature v točki nad žarnico.

V preteklosti je bil za merjenje temperature večinoma uporabljan termočlen, katerega največja pomanjkljivost je bila nezmožnost postavitev zaznavala na površino.

Z izmerjenimi vrednostmi smo kasneje določili približno funkcijo porazdelitve temperature. Določitev natančne temperature površin ter njena porazdelitev sta zelo pomembni za analize toplotnih obremenitev okrova ([5] in [6]). Zaradi statistične analize rezultatov smo avtomatizirali zbiranje in shranjevanje podatkov.

Rezultati meritev in postopek določitve temperaturnega polja bodo omogočali kasnejši preračun meglenk z manjšim številom meritev, oziroma bo pri začetnih različicah meglenke omogočal toplotno-mehanski preračun brez meritev na žarometu. Tak način omogoča hitrejši in cenejši razvoj izdelka ter odpravljanje napak, povezanih s toplotno obremenitvijo v zgodnjih fazah razvoja. Tak postopek je skladen s postopkom zagotovljivosti.

Postopek določanja temperaturnega polja bo predstavljen na primeru meglenke podjetja Saturnus avtooprema d.d.

1 PRIPRAVA MERITVE

V okviru raziskave smo izdelali zasnova meritne verige, izdelali program za zbiranje in shranjevanje podatkov, celoten sistem smo umerili in na koncu smo izvedli meritev in rezultate statistično ovrednotili.

1.1 Zasnova meritne verige

Meritve smo izvajali z 10 uporavnimi temperaturnimi zaznavali Pt-1000 z linearno karakteristiko. Pri meritvi je bila uporabljena dvožilna meritna metoda, kar pomeni, da je bilo za zbiranje podatkov mogoče uporabljati analogni desetkanalni multimeter Kiethely, na katerega je mogoče z dodatno rejevno kartico priključiti do 10 zaznaval. Kartica ima 10 rejev, ki preklaplajo med 10 kanali. Merilnik namreč lahko meri samo eno vrednost naenkrat. To za meritev zadostuje, kajti počakamo, da dosežemo ustaljeno stanje in nato preberemo rezultate.

Meritno verigo (sl. 1) sestavljajo naslednje komponente: žaromet (1), 10 uporavnih meritnih zaznaval Pt-1000 (2), univerzalni analogni meritni

analysis with the finite-element method (FEM). The measurements with the thermal camera also showed, that the temperature fields of different fog lamps look very similar to each other: the temperature falls linearly with the height and depth coordinates. The results also showed a local temperature peak above the bulb.

In the past the main sensor for measuring temperature was the thermocouple. The main drawback with a thermocouple is the enormous effort associated with positioning the sensor exactly on the surface of the part being measured.

The results from the measurement were later used to determine the approximation temperature function. A determination of the exact surface temperature and its distribution over the lamp casing is very important for the thermal analysis of the headlamp ([5] and [6]). The measurement procedures were automated, which also helped when performing the statistical analysis.

The results of the measurement and the determination of the temperature field of the housing will help in the development of new fog headlamps because fewer temperature measurements are needed. In the early development stages the results will make it possible to perform a thermo-mechanical FEM analysis without building prototypes. With this kind of development a faster and cheaper development process is ensured as eliminations of temperature-caused defects in the early development stages. This kind of development is also in accordance with Reliability Maintainability and Supportability (RMS) R&D procedures.

The measurement procedure for estimating the temperature field will be presented using an example of a fog headlamp from the company Saturnus avtooprema Ltd.

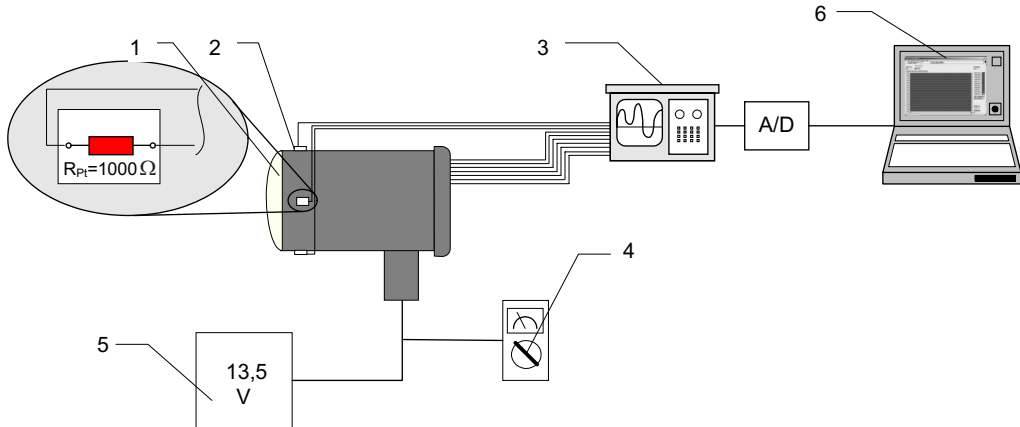
1 PREPARING THE EXPERIMENT

In this experiment the measuring chain was designed and a computer program for the data acquisition and storage was written. The measuring chain was calibrated and the measurements, which were statistically calculated, were performed.

1.1 Measuring chain concept

The measurements were made using 10 Pt-1000 resistance-temperature detectors (RTD) with linear characteristics. A twin-wire method and a Kiethely analog 10-channel multimeter with a 10-relay measuring card was used. The measuring unit can measure only one value at a time, but with the help of the relay card the unit can switch over to different measured channels. Although only one value at a time can be measured, this was sufficient for our purpose because we want to determine the steady temperature state.

The measuring chain (Fig. 1) has the following components: a fog headlamp (1), 10 Pt-1000 RTD sensors (2), a universal analog measuring



Sl. 1. Shema merilne verige
Fig. 1. Scheme of the measuring chain

instrument Keithely, model 2000 (3), voltmeter (4), laboratorijski napajalnik (5), osebni računalnik s programskim paketom LabVIEW (6).

Zahtevana napetost na žarnici je 13,5 V. Napetost na žarnici merimo na sponkah žarnice z uporabo voltmетra (sl. 1).

1.2 Izbiro uporovnih temperaturnih zaznaval

Pri merjenju temperatur, topotnih tokov ali topotne energije se največ uporabljajo dotikalna zaznavala [3]. Glavno vodilo pri izbiro zaznaval je pomenilo dejstvo, da se zaradi postavitev zaznaval lokalno ne spremeni odvod topote. Iz tega pogoja je nastala tudi zadrega pri izbiro, kajti termočleni so manjši, zato je manjši tudi odvod topote prek zaznavala in priključnih žic. Slaba stran termočlenov pa je natančno merjenje temperature na površini, kajti zaradi same oblike le tega težko zagotovimo namestitev zaznavala na površino. Najpogosteje se za merjenje temperatur uporabljajo uporovna temperaturna merilna zaznavala. Med uporovnimi temperaturnimi merilnimi zaznavali so največ v uporabi platinasta. Dobra lastnost platinastih zaznaval je linearna odvisnost spremembe upornosti od temperature v širokem temperaturnem področju.

Za meritev smo uporabljali uporovna zaznavala nemškega podjetja Heraeus Sensors. Namenjena so za meritve, kjer sta pomembna dolgoročna stabilnost in natančnost zaznavala. Oznaka Pt-1000 pomeni, da je merilna rešetka narejena iz platine in imajo imensko upornost pri 0 °C 1000 Ω. Rešetka je nanesena na keramični osnovi, kar zagotavlja dobro prevodnost topote. Zaznavala Pt-1000 so tretjina merilne točnosti B. Tudi sama velikost zaznavala (4 mm × 2 mm) zagotavlja majhen odvod topote prek zaznavala.

1.2.1 Lega in namestitev zaznaval

Zaznavala so nameščena na zunanjih (zaznavala št. 3, 7, 9) in notranji strani (zaznavala št. 4, 8, 10) okrova žarometa (zaznavala so drug nad drugim) in na notranji strani pokrova (zaznavali št. 1, 2) okrova ter na paraboli (zaznavalo št. 6) in senčniku (zaznavalo

instrument (Keithely, model 2000) (3), a voltmeter (4), a laboratory voltage source (5), a personal computer with the LabVIEW program (6).

The required voltage across the bulb is 13.5 V. The voltage is measured with the voltmeter (Fig. 1).

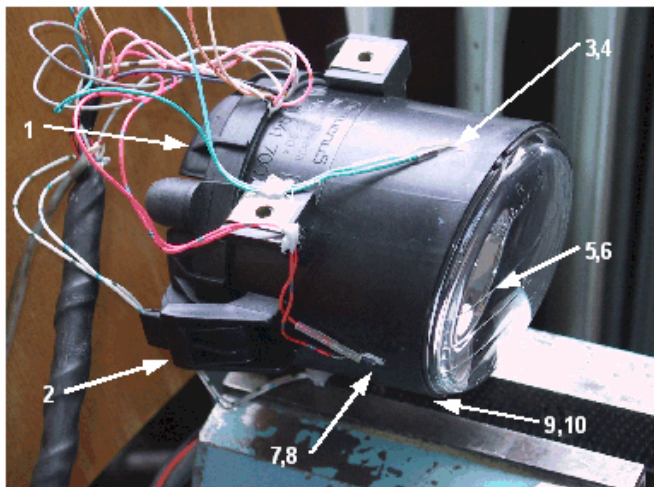
1.2 Temperature sensor selection

Measurements of temperature, heat flow or heat energy are usually made with contact sensors [3]. The basic rule for choosing a sensor is that the sensor should not locally change the heat flow. This problem is associated with thermocouples size. They are small, so a small heat flow is transferred through the sensor and its wiring; however, on the other hand, due to their shape it is hard to position thermocouples directly on the surface. The other most common method for temperature measurements is the use of RTD sensors. These sensors are usually made from platinum. RTD sensors also have a wide temperature range and a linear relationship between resistance and temperature change.

The measurements were made with RTD sensors from Heraeus Sensors. These sensors are used in cases where long-term stability and accuracy are needed. They are made from platinum and have a nominal resistance of 1000Ω at 0°C. The base on which the platinum wire is placed is made of ceramic, which offers good heat conduction. The sensors are in the tolerance class 1/3. Because of their small size (4 mm × 2 mm), heat conduction through the sensor is minimized.

1.2.1 Sensor position and fixation

The RTD sensors are mounted on the outer (sensors No. 3, 7, 9) and inner (sensors No. 4, 8, 10) sides of the fog-lamp housing (the sensors are one above another). Four other sensors are on the inner side of the housing lead (sensors No. 1, 2), on the



Sl. 2. Namestitev zaznaval na zunanjji strani okrova
Fig. 2. Positioning of the sensors on the lamp housing

št. 5) žarometa (sl. 2). Lega zaznaval 3 in 4 je bila izbrana kot predvidoma najbolj vroče mesto na okrovu, in sicer točno nad mestom žarnice. Preostala zaznavala so postavljena tako, da bomo lahko dobljene vrednosti uporabili za izračun funkcije porazdelitve temperature po celotnem žarometu. Zaznavalo na senčniku ter na paraboli je postavljeno na najbolj vroči mesti.

Zaznavala prilepimo na površino merjenca z lepilom. Pri merjenju temperature je treba posebej paziti, da ima lepilo enako toplotno prevodnost in enako temperaturno razteznost. Plast lepila, s katero je zaznavalo prilepljeno, mora biti čim tanjša. Lepilo mora biti tudi temperaturno obstojno. Za lepljenje zaznaval na plastičen okrov smo uporabili dvokomponentno lepilo, ki je temperaturno obstojno do 250 °C. Ker je pričakovana temperatura na senčniku in paraboli zelo visoka (500 °C), je lepljenje zaznaval velik problem. Zaznavali, prilepljeni na kovinsko parabolo in senčnik, sta prilepljeni z uporabo tekoče kovine, ki je namenjena zalivanju razpok na kovinskih delih. To lepilo ima zelo podobno toplotno prevodnost kakor železo. Problem pa je bil pri obeh lepilih zagotoviti čim manjšo debelino lepila. Dodatne meritve s sevalnim infrardečim inštrumentom za merjenje temperature so pokazale, da je vpliv lepila na meritev zanemarljiv.

1.3 Program za zbiranje podatkov

Program za zbiranje podatkov in nadzor meritev sta narejena s programskega paketom LabVIEW. Kakor je razvidno s slike merilne verige (sl. 1), peljemo signale prek kartice za zbiranje več signalov na univerzalni analogni merilni inštrument, od tod pa na vzporedni vhod računalnika, kjer signale obdelamo in analiziramo s programskega paketom LabVIEW.

Program omogoča zagon, vodenje in nadzor celotnega postopka. Na prednji plošči programa so krmilniki in kazala s katerimi se merilni postopek vodi in nadzira.

parabola (sensor No. 6) and on the lampshade (sensor No. 5) as shown in Fig. 2. The sensors No.3 and No.4 are positioned on the hottest spot of the housing – above the bulb. The other sensors are positioned so that their results can be used for a calculation of a distribution function over the whole lamp housing. The sensors on the parabola and the lampshade are positioned on the hottest spots.

The sensors are fixed on the surface with an adhesive. The adhesive has the same heat-conduction and temperature-extension coefficient as the sensors. The layer thickens of adhesive has to be as thin as possible. The adhesive should withstand high temperatures. A two-component adhesive that withstands temperatures up to 250 °C was chosen. The expected temperatures on the parabola and the lampshade will be around 500 °C. This presents a huge problem for fixing the sensors. A liquid steel was used, which is used for the cold welding of cracks in metal parts. It has very similar heat-conduction properties to iron. The biggest problem is to ensure that the layer of the adhesive is thin. The influence of the adhesive was tested with an infrared temperature-measurement instrument, which showed that the influence of the adhesive was negligible.

1.3 Data-acquisition program

A data acquisition program was written with the LabVIEW program. As shown in Fig.1, the signals are directed to the measuring card in an analog measuring instrument and then to the parallel port of a PC, where they are processed and analyzed with the help of LabVIEW.

The program enables us to start, control and observe the whole measurement. The front panel of the program has controllers and indicators to control the measuring process.

2 MERITVE IN REZULTATI

Meritev je potekala pri nespremenljivi napetosti na žarnici 13,5 V. Posamezna meritev je trajala več ko eno uro, ker je morala temperatura doseči ustaljeno stanje. Meritev je potekala na 12 različnih mestih, merilni instrument pa je imel možnost zbiranja samo desetih podatkov, zato je bilo treba meriti dva parametra posebej. To smo storili tako, da smo pokrov okrova z zaznavali odstranili in namesto njih priključili zaznavali na paraboli in senčniku ter meritev ponovili.

2.1 Preverjanje umerjanja merilne verige

Zaznavala Pt-1000 so izdelana iz platine, kateri se s spremembijo temperature spreminja upornost. Merilno verigo smo umerjali tako, da smo žaromet s priključenimi zaznavali dali v toplotno komoro in primerjali izhodni signal oz. temperaturo zaznaval in etalonskega termometra. Etalonski termometer je bil na isti višini in na mestu kakor druga zaznavala, zato lahko vzamemo, da je na tem delu komore homogeno temperaturno polje. Merilno verigo smo preverjali pri temperaturah 20 °C, 40 °C ter 60 °C. Etalonski termometer ima merilno negotovost $\pm 0,01^\circ\text{C}$. Primerjavo med temperaturo, izmerjeno z zaznavali Pt-1000 in etalonskim termometrom, prikazuje slika 3.

Opozimo lahko temperaturni odmik navzgor od etalonskega termometra. Pri 40 °C se pokažejo kar velika nihanja temperature v temperaturni komori (sl. 3). Vendar se pokaže, da niso sporna zaznavala, ker ta

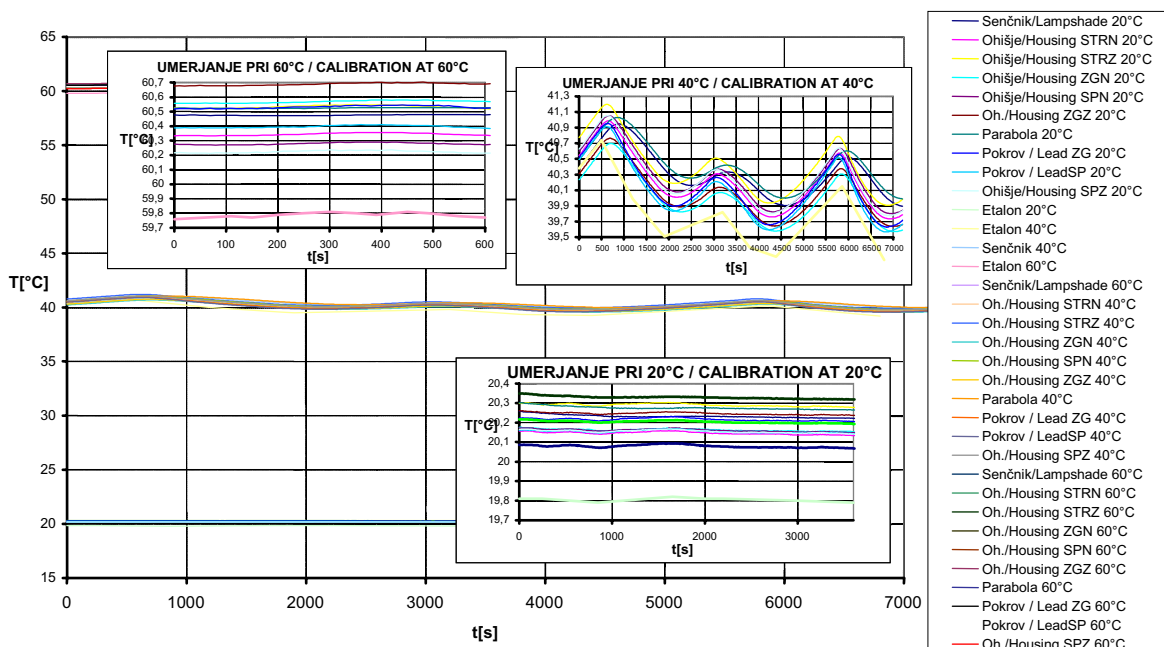
2 MEASUREMENTS AND RESULTS

The bulb was powered with a constant voltage of 13.5V. The measurement lasted more than an hour, because the temperature field needed to reach a steady state. Measurement was taken at 12 different spots, so two spots had to be measured separately. This is the way we measured all the spots on the housing and the lead. The sensors on the lead were then disconnected and the sensors on the parabola and the lampshade were connected and the whole measurement was repeated.

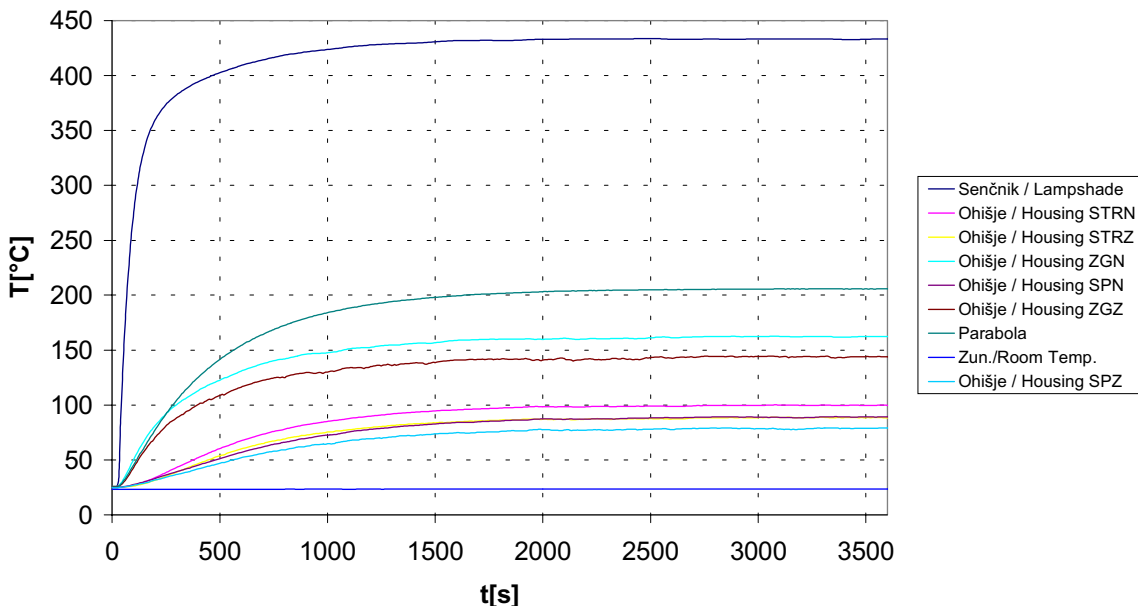
2.1 Measuring chain verification

The Pt-1000sensors are made from platinum, the resistance of which varies with temperature. The whole measuring chain together with the lamp was verified in a heat chamber and a temperature comparison was made with an etalon thermometer. The etalon thermometer was at the same height as the other sensors and we assumed a homogeneous temperature distribution in that part of the temperature chamber. The measuring chain was verified at the temperatures 20°C, 40°C and 60°C. The etalon thermometer has a measurement uncertainty $\pm 0,01^\circ\text{C}$. The results of the Pt-1000 sensor verification are shown in Fig.3.

A positive temperature offset was observed for the sensors. A temperature oscillation at 40°C (Fig.3) was also detected. The problem of the oscillation is related to the heating chamber, which



Sl. 3. Odstopek zaznavala od etalonskega termometra pri različnih temperaturah
Fig. 3. Verification of the sensors using an etalon thermometer



Sl. 4. Meritev temperature na okrovu in pokrovu žarometa
Fig. 4. Temperature measurement on the housing and the lead of the fog lamp

lepo sledijo kalibracijskemu termometru, temveč komora, ki težko vzdržuje nespremenljivo temperaturo 40 °C. Amplituda nihanja temperature pri zaznavalih je 1,9 °C.

Iz meritev je razvidno, da kažejo zaznavala Pt-1000 nekaj višjo temperaturo kakor etalonski termometer. Opazimo pa lahko, da zaznavala lepo sledijo spremembam temperature in so zelo stabilna. Zaradi razlike med zaznavali in etalonskim termometrom izračunamo merilno negotovost merilne verige [4].

2.2 Rezultati meritev

Meritve so potekale v dveh delih, ker smo imeli na voljo omejeno število merilnih mest.

Tako smo najprej izvedli meritve na osmih merilnih mestih in dveh mestih na pokrovu žarometa. Nato smo zamenjali pokrov žarometa ter parabolo s senčnikom, kjer sta bili dodatni merilni mesti in ponovili meritve. Tako smo dobili 4 meritve temperature na pokrovu žarometa in 8 meritve na senčniku in paraboli. Za preostala merilna mesta smo dobili 12 meritev. Primer rezultata meritve je na zgornji sliki (sl. 4).

Za nadaljnjo obdelavo podatkov smo vzeli odčitke temperature po času 3000 s, kjer se temperatura ustali. Nato smo za vsako merilno mesto posebej izračunali povprečno vrednost ter 95-odstotni interval zaupanja za izmerjeno temperaturo. Spodnja slika prikazuje temperaturo v ustaljenem stanju, srednjo vrednost ter spodnjo in zgornjo mejo 95-odstotnega območja zaupanja za eno izmed merilnih mest (sl. 5).

Iz primerjave leve in desne strani na zgornji sliki za zaznavalo na notranji in zunanj strani vidimo

cannot be kept at a constant 40°C. At 40°C the sensors follow the etalon thermometer closely. The amplitude of the temperature oscillations at 40°C is 1.9°C.

The verification measurements show that the Pt-1000 sensors show higher temperatures than the etalon thermometer. The verification measurements also show that the sensors follow the changes in temperature very well, and that they are very stable. Based on the differences in the measurements between the sensors and the etalon thermometer the measurement uncertainty of the measuring chain was calculated [4].

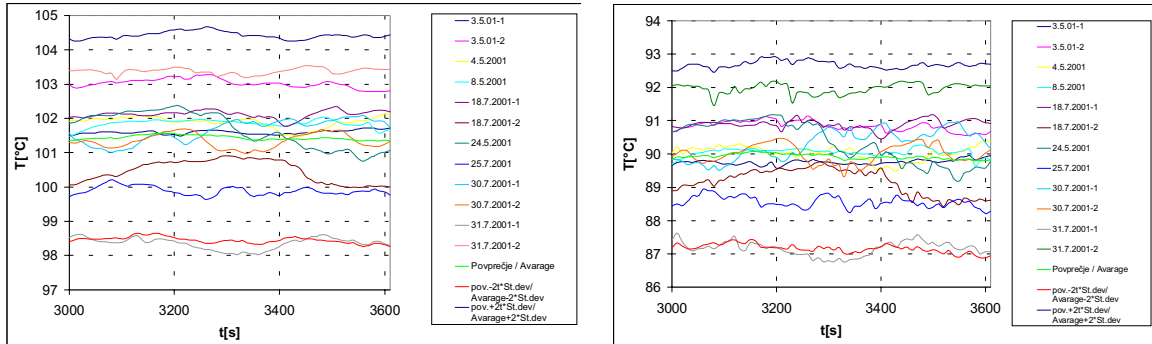
2.2 Results

Because of the limited number of measuring points, the measurements were carried out in two parts.

First the measurements were carried out on the eight points on the housing and the two points on the lead of the housing. Then the lead of the housing, the parabola and the lampshade were changed, so that the temperature on the parabola and the lampshade were measured. Altogether, four measurements on the lead and eight measurements on the parabola and the lampshade were made. An example of the measurement is shown in Fig. 4.

For subsequent analysis, the results after 3000 s were taken, because after this time the temperatures were stable. From these data a mean value and a 95% confidence interval were calculated. Fig. 5 shows the measurements at steady state for one measuring point, the mean value, and the lower and upper 95% confidence intervals.

From a comparison of the left- and right-hand side of Fig. 5, which shows the results for the inner and outer sensors, the large influence of heat



Sl. 5. Ustaljena temp. na zunanjji (desno) in notranji (levo) stran srednjega dela okrova
Fig.5. The steady temperature on the outer (right) and the inner (left) sides of the middle part of the housing

močan vpliv odvoda toplotne zaradi cirkulacije zraka v prostoru okrog zunanjih zaznaval (sl. 5). Ta nastane zaradi prepiba oziroma drugih motenj. Na notranjih zaznavalih se ta vpliv zmanjša (bolj gladka krivulja), pojavi se s časovnim odmikom.

Končni rezultati, ki upoštevajo še sistemsko ter naključno negotovost, so predstavljeni v preglednici 1. Temperature se s 95% odstotno verjetnostjo gibljejo v spodnjem intervalu zaupanja.

3 SKLEPI

Kakor smo že poudarili, je pomembna pravilna izbira zaznavala, kajti toplotna zmogljivost žarometa je razmeroma majhna in je zato vsak pritrjeni element "velik" odvodnik toplotne. To lahko povzroči,

Preglednica 1. Rezultati meritev temp. na posameznih delih žarometa
Table 1. Measuring results for the fog-lamp parts

Merilno mesto/ Measuring point	Temperatura/ Temperature [°C]
Zunanja stran zgornjega dela okrova / Outer upper side of the housing (Oh. ZGZ)	144,6 ± 2,5
Notranja stran zgornjega dela okrova / Inner upper side of the housing (Oh. ZGN)	166,8 ± 2,9
Zunanja stran srednjega dela okrova / Outer middle side of the housing (Oh. STRZ)	89,9 ± 0,9
Notranja stran srednjega dela okrova / Inner middle side of the housing (Oh. STRN)	101,4 ± 1,0
Zunanja stran spodnjega dela okrova / Outer lower side of the housing (Oh. SPZ)	80,5 ± 1,0
Notranja stran spodnjega dela okrova / Inner lower side of the housing (Oh. SPN)	90,7 ± 1,0
Notranja stran zgornjega dela pokrova / Inner upper side of the lead (Pok. ZG)	98,3 ± 0,8
Notranja stran spodnjega dela pokrova / Inner lower side of the lead (Pok. SP)	77,6 ± 0,7
Notranja stran zgornjega dela parabole / Inner upper side on the parabola (Parabola)	206,3 ± 1,2
Zunanja stran zgornjega dela senčnika / Outer upper side of the lampshade (Senčnik)	434,1 ± 2,5

transfer, as a result of air flow circulation in the room, on the outer sensor can be observed. This influence is a result of the air circulation and other air distortions in the room. The influence of the air flow in the room is less influential on the inner sensor (the temperature curve is smoother and distortions are delayed).

The results presented in the Table 1 below also take into account a systematic and coincidental uncertainty. The presented temperatures lie within the confidence interval with a 95% probability.

3 CONCLUSIONS

A fog lamp has a relatively small heat capacity, and therefore choosing a sensor with a very small heat capacity is essential because each sensor acts as a big heat conductor. As a result, the measured

da je merjena temperatura na mestu zaznavala manjša od dejanske. Zaradi tega smo izbrali zaznavala s čim manjšo površino ter priključne žice s čim manjšim prerezom. Vse priključne žice so pritrjene tako, da se ne dotikajo okrova na mestih merjenja. S tem smo zmanjšali odvod toplote na minimum.

Meritve so tudi potrdile domnevo, da ima temperaturno polje v žarometu velik gradient. Ta nastane zaradi vpliva naravne konvekcije in sevanja žarnice. Pokazalo se je, da je največja temperatura na okrovu žarometa na mestu nad začetkom parabole, kjer se topel zrak dviga in lokalno segreva okrov. Na isti višini zadnjega dela okrova se temperatura zmanjša kar za 60°C. Pokazalo se je tudi, da se pojavi kar velika razlika v temperaturi zunanje in notranje površine. Zaradi razlike temperatur po obliki žarometa in temperaturnih razlik na površini žarometa pride do deformacije okrova žarometa, kar privede do netesnosti okrova. Z ugotovitvami, pridobljenimi z meritvami, smo določili temperaturno porazdelitveno funkcijo [4], ki je bila podlaga za nadaljnje analize z uporabo končnih elementov.

temperature is lower than the true one. That is why we selected sensors with a small area and a small wire cross-section. All the connecting wires do not touch the housing near the measuring points. This also reduced the heat transfer from the housing to a minimum.

The measurements also showed that the temperature field in the lamp has a high temperature gradient. This is a consequence of the two forms of heat transfer: natural convection and bulb radiation. The measurements showed that the highest temperature on the housing is right above the end of the parabola. On that part the hot air is rising and it locally heats the housing. At the same height on the back part of the housing the temperature is 60°C lower. The temperature difference between the inner and the outer housing surfaces is quite large. These differences on the housing surfaces cause housing deformation, which can lead to sealing problems with the housing. The measurement results helped us to determine a temperature distribution function [4]. This function was the basis for subsequent calculations with the finite-element method.

4 LITERATURA 4 REFERENCES

- [1] Wagner, A. (2001) Eksperimentalno določanje temperaturnega stanja v ohišju žarometa za vozilo VW Lupo (seminarska naloga pri predmetu Eksperimentalne metode v raziskovanem delu). Ljubljana.
- [2] Holman, J.P., W.J.Jr Gajda (1984) Experimental methods for engineers, IV.izdaja, McGraw-Hill International Book Co., London, , ISBN 0-07-Y66337-8.
- [3] Bajšić, I. (marec 2001). Primerjava temperaturnih merilnih zaznaval. Ljubljana.
- [4] Wagner, A. (2003) Izboljšanje razvojnih vrednotenj z napovedovanjem zagotovljivosti izdelka. Magistrsko delo. Univerza v Ljubljani, Fakulteta za strojništvo. Ljubljana.
- [5] Moore, W. I., E.S. Donovan, C.R. Powers (1999) Thermal analysis of automotive lamps using the ADINA-F coupled specular radiation and natural convection model. *Computers and Structures* 72, London, 17-30.
- [6] Okada, Y., T. Nouzawa, T. Nakamura (2002) CFD analysis of the flow in an automotive head lamp. *JSAE Review* 23, 95-100.
- [7] Shiozawa T., M. Yoneyama., K. Sakakibara, S. Goto, N. Tsuda, T. Saga, T. Kobayashi T. (2001) Thermal air flow analysis of an automotive headlamp: the PIV measurement and CFD calculation for a mass production model. *JSAE Review* 22, 245-252.

Naslov avtorjev: mag. Andrej Wagner
 prof. dr. Ivan Bajšić
 prof.dr. Matija Fajdiga
 Fakulteta za strojništvo
 Univerza v Ljubljani
 Aškerčeva 6
 1000 Ljubljana
 andrej.wagner@fs.uni-lj.si
 ivan.bajsic@fs.uni-lj.si
 matija.fajdiga@fs.uni-lj.si

Authors' Address: Mag. Andrej Wagner
 Prof. Dr.Ivan Bajšić
 Prof.Dr. Matija Fajdiga
 Faculty of Mechanical Eng.
 University of Ljubljana
 Aškerčeva 6
 1000 Ljubljana, Slovenia
 andrej.wagner@fs.uni-lj.si
 ivan.bajsic@fs.uni-lj.si
 matija.fajdiga@fs.uni-lj.si

Prejeto:
 Received: 27.11.2003

Sprejeto:
 Accepted: 8.4.2004

Odperto za diskusijo: 1 leto
 Open for discussion: 1 year

Vključitev numeričnih analiz v zgodnjih fazah konstrukcijskega postopka

Introducing Numerical Analyses in the Early Phases of the Design Process

Tomaž Bučar - Miha Janežič - Primož Pangeršič - Matija Fajdiga

Odločitve, sprejete v razvojnem postopku izdelka, bistveno vplivajo na končno ceno, zmogljivost, zanesljivost, varnost in vpliv izdelka na okolico. Ker je poznavanje konstrukcijskih zahtev in omejitev v zgodnjih fazah proizvodnega postopka izdelka pogosto omejeno, je sprejemanje vsakršnih odločitev za konstrukterja zelo zahtevno. Soočeni s tako zapletenostjo so se posamezni konstrukterji omejili na ozke in dobro opredeljene podnaloge, kar ima za posledico neenotnost napredka na tem področju. V mnogih primerih je bil razvojni postopek izboljšan z računalniško podprtим konstruiranjem (RPK) in tehnikami numeričnih vrednotenj, kakor je metoda končnih elementov (MKE). Združitev obeh postopkov omogoča izračun napetostno-deformacijskih stanj izdelka in njegovo obnašanje pri različnih oblikovnih variantah. Podatke o napetostno-deformacijskih stanjih lahko pridobimo tudi z eksperimentalno analizo fizičnih preizkušancev, toda prednost postopka RPK-MKE je možnost spremicanja oblikovnih in materialnih parametrov izdelka ter takojšnja numerična vrednotenja pred izdelavo fizičnih prototipov. Ker so računalniški modeli zgrajeni na podlagi mnogih predpostavk in omejitev, tudi rezultati analiz z metodo končnih elementov brez ustrezne razlage nimajo prave vrednosti. V prispevku je zato predlagana metoda za pridobitev referenčne baze podatkov, na podlagi katere poteka vrednotenje rezultatov numeričnih izračunov. Postopek gradnje baze podatkov je prikazan na konkretnem primeru ročne zavore in zavornega pedala osebnega vozila.

© 2004 Strojniški vestnik. Vse pravice pridržane.

(Ključne besede: procesi konstruiranja, CAD, metode končnih elementov, načrtovanje preskusov)

Decisions made during the product development process have a significant influence on factors such as costs, performance, reliability, safety and the environmental impact of a product. However, since the knowledge of all the design requirements and constraints during this early phase of a product's life cycle is usually imprecise, approximate or unknown, the designer's decision-making is a very demanding task. Faced with such complexity, individual designers have restricted themselves to narrow, well-defined sub-tasks and, as a result, progress in this area has been patchy and spasmodic. In many cases, product design has been improved by the help of computer-aided design (CAD) and structural analyses based on the finite-element method (FEM). These two methods, coupled together, allow the calculation of mechanical quantities (such as stresses, deformations and contact pressures) and the investigation of the different behaviour of products with various designs. Such quantities can also be measured by means of in-vitro tests, but the advantage of CAD-FEM is the possibility of changing the geometrical and material properties of the product and evaluating its different behaviour before manufacturing prototypes. However, because the numerical models are based on many suppositions and restrictions, without proper interpretation the finite-element analysis (FEA) results are also of almost no use. Thus, in this article a method of acquiring a reference database, which serves for FEA results validation, is suggested. The procedure of building a suitable reference database is demonstrated by means of two examples, a car's handbrake and brake pedal.

© 2004 Journal of Mechanical Engineering. All rights reserved.

(Keywords: product design, CAD, finite element methods, experiment planning)

0 UVOD

Konstruiranje je zahteven postopek, s katerim se zamisel o zadostitvi nove funkcije v naravi smiselnopredeli do najmanjše podrobnosti in predstavi v nematerialni obliki kot izdelek. Postopek

0 INTRODUCTION

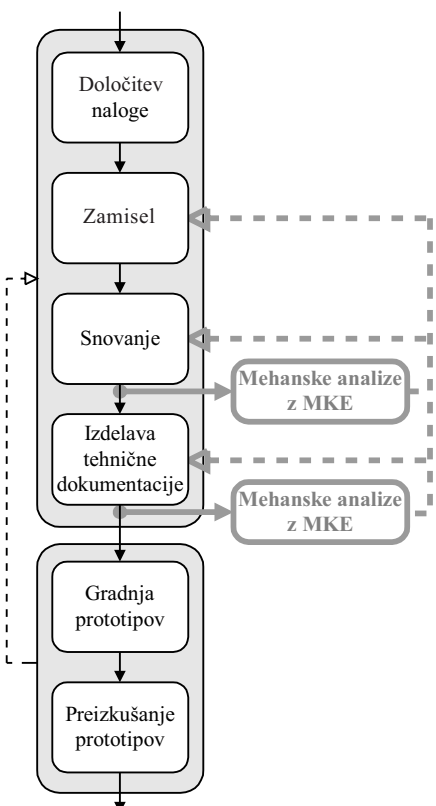
Product design is a complex, iterative, decision-making engineering process, the result of which is transforming an abstract principle into a concrete technical solution. It usually starts with the identifi-

konstruiranja se običajno prične z razpoznavanjem in analizo naloge, ki jima sledi zaporedje dejavnosti, s katerimi iščemo optimalno rešitev problema, in konča s podrobnim opisom izdelka. Posamezne faze konstrukcijskega postopka so pri različnih avtorjih modelov opredeljene različno. Pregled najbolj znanih metod je podan v [1]. V splošnem je konstrukcijski postopek razdeljen na štiri glavne faze [2]. Prva faza je specifikacija naloge, pri kateri se natančno zberejo in določijo informacije o izdelku. Zasnova je druga faza konstrukcijskega postopka, katerega osnovni namen je iskanje idejnih rešitev, ki izpolnijo dano nalogu. Fazi zasnove sledi faza snovanja. V tej fazi se izdela natančen osnutek z določenimi osnovnimi merami in končno obliko. Zadnja faza je dodelava, ki vključuje optimiranje podrobnosti in izdelavo vse potrebne dokumentacije za izdelavo prototipov. S to fazo se konča konstrukcijski postopek v ožjem pomenu, kateremu sledijo še izdelava in preizkusi prototipov. Vse omenjene faze konstruiranja so prikazane na sliki 1. Računalniško podprta orodja so uveljavljena predvsem v končnih fazah konstruiranja, ki obsega določanje oblike in izmer. Razširitev računalniške podpore na zgodnje faze konstruiranja je v zadnjih letih glavni cilj raziskav na tem področju. Nekateri rezultati tovrstnih raziskav so podani v [3] do [5]. Običajno je končna oblika izdelka potrjena šele po intenzivnih in uspešnih eksperimentalnih vrednotenjih dragih fizičnih prototipov. Če testiranja niso uspešna, je treba izdelek na podlagi povratnih informacij večkrat popravljati, kar pomeni dodatne razvojne stroške in je lahko časovno precej zamudno. Da se izognemo nepotrebnemu izdelovanju dragih fizičnih prototipov, se razvoj računalniške podpore konstruiranju vedno bolj usmerja tudi na uporabo numeričnih vrednotenj in računalniških prototipov. Uporaba tehnik numeričnih analiz omogoča sprotno in učinkovito vrednotenje izdelkov brez izdelave fizičnih prototipov. Namen tega prispevka je prikazati trdnostno analizo z metodo končnih elementov kot eno od tehnik numeričnih vrednotenj, ki bo uporabna v zgodnjih fazah konstrukcijskega postopka (sl. 1). Ker tovrstne numerične analize temeljijo na poenostavljenih matematičnih modelih, je treba imeti za vrednotenje rezultatov na voljo primerjalno bazo podatkov. Glavni cilj raziskovalnega dela je zato razviti ustrezno metodo, ki bo ob najmanjšem dodatnem delu in stroških omogočala gradnjo kakovostne baze primerjalnih podatkov. Z uporabo kombinacije numeričnih vrednotenj in tehnik postopka RMS (FMEA, FTA) [6] lahko pridemo v zgodnjih fazah razvoja izdelka bistveno hitreje in z manj porabljenimi sredstvi do kakovostnih rešitev.

V nadaljevanju prispevka je najprej opisana predlagana metoda za gradnjo omenjene primerjalne baze podatkov. Uporaba metode je nato prikazana na dveh dejanskih primerih. Na koncu so podane še nekatere ugotovitve in sklepi.

cation of a need, proceeds through a sequence of activities to seek an optimal solution to the problem, and ends with a detailed description of the product. Researchers define individual phases of the design process in various ways. An overview of the most-known methods can be found in [1]. Generally, a design process consists of four phases [2]. The first phase is product design specification, where information about the product is collected and defined in precise yet neutral terms. Conceptual design represents the second phase of the design process, whose primary concern is the generation of physical solutions to meet the design specification. The conceptual design phase is followed by the embodiment design phase. In this phase, the precise layout and the form of the final product are developed. The final phase is the detailed design, where final decisions on dimensions, arrangement and shapes of individual components and materials are made and production documentation for manufacturing prototypes is completed. With this phase the product design, in a narrow sense, is concluded and followed by prototype manufacturing and testing. Figure 1 summarizes all the mentioned phases of the design process. Computer-aided tools are well established in the later phases of the design process, namely detailing and embodiment with modelling. Extending computer support to the early phases of the design process has been the main research aim in this area in the past few years. Some findings acquired in such researches can be found in [3] to [5]. Usually, the final product form is confirmed after intensive and successful experimental analyses of expensive physical prototypes. Unless experimental testing is successful, the product needs to be redesigned according to feedback information, which leads to further costs and time consumption. In order to avoid expensive and unnecessary prototype manufacturing, computer support for design is aimed at numerical validation and computer prototypes. The use of numerical analysis methods allows a consistent and efficient product evaluation without the need for expensive physical prototypes. The aim of this paper is to demonstrate the structural analysis based on FEM as a numerical analysis method applicable in the early phases of the design process (see Fig. 1). Since such numerical analyses are founded on simplified numerical models, a reliable reference database is required for the validation of FEA results. The main objective of such an approach, and therefore the focus of this paper, is to develop a suitable method that enables us to build a reference database of high quality with minimal additional efforts and costs. Using a combination of numerical analyses and RMS methods (FMEA, FTA) [6] in the early phases of the product design, we can solve the problem in a significantly faster and cheaper fashion.

In the next sections the method for acquiring the reference database is proposed and the procedure is then demonstrated in practice. To end with, some conclusions are given.



Sl. 1. Faze konstrukcijskega postopka

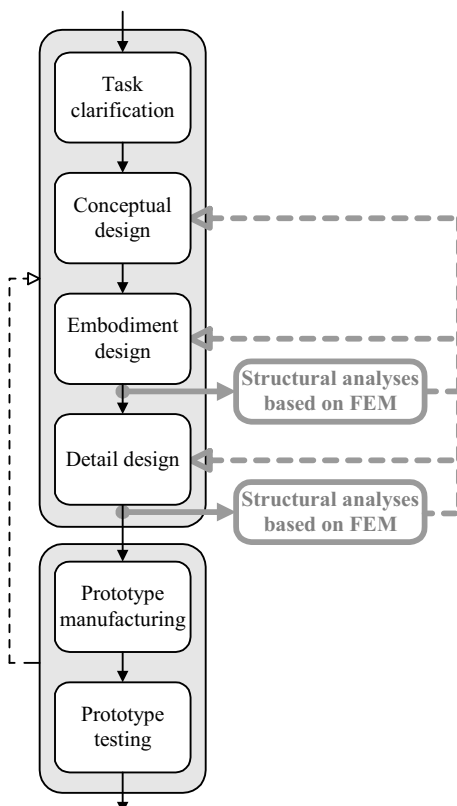


Fig. 1. The phases of product design

1 GRADNJA PRIMERJALNE BAZE PODATKOV

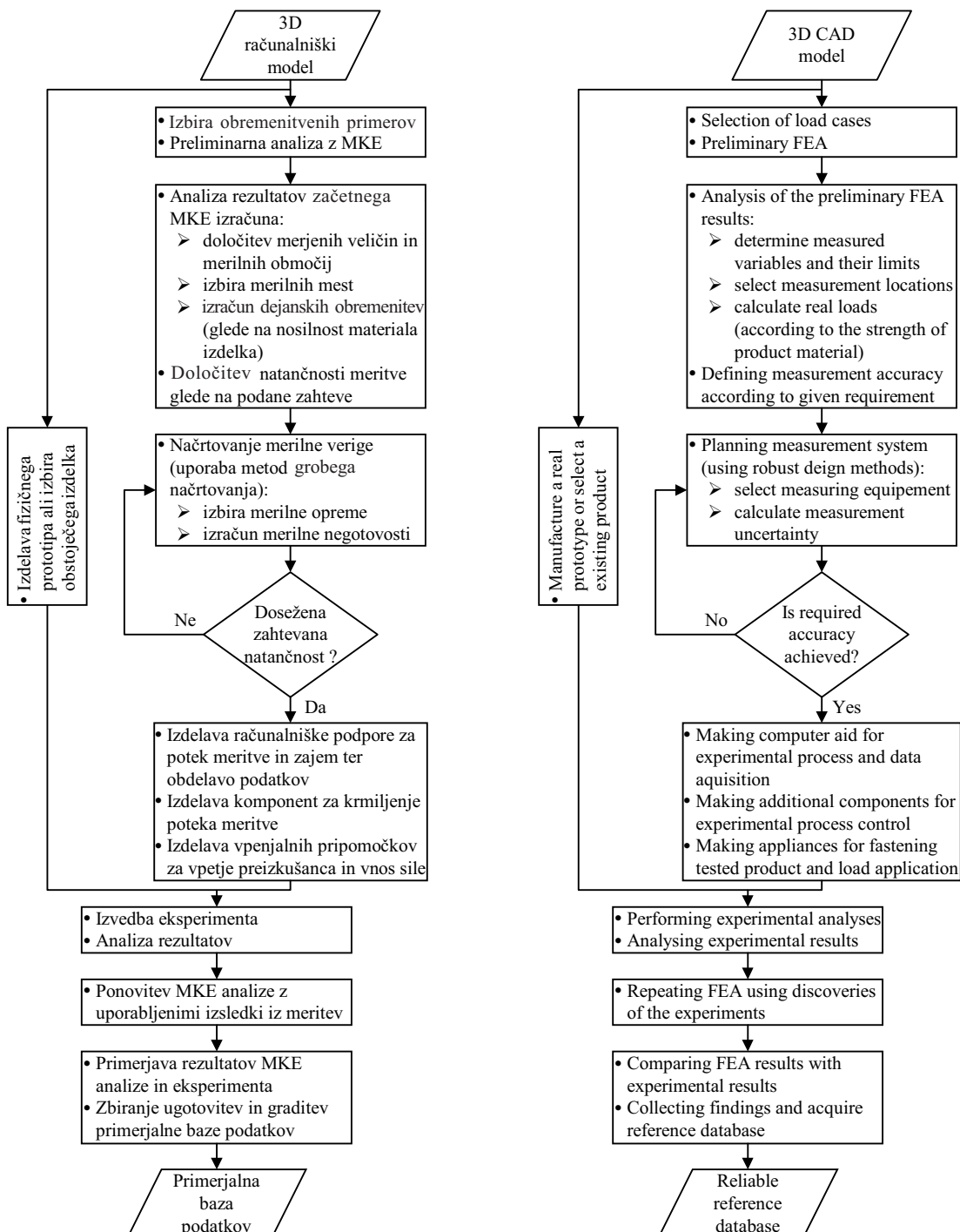
V fazi razvoja izdelka se za numerične analize z metodo končnih elementov uporabljajo bolj ali manj zahtevni matematični modeli, ki temeljijo na različnih omejitvah in predpostavkah. Tako ustvarjeni matematični modeli so nenatančni in dejanski izdelek opišejo le približno. Ker so zaradi tega približni tudi rezultati numeričnih analiz, morajo za njihovo vrednotenje obstajati primerne primerjalne vrednosti. Primerjavo za vrednotenje rezultatov pomeni primerjalna baza podatkov, ki jo pridobimo s predhodnimi numeričnimi izračuni in preizkusi. Predlagana metoda gradnje baze primerjalnih podatkov je prikazana na sliki 2. Predstavljeni postopek se opravi le enkrat, bodisi na že znanem izdelku ali na izdelku v razvoju. Izdelano primerjalno bazo podatkov je mogoče uporabiti tudi pri razvoju sorodnih izdelkov. Konstrukcijski postopek izdelkov se tako pospeši, saj ovrednoteni rezultati numeričnih analiz v veliki meri nadomestijo izdelavo in eksperimentalno analizo dejanskih prototipov. Uvajanje sprotnega in učinkovitega vrednotenja ter preizkušanja izdelkov na tako imenovanih računalniških prototipi je torej naš glavni namen.

Kakor smo že omenili, je na sliki 2 prikazan postopek za gradnjo kakovostne baze podatkov, na podlagi katere se v zgodnjih fazah razvoja izdelka vrednotijo rezultati numeričnih izračunov. V pretočnem diagramu je nazorno prikazano zaporedje posameznih

1 REFERENCE DATABASE ACQUISITION

During product design, various numerical models based on many suppositions and restrictions are used for finite-element analyses. Thus, such models are inaccurate and describe the physical product only approximately. Consequently, FEA results are also approximate, which is why comparative examples are required for their validation. These comparative examples are a reliable reference database that is acquired through preceding numerical calculations and experimental analyses. The suggested method for building a reference database is shown in Figure 2. The shown procedure is performed only once on the existing product or on the product in the development process. The elaborated reference database can also be used in the development of similar products. This way the product development process is accelerated, for the evaluated FEA results largely substitute for expensive prototype manufacturing and experimental analyses. The introduction of a consistent and efficient product evaluation using so-called computer prototypes is therefore our main purpose.

As mentioned, Figure 2 presents the procedure for reference database elaboration on which the evaluation of numerical calculations in the early phases of product design are based. The block diagram shows the sequence of tasks clearly. It is worth



Sl. 2. Metoda za gradnjo primerjalne baze podatkov

opravil, podrobnejša razlaga pa sledi na stvarnih primerih. Omeniti je treba le to, da je eksperimentalno preverjanje numeričnih rezultatov mogoče le z zelo kakovostnimi in premišljeno načrtovanimi preizkusi ([7] in [8]). Ker ima pri tem primeren in pravilno zasnovan merilni sistem pomembno vlogo, si pri izdelavi zamisli meritve pomagamo tudi z metodami grobega načrtovanja ([9] in [10]). Glavno načelo omenjene metode je izboljšanje kakovosti eksperimentalne analize z zmanjšanjem občutljivosti

Fig. 2. The method for reference database acquisition

mentioning that experimental verification of the FEA results is only possible by means of perfected and well-planned tests ([7] and [8]). Since a suitable and properly conceptualised measurement system plays an important role here, the method of robust design ([9] and [10]) can be of great help when preparing the experiment concept. The key principle of this method is to improve the quality of the experimental analysis through reducing the measurement system's sensitivity to disturbing factors. Our task is

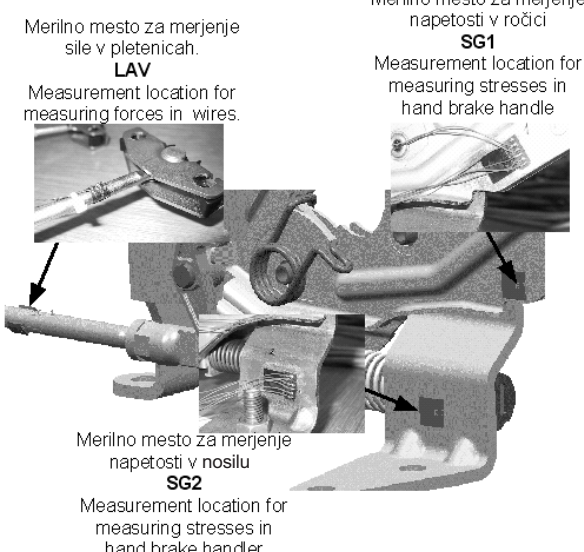
merilnega sistema na motilne dejavnike. Naša naloga je torej, da izberemo komponente merilnega sistema tako, da bo na izhodu iz sistema vpliv motilnih signalov na želenega čim manjši. Postopek izgradnje primerjalne baze podatkov bo v nadaljevanju prikazan na dveh realnih primerih.

2 ZGLEDI

2.1 Ročna zavora

V tem poglavju je predstavljen sistem eksperimentalnega preverjanja numerične analize ([12] in [13]), s kakršnim na izdelkih določenega tipa gradimo bazo znanja. S tako pridobljeno bazo podatkov si v konstrukcijskem postopku podobnih izdelkov pomagamo pri gradnji modelov končnih elementov in pri vrednotenju rezultatov.

Da bi pred meritvami bolje spoznali napetostno in deformacijsko stanje pri izbranih obremenitvah, je bila izdelana začetna analiza z metodo končnih elementov. Z začetno analizo napetostnega stanja smo določili najprimernejša mesta na konstrukciji za merjenje napetosti. Ker smo za merjenje mehanskih napetosti izbrali merilne lističe, morajo imeti merilna mesta pri vseh obremenitvenih primerih razmeroma veliko napetost, njen gradient po površini pa naj bi bil čim manjši. Merilno mesto mora biti tudi geometrijsko primerno za namestitev merilnega lističa. Na podlagi rezultatov začetne analize sta se za najugodnejši mesti za merjenje napetosti izkazali mesti SG1 in SG2 (sl. 3). Na teh mestih se pojavijo razmeroma velike napetosti pri vseh obremenitvenih primerih. Izbrani mesti sta geometrijsko ustreznii za namestitev merilnih lističev in sta eno na ročici drugo pa na nosilu ročne zavore.



Sl. 3. Merilna mesta
Fig. 3. Measurement locations

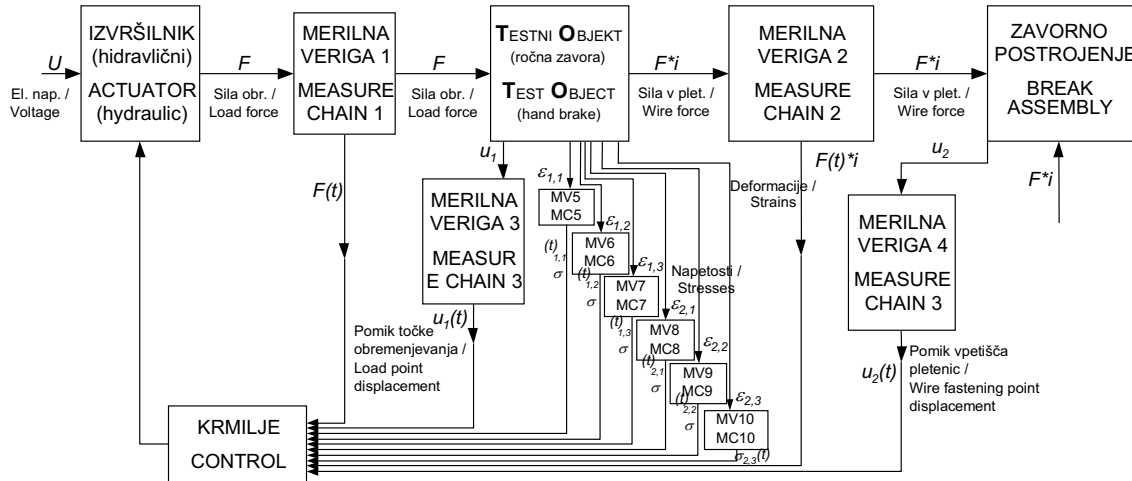
to select the components of the measurement system in such a way that the influence of the disturbing signals on the chosen one is minimised. In the rest of the paper the procedure of reference database acquisition is demonstrated by means of two practical examples.

2 EXAMPLES

2.1 Handbrake

In this section we present a system for the experimental validation of numerical analysis ([12] and [13]) with which we can build a reference database that would help us when designing and validating similar structures. Such a database can, in the design processes of similar structures, help us to build finite-element models and validate numerical simulation results.

A preliminary analysis using the finite-element method was made in order to get to know better the stress and strain states in the chosen load cases. This preliminary stress-state analysis helped us define the most suitable locations to measure the stresses on the structure. Since we chose strain gauges to measure the mechanical stresses, all the measurement locations need to have a relatively high stress in all load cases, and the stress gradient on the surface needs to be as low as possible. Measurement locations also have to be geometrically suitable for placing strain gauges. On the basis of a preliminary analysis we found that the best locations for stress measurement were locations SG1 and SG2 (see Fig. 3). On these locations stresses are relatively high in all the load cases. They are also geometrically suitable for placing strain gauges: one is on the hand-brake handle and the other on its holder.



Sl. 4. Sistemska slika preizkuševališča
Fig. 4. Experimental system scheme

Celotno merilno verigo, uporabljeno pri eksperimentalnem delu, prikazuje slika 4. Poleg mehanskih napetosti so bile merjene tudi naslednje veličine: sila obremenjevanja ročne zavore, pomik točke vnosa obremenitev, sila v pletenicah in pomik vpetišča pletenic.

Napetosti na predhodno izbranih mestih so bile določene na podlagi deformacij, ki so bile merjene z merilnimi lističi s tremi mrežami HBM-RY91. Enako načelo je bilo uporabljeno tudi za merjenje sile v pletenicah, le da so bili pri tem uporabljeni merilni lističi z dvema mrežama HBM-XY11. Za merjenje sile obremenjevanja ročne zavore je bila uporabljena tlačno/natezna sonda proizvajalca HBM z znanimi karakteristikami. Merjenje pomika točke vnosa sile je bilo izvedeno z vrtljivo merilno letvijo (PMS-RML), ki deluje na načelu prirastkovnega dajalnika sunkov. Pomik vpetišča pletenic je bil merjen z linearnim variabilnim diferencialnim transformatorjem (LVDT). Karakteristike obeh zaznaval za merjenje pomikov so bile podane od izdelovalca. Za celoten merilni sistem je bila izdelana tudi analiza merilne negotovosti [11].

Obremenitveni primeri so bili prilagojeni za preračun z metodo končnih elementov. Za osnovo je rabil prevod tehničnih določil naročnika. V tem dokumentu bo obravnavan le najznačilnejši obremenitveni primer, tj. obremenitev ročice navzgor (sl. 5). Poleg tega sta bila obravnavana še obremenitvena primera z bočno obremenitvijo, in sicer prvi v sproščenem in drugi v napetem stanju.

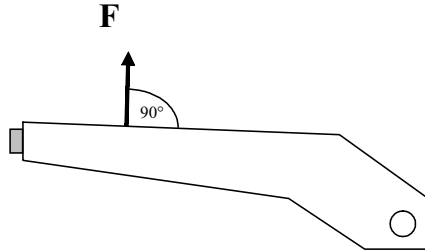
Slika 6 prikazuje z metodo končnih elementov dobljeno porazdelitev napetosti na mestih, kjer sta pri meritvi nameščena merilna lističa, pri obremenitvi 248 N. Na podlagi takšnih slik pri različnih obremenitvah dobimo sliko spremenjanja povprečne napetosti na merilnem mestu v odvisnosti od obremenitve. Primerjavo tako dobljenih rezultatov analize z MKE in

The complete measurement chain in the experiment is shown in Figure 4. Besides mechanical stresses the following quantities were also measured: handbrake loading force, displacement of the load-applying point, force in the wire and displacement of the wire-fastening point.

Stresses on the preliminarily chosen locations were defined on the basis of deformations that were measured by 3-grid strain gauges HBM-RY91. The same method was used for measuring the force in the wire, but 2-grid strain gauges HBM-XY11 were applied. To measure the handbrake loading force we used an HBM load cell RSCA 1t with known characteristics. The displacement of the load-applying point was measured by means of a linear incremental encoder (PMS-RML), which functions on the incremental rotary encoder principle, and the displacement of the wire-fastening point was measured by means of a linear variable differential transformer (LVDT). The characteristics of both sensors used were defined by the producers. For the entire measurement system an analysis of the measurement uncertainty was also performed [11].

All load cases were adapted for the finite-element method calculation, and based on the customer's technical specifications. This paper deals only with the most typical load case, that is, when the handle is loaded upwards (see Fig. 5). In addition to this, however, we also studied two load cases with the load directed sideways, one with the handbrake in loose state and the other in pretense state.

Figure 6 describes the stress distribution on the strain-gauge locations at maximum load 248 N as obtained with the finite-element analysis. On the basis of such figures at different loads, we can get a chart representing the dependence of the average stresses at measuring locations on the applied load. Figure 7 shows the comparison of the results obtained with the finite-element analysis with the results obtained from meas-



Sl. 5. Vnos obremenitve
Fig. 5. Load application

eksperimentalne analize prikazuje slika 7. Na ta način pridemo do spoznanja o velikosti odstopanja rezultatov simulacij od rezultatov meritev. Ker se rezultati simulacij nikdar ne ujemajo popolnoma z rezultati meritev, takšne primerjave ponovimo večkrat na podobnih konstrukcijah. Ob večkratnem ponavljanju meritev na podobnih konstrukcijah najdemo povezavo med rezultati simulacij in rezultati meritev. Takšni izsledki so že pomemben del baze znanja, ki bo pri prihodnjih konstrukcijah namenjena za to, da bomo lahko s simulacijo kar se da natančno ugotovili napetostno deformacijsko stanje ročne zavore.

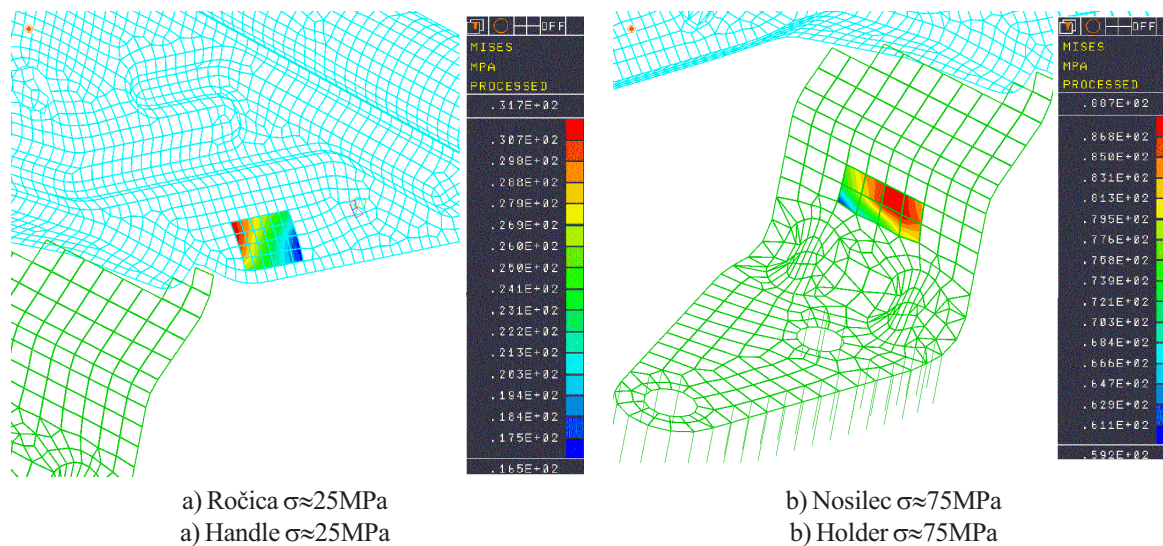
Krivilji na sliki 8 prikazujeta drugo vrsto rezultatov, ki prav tako sodijo v bazo znanja. Omenjeni potek predstavlja odvisnost sile v vpetišču pletenic od pomika le-tega, torej predstavlja togost celotnega zavornega sistema. V obravnavanem primeru se je izkazalo, da je izmerjena karakteristika bilinearna. To je sicer bolj ali manj splošno znano dejstvo, pa vendar značilen primer ugotovitev meritev, ki skupaj z numeričnima vrednostma obeh togosti sodi v bazo znanja. Značilna ugotovitev, ki sledi iz takšnega spoznanja je, da za natančno analizo podobnih konstrukcij z MKE uporaba linearnih reševanj zaradi nelinearnosti robnih pogojev ni zadostna. Za nadaljnje numerične simulacije podobnih konstrukcij je torej pomembno, da poprej pridobimo ali izmerimo podatek o togosti zavornega sistema ter nato izdelamo nelinearno analizo z MKE. Vsa zgoraj našteta spoznanja pa nenazadnje pripomorejo k znatnemu skrajšanju časa, potrebnega za izvedbo podobnih simulacij ob hkratnem izboljšanju zanesljivosti rezultatov.

Matematični model ročne zavore je bil v konkretnem primeru zgrajen z uporabo končnih elementov, izračunane vrednosti so nato primerjane z izmerjenimi vrednostmi. Po pričakovanju se je izkazalo, da se med dobljenimi rezultati pojavi določeno razhajanje, kar je v veliki meri posledica poenostavitev in predpostavk, uporabljenih pri analizi z MKE, ki dejanski model idealizirajo, npr. zveza med napetostjo in deformacijo je v celotnem območju obremenjevanja linearna (Hookeov zakon), vrednost elastičnega modula E je stalna, material je izotropen, debelina pločevine je po končnem elementu nespremenljiva.

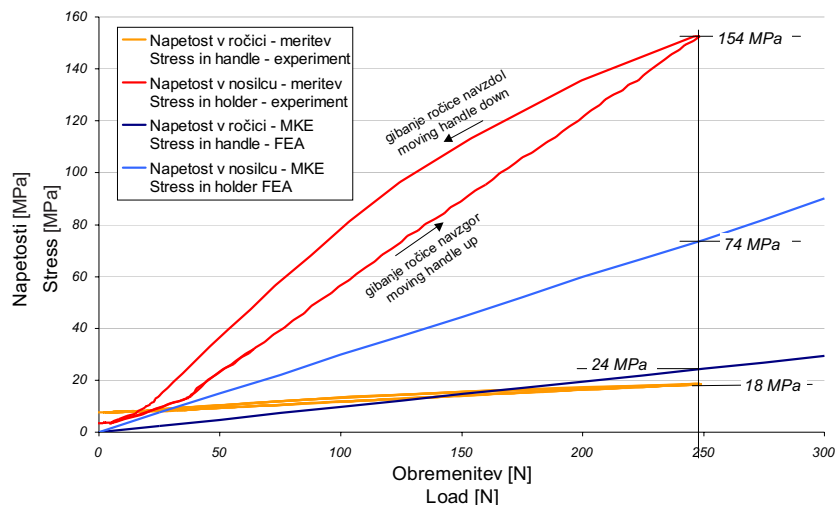
urements. From this we can find the difference between the simulation results and the measurement results. Since the simulation results always vary from the measurement results, the comparison between the simulation and the measurement should be repeated and statistically treated on similar structures. With this method, the general rules of dependency between the measured and the simulated results that apply well to other similar structures can be acquired. Such general rules are an important part of a reference database, which would help us with an accurate stress-state estimation with simulations on similar structures in the future.

The diagram in Figure 8 shows other kinds of results, which can also play a significant role in building a quality reference database. This diagram represents the measured results of the dependency of the force in the wire on the displacement of the wire-fastening point, which represents the stiffness of the whole breaking system. In the discussed case, we can see that the stiffness has a bilinear characteristic. Although this is more or less a commonly known fact, it is still a characteristic example of a measurement result, which, together with both values of stiffness, belongs to a reference database. A characteristic finding, which follows from such a result, is that because of the nonlinearities (bilinear) included in restraints of this and similar structures, a simple, linear finite-element analysis for estimating stress states of this type of structure cannot be used. For further finite-elements analyses it is very important to measure or somehow provide a breaking system's stiffness characteristics and to use appropriate non-linear finite-element solvers. Finally, all the findings mentioned above contribute to a considerable shortening of the time needed for a realization of a finite-element analysis of similar structures and a simultaneous improvement of the results' reliability.

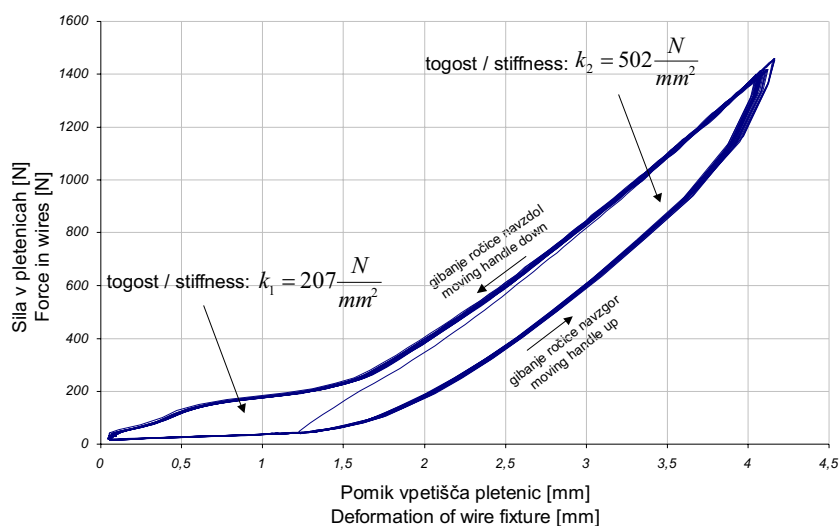
The mathematical handbrake model in this case was constructed with the help of finite elements. The calculated values are compared to the measured values. As we anticipated, it turned out that there was a considerable difference between the results obtained with each method, particularly with respect to the stresses. The finite-element analysis is based on a set of simplifications and suppositions that idealize the real model, e.g., the relationship between stress and strain is linear everywhere (Hooke's law), the value of Young's modulus (E) is constant, the material is isotropic, the thickness of the sheet is constant according to the finite element, etc.



Sl. 6. Napetosti, dobljene z MKE na mestih merilnih lističev pri največji obremenitvi
Fig. 6. Stress distribution at strain-gauge locations during maximum load, obtained by FEA



Sl. 7. Napetosti kot funkcije obremenitve
Fig. 7. Stresses in the handbrake



Sl. 8. Togost zavornega sistema
Fig. 8. Stiffness of the whole braking system

Pri izdelavi matematičnega modela se pojavlja tudi vprašanje modeliranja zračnosti in naleganja posameznih sestavnih delov. V primeru, da je naleganje dveh elementov v matematičnem modelu napačno, dobimo močno spremenjen fizikalni sistem, ki obravnavani dejanski sistem opiše napačno. Za izboljšanje zanesljivosti rezultatov simulacij in nenazadnje tudi baze znanja, bi bilo treba natančno raziskati tudi vpliv zgoraj navedenih parametrov na rezultate numeričnih simulacij in predvsem na njihovo odstopanje od rezultatov meritev.

2.2 Zavorna stopalka

Drugi zgled ustvarjanja baze podatkov in izpopolnjevanja postopka konstruiranja je predstavljen na primeru zavorne stopalke [14]. Na sedanji konstrukciji je bilo treba odpraviti problem prevelike bočne deformacije, ki se je pojavila v primeru testiranja ene od konstrukcijskih zahtev. Problem se je pokazal v primeru simulacije izstopanja voznika iz vozila, pri čemer si pomaga z odrivanjem desne noge od stopalke zavore. Za izboljšanje togosti konstrukcije je bilo treba to spremeniti, vendar s poudarkom na najmanjših stroških, ki bi spremljali to spremembo. Poglavitni namen je bil poiskati najšibkejši del konstrukcije in ga ustrezno izboljšati, tako da bi konstrukcija ustrezala predpisani zahtevi, tj. dovoljena bočna deformacija sredine stopalke zavore, kar je prikazano na sliki 9.

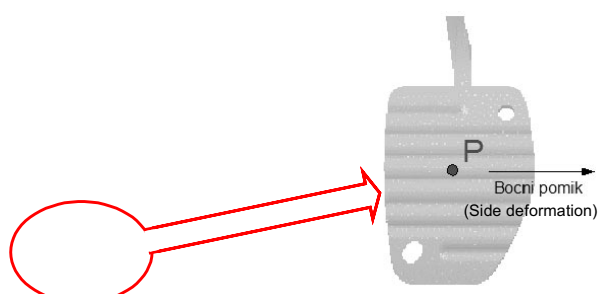
Za sedanjo konstrukcijo je bila najprej izdelana linearna napetostno-deformacijska analiza z MKE. Dobrijeni rezultati vedno pomenijo določeno odstopanje od dejanskega stanja, zato je nujno potrebno določiti velikostni razred odstopanja. Tega določimo z ustrezno izvedenim preizkusom oziroma meritvijo, ustreznost rezultatov meritev pa je mogoča le z natančno izdelanim merilnim sistemom. Do razlik pride zaradi poenostavitev pri analitičnem delu in meritve negotovosti pri eksperimentalnem delu. Ob poznavanju obeh pa lahko določimo usmeritev oz. neko bazo znanja, ki omogoči cenejše in hitrejše

When making the mathematical model, we face two problems: how to model looseness and how to model contacts between component parts. If the contact between two elements in the mathematical model is not correct, we get a totally different physical system, which describes the discussed real model incorrectly. To improve the reliability of the simulation results and the reliability of the reference database, we should make an exact investigation of the influence of the mentioned parameters on the results of the numerical simulations and on their deviation from the measurement results.

2.2 Brake Pedal

The second example of database acquisition and the imperfection of the design procedure is shown for the case of a pedal assembly [14]. The existing design needed to be improved because its lateral deformation, when testing one of the structural demands, was too large. This boundary condition simulates a driver leaving the vehicle, while using the brake pedal as a support for his/her right leg. The design had to be modified to improve the stiffness, but with minimum costs. The weakest part of the structure was identified and improved so that the new structure will fulfil all the structural demands, in particular the allowed size of the lateral deformation (the centre of stepping area of a brake pedal - point P), shown in Fig.9.

A linear stress-strain analysis was made for the existing structure with a finite-element method (FEM). The results always deviate from reality, so the magnitude of the deviation had to be established. This was done with an appropriately performed experiment together with an exact measurement system. The differences are a result of simplifications in the analytical work and the measurement uncertainty of the experiment. When both of them are known, a database can be created, and this can be helpful when cheaper and faster modifications to similar structures have to be produced. The results of the strength analysis can be



Sl. 9. Predmet testiranja
Fig. 9. Testing object

spreminjanje sorodnih konstrukcij s podobnimi poenostavivami. Pri načrtovanju merilnega sistema torej bistveno pomagajo rezultati analitičnega dela, tj. trdnostnih analiz, s katerimi določimo npr. velikost merilnih območij in ustrezno izberemo merilno opremo.

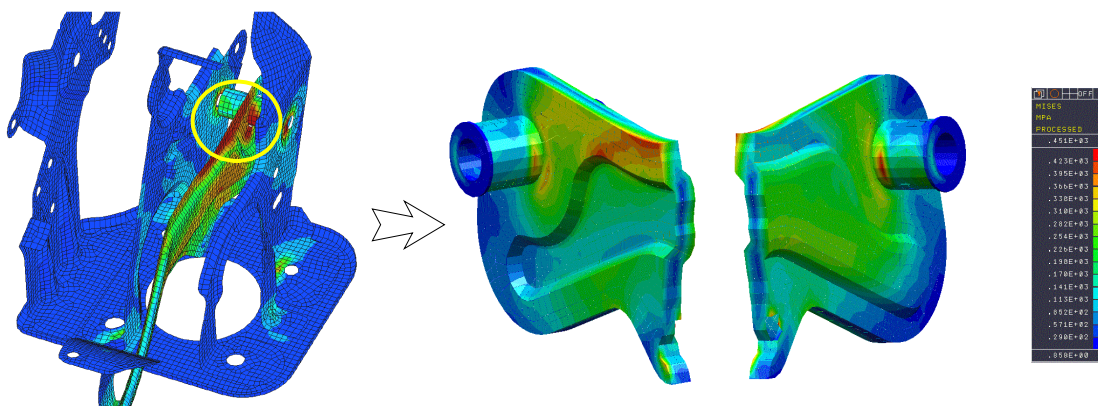
Trdnostna analiza je potekala v dveh delih. Prvi del analize je potekal na celotnem sestavu zavore in rezultat je pokazal, da se večinoma deformira stopalko zavore, nosilo pa precej manj. Posebej veliko področje velike napetosti v materialu naj bi bilo na zgornjem delu stopalke zavore in okoli spoja med stopalko in jekleno cevjo (=vrtišče). Omenjeni spoj na sedanji konstrukciji je bil izveden kot krčni nased in rezultat prvega dela trdnostne analize je nakazoval, da ta spoj lahko bistveno prispeva k velikosti bočne deformacije. S preoblikovanjem tega spoja bi torej lahko zmanjšali nastali problem. Drugi del trdnostne analize je bil narejen na bolj natančnem modelu stopalke zavore, s tem, da so bile upoštevane tudi plastične puše, ki so montirane v vrtišču stopalke. Ker stanja v krčnem nasedu med stopalko in cevjo ne moremo zadovoljivo modelirati, je bila uporabljena srednja možnost med krčnim nasedom in varjenjem pedala in cevi. Torej smo že uporabili zamisel, kako bi preoblikovali sedanjo stopalko zavore. Tudi natančnejša analiza je potrdila velike napetosti v okolini spoja cevi in stopalke (sl. 10).

Glede na dobljene rezultate drugega dela trdnostne analize smo povzeli, da ta del konstrukcije bistveno prispeva k velikosti bočnih deformacij, predvsem zaostalih bočnih deformacij v primeru preobremenitev. To predpostavko je bilo treba potrditi ali ovreči z izvedbo meritve na stopalki zavore. Dobljeni rezultati so pomagali pri nadaljnji izbiri merilne opreme in načrtovanju merilnega mesta. Zaradi prej omenjenega dogovora pri modeliranju stopalke zavore smo načrtovali izvajanje meritve na sedanji in spremenjeni izvedbi stopalke zavore. Pri varjeni izvedbi smo pričakovali boljše ujemanje rezultatov.

very helpful when planning the measurement system because it is easier to define a measurement range and choose the appropriate equipment.

The strength analysis was made in two steps. First, the whole structure was analyzed. The results showed that the most deformable part of the structure is the brake pedal and not the support. The areas with stresses higher than the yield stress are on the top of the brake pedal and around the joint of the pedal and the steel tube (= revolution point). The joint on the existing structure was made with a compressive forming technology, and because the results of the stress analysis imply that this joint could have a large influence on the magnitude of lateral deformations and its modifications could result in resolving the problem. The second step of the strength analysis was done on a more exact model of the brake pedal, where the plastic sliding elements in the revolution joint were also considered. Because the stress-strain state in the compression joint cannot be modelled satisfactorily, a compromise between the compression-forged joint and welded joint of the pedal and tube was used. Basically, the idea of how to modify the existing brake pedal had been already used. The results of the second step of the strength analysis confirmed that areas of high stress appear around the joint of the pedal and tube (see Fig.10).

According to the results of the second part of the strength analysis we concluded that this structural part contributes significantly to the size of the lateral deformations, mostly to the residual deformations in the case of overloading. This assumption should be confirmed or refuted with an experiment. The results of the strength analysis were helpful when we planned the measurement system and choose equipment for it. Because the model used for the FEA was a compromise between a compressed and a welded joint, measurements were planned for both the existing and the modified brake pedal. The results for the welded brake pedal were expected to be closer to the results of the FEA.



Sl. 10. Rezultati napetostno deformacijske analize – primerjalna napetost
Fig. 10. Results of stress-strain analysis – comparative stress

Predpisani pogoji preizkušanja zahtevajo, da je merilni sistem sestavljen tako, da je mogoče nadzorovati dejanske vhodne signale glede na zahtevane vhodne signale (dejanska sila F_D proti zahtevani obremenitvi F_R). Med testiranjem je treba zbirati podatke v točki P (pomik).

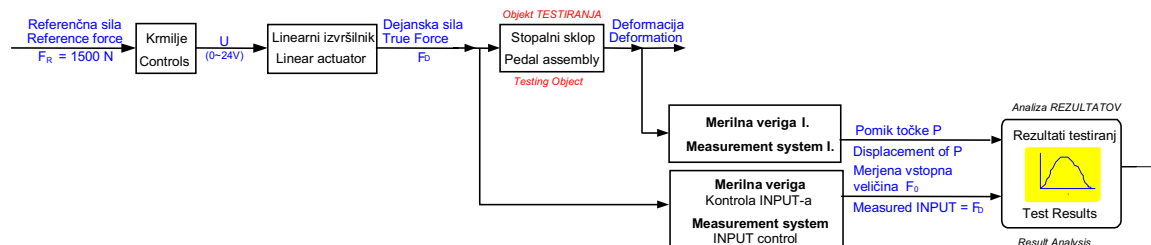
Na izbiro elementov merilnega sistema so bistveno vplivali rezultati trdnostne analize, saj smo tako lahko določili zahtevano merilno območje opreme in zaznaval ter preverili merilno negotovost obeh merilnih verig, ki naj bi bila nižja od 0,5%. Negotovost je bila določena za vsako merilno verigo posebej, in sicer z metodo najmanjših kvadratov. Zaradi statične obremenitve konstrukcije so bile za nas pomembne statične karakteristike merilne opreme. Na slikah 12 in 13 je v shemah prikazana izbira merilne opreme.

Meritve bočnih deformacij smo izvedli na treh nakrčenih stopalkah in treh varjenih stopalkah. Dobljeni rezultati meritev so potrdili naše domneve, ki so izhajale iz rezultatov trdnostnih analiz z MKE. Slike 14 je razvidno, da so razlike med analitičnimi in eksperimentalnimi rezultati, pri obremenitvi 1000 N, manjše kakor pri obremenitvi 1500 N, kar je posledica omejitve linearne trdnostne analize, saj ta ne upošteva plastifikacije materiala. Dobljeni rezultati potrjujejo domneve, da so rezultati pri varjeni izvedbi bližje rezultatom analize z MKE. Ugotovimo lahko, da nakrčena izvedba stopalke zavore omogoča večje bočne pomike pri preobremenitvi s silo 1500 N kakor varjena izvedba. Prav tako pa se pojavijo večje trajne deformacije

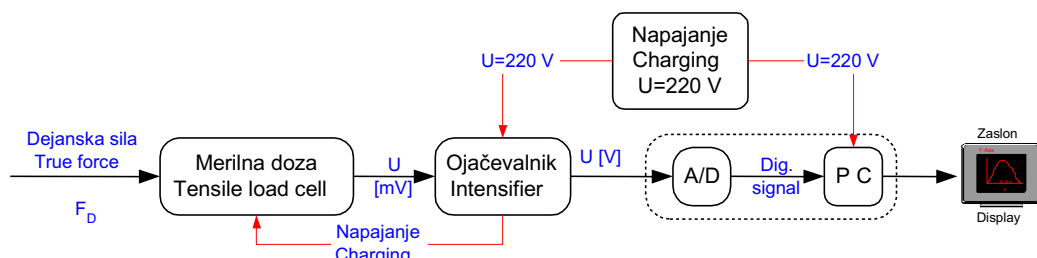
The prescribed testing conditions state that the measurement system should be able to control the true input signal given by the reference input signal (F_D vs. F_R). During the testing procedure a data acquisition of the displacements of the point P should be performed automatically.

The selection of the elements for the measurement system (the measurement range of the sensors and other equipment) was influenced by the results of the strength analysis. The measurement uncertainty for both measurement systems was checked. It needed to be lower than 0.5%. The measurement uncertainty was calculated with a mean-square method. The implied load was static, and that is the reason why we were only interested in the static characteristics of the measurement equipment. Figures 12 and 13 show the equipment that was chosen for both measurement systems.

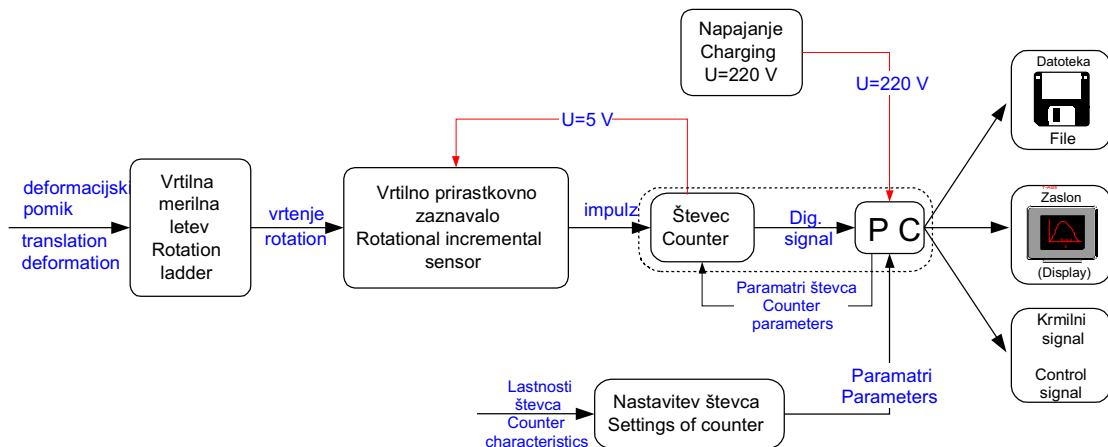
A measurement of the deformation was carried out on three brake pedals with a compression-formed joint and on three pedals with a welded joint. The results of the experiment confirmed our assumptions based on the FEA results. Figure 14 shows that the differences between the analytical and the experimental results at the lower load (1000N) are smaller than at the higher load (1500N). The reason for this is that the linear strength analysis does not consider different material properties after the yield-stress limit is reached. The results of the experiment for the welded pedal also confirmed our assumption that the FEA results should be closer to the experimental results. We concluded that the compressed joint allows a larger lateral deformation when an overload of 1500N is applied. After the load is



Sl. 11. Shema merilnega sistema
Fig. 11. The measurement system scheme



Sl. 12. Merilna shema - merilna veriga nadzora vstopnega signala
Fig. 12. Measurement scheme - measurement system: control of input



Sl. 13. Merilna shema - veriga I
Fig. 13. Measurement scheme - system I

po razbremenitvi stopalke. To je potrdilo rezultate trdnostne analize, da je pedal eden kritičnih delov, ki jih moramo spremeniti, da bi izpolnili zahtevane pogoje. Stopalka zavore prispeva precejšen delež k velikosti zaostalih deformacij tudi takrat, ko je montiran v sestavu stopalke.

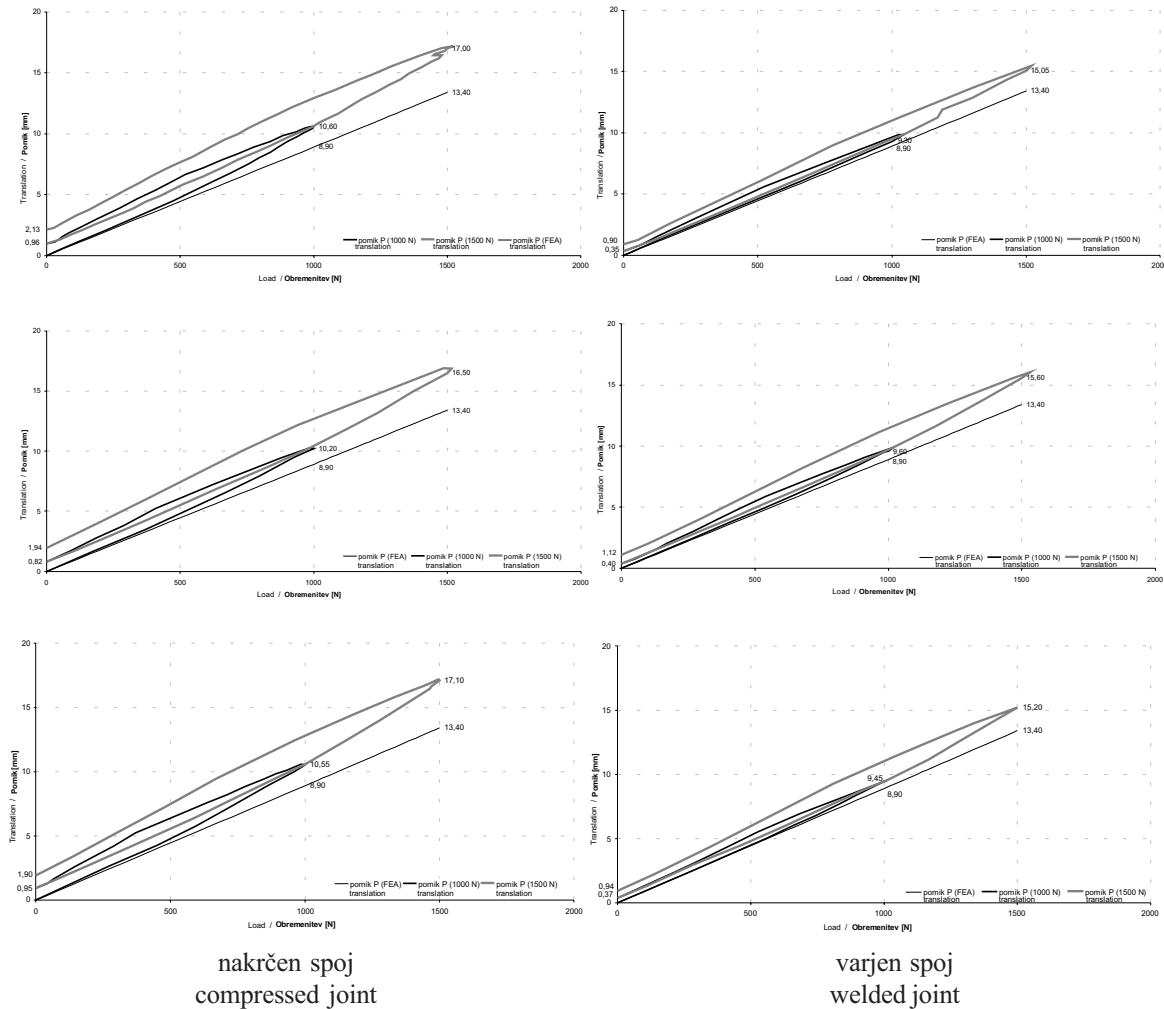
Nakrčen spoj očitno omogoča lokalne deformacije oziroma popustitev pri preobremenitvi. Varjena izvedba se zato izkaže za ugodno spremembo pri postopku izdelave, kljub temu, da to prispeva nekaj dodatnih stroškov. Ta izvedba pomeni zmanjšanje elastične in trajne bočne deformacije pedala. Slednja se zmanjša za približno 1 mm.

Izkazalo se je, da je način s katerim smo se lotili reševanja problema pravilen in da se s tem precej skrajša celoten postopek popravljanja sedanje konstrukcije. Z izdelavo analize sedanje konstrukcije smo dovolj dobro ocenili kritična mesta in sestavne dele, ki pojasnjujejo problem, tj. prevelika trajna bočna deformacija sredine stopalke zavore. Na vsak način je treba poznati omejitve programa, s katerim je bilo opravljeno analitično delo, in seveda vse poenostavitev, ki smo jih privzeli pri izdelavi modela, ki naj bi pomenili približek k dejanskemu stanju. Rezultate trdnostnih analiz smo uporabili le kot smernice k načrtovanju merilnega mesta za testiranje, saj zaradi poenostavitev modela ne morejo biti izraz dejanskega stanja. Dejansko stanje smo določili z eksperimentalnim delom. Dobljene smernice so pomenile predvsem določitev kritičnega elementa konstrukcije (stopalka zavore) in pričakovano merilno območje (0 do 20 mm), ki ga bodo morala pokrivati zaznavala. Po teh podatkih je potekalo načrtovanje merilnega mesta in določitev merilne negotovosti za posamezno merilno verigo. Pokazala se je pomembnost te faze načrtovanja merilnega mesta, saj se je izkazalo, da izbrana oprema omogoča zahtevano natančnost meritev (0,5%). Rezultati testiranj so potrdili kritičnost sestavnega dela, ki smo ga določili s trdnostno analizo. Ker so razlike med analitičnimi in eksperimentalnimi rezultati razmeroma velike, se je z opisanim postopkom ustvarila pomembna primerjalna baza podatkov za vrednotenje rezultatov podobnih analiz z MKE.

removed, the remaining permanent deformation is also bigger. That is why we are convinced that the pedal is one of critical parts in the structure that had to be changed to satisfy structural demands. The brake pedal contributes a significant share to the total deformation of a structure when it is mounted.

A compression-formed joint obviously allows local deformations to appear when an overload is applied. We saw that this joint suddenly relaxes. Although the welded joint is more expensive it does have benefits. This modification results in a reduction of the elastic and residual plastic deformation of the brake pedal by approximately 1mm.

We showed that the method used for resolving the problem was correct. The process of design modification was shortened. Based on the results of the FEA we are able to correctly define the weakest part of a structure, which is the reason for the inadequate stiffness of the overall structure. However, we have to keep in mind the limitations of the FEA software and all the simplifications used to create the finite-element model. The results of the FEA were only used as guideline for system measurement planning and they are not a true representation of reality. The real stress-strain state of the structure was defined by the experiment. Guidelines were used to define the weakest part of structure (the brake pedal) and to define the measurement range (0-20mm) of the sensors. Based on those data we planned the measurement systems and later defined the measurement uncertainty. Our work showed the importance of this phase, because it proved that the measurements were accurate (0.5% deviation). The test results proved that using FEA the defined critical part is the actual one. Because the differences between the analytical and the experimental results were still relatively large, the described method helped us to supplement the comparative database for similar structures and similar analyses.



Sl. 14. Primerjava rezultatov meritev in trdnostne analize nakrčene in varjene izvedbe spoja na stopalki zavore

Fig. 14. Comparisons of the experimental results and the results of the FEA on compressed and welded joints

3 SKLEP

Glavni cilj raziskave je vpeljava trdnostnih analiz z metodo končnih elementov v zgodnje faze konstrukcijskega postopka. Rezultati tovrstnih analiz brez ustreznih razlage žal nimajo prave vrednosti. V prispevku je zato predlagana in na stvarnih primerih prikazana metoda za pridobitev primerjalne baze podatkov, na podlagi katere poteka vrednotenje rezultatov numeričnih izračunov. Glavna značilnost omenjene metode je ugotoviti ujemanje rezultatov preračuna z metodo končnih elementov in rezultatov eksperimentalne analize, s čimer se dokaže pravilnost v numeričnem modelu narejenih predpostavk in poenostavitev. Prednost numeričnih analiz, kakor je npr. analiza z metodo končnih elementov, je velika stopnja prilagodljivosti, saj tovrstne analize omogočajo izračun napetostno-deformacijskih in drugih stanj izdelka pri različnih vrednostih konstrukcijskih parametrov brez izdelave fizičnih prototipov, če so na voljo le ustreznii trirazsežni računalniški modeli.

3 CONCLUSION

The objective of the study was to introduce structural analyses based on the finite-element method in the early phases of the design process. Unfortunately, the results of such analyses without a proper interpretation are of almost no use. Therefore, in this article we suggest a method for acquiring the reference database, which serves for the validation of the FEA results. The main characteristic of this method is to find out the consistency of the results computed on the basis of the FEM model with the experimental analyses, which proves the correctness of the assumptions concerning the static scheme of the mechanical structure. The advantages of the FEM lie in its great flexibility, which means that many design parameters can be changed to predict how they can influence the mechanical behaviour of the product without prototyping new models, once the 3D CAD files are available.

Če povzamemo, numerične in eksperimentalne analize imajo pomembno vlogo pri konstruiranju zanesljivih izdelkov. Prve so uporabne za vrednotenje rešitev v zgodnjih fazah konstrukcijskega postopka, ko se ukvarjamo z izbiro materialnih lastnosti, izmer posameznih komponent, strukturo, obliko dotikalnih površin itn. Eksperimentalne analize se v tem primeru uporabljajo le za potrditev ustreznosti končnega fizičnega prototipa, pri katerem se izvaja testiranje oblike, materiala in tehnološkega postopka.

In conclusion, both computational and experimental methods play an important role in designing reliable products. The former is useful in the evaluation of the initial designing phase, where some parameters dealing with material properties, dimensions of components, structures and the shapes of contacting surfaces have to be chosen. The latter finds its proper application in the validation phase where a final prototype, which includes shape, material and technological process, has to be tested.

4 LITERATURA 4 REFERENCES

- [1] Duhovnik, J., J. Tavčar (2000) Elektronsko poslovanje in tehnični informacijski sistemi: PDMS-product data and management systems. *Fakulteta za strojništvo*, Ljubljana.
- [2] Pahl, G., W. Beitz (1993) Konstruktionslehre. *Springer Verlag*, Heidelberg, New York.
- [3] Golob B., A. Ježernik (2003) Predlog funkcijskih značilnosti faze zasnove v konstrukcijskem postopku. *Strojniški vestnik*, 49(2003)5, 275-286.
- [4] Hsu, W., I.M.Y. Won (1998) Current research in the conceptual design of mechanical products. *Computer-Aided Design*, Vol. 30, No. 5, 377-389.
- [5] Brunetti, G., B. Golob (2000) A feature-based approach towards an integrated product model including conceptual design information, *Computer-Aided Design*, 32, 877-887.
- [6] SAE (1995) RMS - Reliability, maintainability and supportability guidebook, 3rd edition. *Society of Automotive Engineers*.
- [7] Holman, J.P. (1984) Experimental methods for engineers, 4th edition. *McGraw-Hill international*, Singapore.
- [8] Pallas-Areny, R., J.G. Webster (2001) Sensors and signal conditioning. *John Wiley & Sons*, New York.
- [9] Peace, G.S. (1993) Taguchi methods: a hands-on approach. *Addison-Wesley*.
- [10] Phadke, M.S. (1989) Quality engineering using robust design. *Prentice-Hall international*, London.
- [11] Janežič, M., T. Bučar (2003) Seminarska naloga pri predmetu Eksperimentalne metode v raziskovalnem delu. *Fakulteta za strojništvo*, Ljubljana.
- [12] Bučar, T., M. Janežič, M. Fajdiga (2003) Eksperimentalna analiza napetostno deformacijskega stanja ročne zavore. 6th Conference and Exhibition Innovative Automotive Technology IAT'03, Portorož.
- [13] Janežič, M., T. Bučar, M. Fajdiga (2003) Primerjava numerične in eksperimentalne analize napetostno deformacijskega stanja ročne zavore. 6th Conference and Exhibition Innovative Automotive Technology IAT'03, Portorož.
- [14] Pangeršič, P., M. Fajdiga (2003) Eksperimentalno preverjanje numeričnih analiz mehanskih sklopov. 6th Conference and Exhibition Innovative Automotive Technology IAT'03, Portorož.

Naslov avtorjev: Tomaž Bučar

Miha Janežič
 Primož Pangeršič
 prof.dr. Matija Fajdiga
 Univerza v Ljubljani
 Fakulteta za strojništvo
 Aškerčeva 6
 1000 Ljubljana
 tomaz.bucar@fs.uni-lj.si
 miha.janezic@fs.uni-lj.si
 primoz.pangersic@fs.uni-lj.si
 matija.fajdiga@fs.uni-lj.si

Authors' Address: Tomaž Bučar

Miha Janežič
 Primož Pangeršič
 Prof.Dr. Matija Fajdiga
 University of Ljubljana
 Faculty of Mechanical Eng.
 Aškerčeva 6
 SI-1000, Ljubljana, Slovenia
 tomaz.bucar@fs.uni-lj.si
 miha.janezic@fs.uni-lj.si
 primoz.pangersic@fs.uni-lj.si
 matija.fajdiga@fs.uni-lj.si

Prejeto:
 Received: 11.11.2003

Sprejeto:
 Accepted: 8.4.2004

Odprto za diskusijo: 1 leto
 Open for discussion: 1 year

Trenutne smeri razvoja pri spajanju materialov v avtomobilski industriji

Current Development Trends For Material Joining In The Automotive Industry

Janez Tušek - Damjan Klobčar

Prispevek opisuje trenutno stanje spajanja materialov v svetovni avtomobilski industriji. Teoretično so opisani in s praktičnimi primeri prikazani postopki spajanja materialov, ki se uporabljajo v največjih avtomobilskih tovarnah v svetu. Prikazano je uporovno varjenje, obločno varjenje, spajkanje, hibridno varjenje, varjenje čepov, lepljenje in mehansko spajanje. Na koncu je podan sklep, ki pove, da gre razvoj na tem področju v smeri uporabe laserja za varjenje in spajkanje, lepljenja in mehanskega spajanja s kovicami in brez njih.

© 2004 Strojniški vestnik. Vse pravice pridržane.

(Ključne besede: spajanje materialov, varjenje, spajkanje, lepljenje)

This paper describes the current state of the field of material joining in the world's automotive industry. The processes of material joining that are used in the biggest automotive factories are theoretically described and confirmed with practical examples. Resistance spot welding, arc welding, brazing, hybrid welding, stud welding, adhesive bonding and mechanical joining are described. We conclude that the future of material joining in the automotive industry is likely to be in the use of laser beams for welding and brazing, adhesive bonding and in mechanical joining with or without rivets.

© 2004 Journal of Mechanical Engineering. All rights reserved.

(Keywords: joining, welding, brazing, adhesive bonding)

0 UVOD

Razvoj v avtomobilski izdelavi je eden izmed najizrazitejših in najpomembnejših v celotni kovinski in elektroindustriji. To še posebej velja za industrijsko razvite države, kamor lahko štejemo tudi Slovenijo. Velika konkurenca na svetovnem trgu narekuje izdelovalcem avtomobilov uporabo novih materialov, sodobnih izdelovalnih tehnologij in sodobnih ter okolju prijaznih tehnik spajanja.

Še pred nedavnim so bile avtomobilske karoserije izdelane skoraj izključno iz malolegiranega jekla, varjene plamensko, obločno in elektrouporovno točkovno. Z uporabo novih materialov, kakor so jekla z veliko trdnostjo, prevlečene jeklene pločevine, aluminij in kompoziti pa so se potrebe po razvoju in uvajanju novih tehnologij spajanja močno povečale.

Na sliki 1 so shematsko predstavljene tehnike spajanja materialov, ki se dandanes najpogosteje uporabljajo v avtomobilski izdelavi. Razdelimo jih lahko v pet večjih skupin, to so; varilni postopki, spajkanje, hibridno varjenje, lepljenje in mehansko spajanje ([1] in [2]).

0 INTRODUCTION

Developments in the automotive industry are some of the most intensive and important in the metal and electrical industries. This is especially true for the group of highly developed industrial countries, of which Slovenia is a member. Fierce competition ensures that the world's car producers use new materials, state-of-the-art production technologies and environmentally friendly joining techniques.

Not long ago, almost all car bodies were made of mild steel, and were flame welded, arc welded or resistance spot-welded. The use of new materials – different grades of high-strength steels, steel sheets with different kinds of surface coatings, aluminium and plastic composites – has increased the need to develop and introduce new joining technologies.

The joining techniques that are commonly used in the automotive industry are schematically shown in Fig. 1. They can be divided into five major groups, i.e. welding, brazing, hybrid welding, adhesive bonding and mechanical joining ([1] and [2]).

1 VARJENJE

Varjenje je še vedno tehnika spajanja, brez katere si sploh ne moremo zamisliti izdelave avtomobila. Razvoj varjenja je sledil novostim, podobno kakor razvoj na drugih področjih. Nastajali so posodobljeni, izboljšani in popolnoma novi postopki varjenja (spajanja) materialov, hkrati pa izginjali stari, neučinkoviti postopki. Že skoraj celo desetletje v avtomobilski industriji ne uporabljamo več plamenske tehnike. Počasi izginja klasično obločno varjenje. Za varjenje vedno več uporabljamo laser, več vrst hibridnih postopkov obločnega varjenja in obločne postopke za varjenje čepov ter še nekatere druge postopke varjenja; kaskršni so ultrazvočno varjenje, varjenje s trenjem, varjenje z elektronskim snopom, difuzijsko varjenje in drugo. Še vedno je med vsemi postopki varjenja, elektrouporovno točkovno varjenje daleč najpomembnejši in najpogosteje uporabljan postopek varjenja v avtomobilski izdelavi [5].

1.1 Uporovno varjenje

Pri uporovnem varjenju izrabljamo joulsko toploto, ki se razvije pri prevajanju varilnega toka skozi dve ali celo več pločevin, ki običajno sestavljajo prekrivni zvarni spoj. Ker je dotikalna upornost na stiku pločevin največja, se v tej točki pojavi največ toplote, ki raztali del materiala obeh varjencev za nastanek zvarne točke.

V sodobnih avtomobilih so že okoli 50 % celotne mase avtomobila jekla z veliko trdnostjo, ki pri uporovnem varjenju zahtevajo nekoliko spremenjen varilni postopek. Zahteva se večja pritisna sila na elektrodah, manjša jakost varilnega toka, daljši čas varjenja in pa daljši čas držanja sklenjenih elektrod po varjenju.

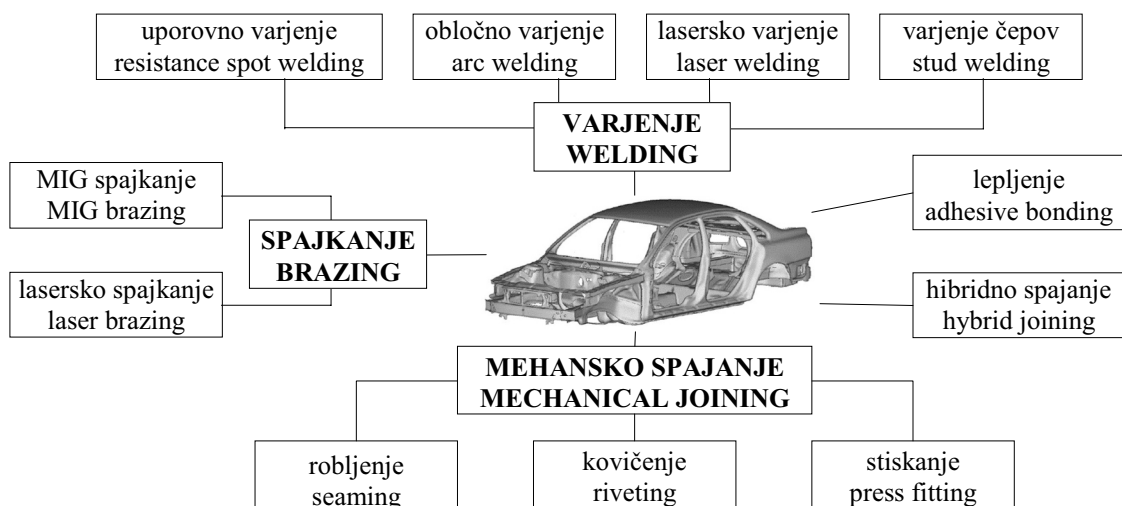
1 WELDING

Welding is still the most important joining technique for car production. The development of welding techniques has followed innovations and developments in other fields. Modernized, improved and completely new joining techniques have been developed, while old and unproductive techniques have disappeared. It has been ten years since flame welding was used in the automotive industry, and classical arc welding is slowly disappearing. These days, laser welding, various hybrid techniques of arc welding and stud welding are frequently used, as well as ultrasonic welding, friction welding, electron-beam welding, diffusive welding, etc. However, of all welding procedures, resistance spot welding is still the most important and the most widely used in automobile manufacturing [5].

1.1 Resistance spot welding

Resistance spot welding makes use of Joule heating, which is produced when a welding current is conducted through two or more steel sheets, which often form a lap joint. Because the resistance is the highest at the sheet contact, most of the heat is produced there. This heat then melts the material and the welding spot is formed.

A modern car body contains approximately 50 weight-% of HSS; this requires different welding parameters when it is resistance spot welded. An increased electrode force, a decreased welding current, an increased welding time and increased holding times for the electrodes are the required welding parameters.



Sl. 1. Tehnike spajanja materialov, ki jih uporabljamo v avtomobilski izdelavi

Fig. 1. Joining techniques used in automobile manufacturing

V praksi se vedno bolj uveljavlja borirano jeklo z veliko trdnostjo od 1200 do 1400 MPa, ki se uporablja za odbojnike, ojačitvene loke pri strehah in za pragove avtomobilskih karoserij.

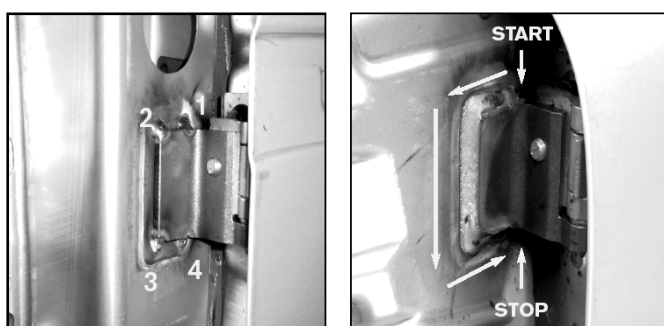
Pri velikem številu avtomobilov so odbojniki privijačeni na karoserijo avtomobila. Boljša rešitev je, če so odbojniki na karoserijo privrjeni, ker se s tem poveča stabilnost, predvsem torzijska togost [3].

Pri uporovnem točkovnem varjenju še vedno ostajata največja težava in največji strošek obraba elektrod; predvsem zaradi prevlečenih materialov. V avtomobilski izdelavi se uporabljajo predvsem pocinkana jeklena pločevina. Čisti cink ima tališče pri 419 °C in vrelišče pri 906 °C, kar pomeni, da cink zavre pri mnogo nižji temperaturi, kakor se jeklo ali baker raztalita. Cink med varjenjem prodira v bakreno elektrodo, dela novo zlitino, ki ima večjo upornost, kar spremeni pogoje varjenja. V novejšem času se uporabljajo sintrane elektrode, izdelane iz bakra in aluminijevega oksida. Vzdržljivost teh elektrod pri uporovnem varjenju pocinkanih materialov je precej boljša in doba trajanja daljša.

Drugi večji problem točkovnega uporovnega varjenja je v zagotavljanju kakovosti in preverjanju kakovosti zvarne točke. Veliko število raziskovalcev po svetu proučuje uporabo različnih metod preizkušanja kakovosti zvarnega spoja brez porušitve. Kljub temu, danes še ne poznamo metode, ki bi bila uporabna v velikoserijski proizvodnji za pregled vseh zvarnih točk na vseh avtomobilih [4].

1.2 Obločno varjenje

Pri izdelavi avtomobilskih karoserij se obločna tehnika varjenja praktično uporablja le še za privaritev tečajev za vrata na karoserijo in za izdelavo posameznih elementov podvozja avtomobilov. Pri tem moramo omeniti obločno varjenje MAG s ploščato elektrodo, ki je bilo razvito prav za izdelavo posameznih elementov za podvozja za različne vrste avtomobilov. S ploščato elektrodo širine od 3 do 5 mm in debeline od 0,5 do 0,8 mm lahko varimo v zaščiti plinske mešanice in dosegamo hitrosti do 2,0 m/min ([5] in [6]).



Sl. 2. Potelek klasičnega varjenja MAG z žico premera 1,2 mm za privaritev tečajev za vrata na karoserijo avtomobila [5]

Fig. 2. The course of MAG welding with a filler wire of 1.2-mm diameter for side-door-hinge welding on a car body [5]

In practical applications, boron-alloyed-type high-strength steel with a strength ranging from 1200 to 1400 MPa is being used more often. This steel is normally used for the car bumpers, the B-pillar roof bow and the B-pillar doorstep reinforcements of car bodies.

Generally, the bumper beam is screwed to the car body, but the body torsion stiffness is much better if a welded solution is applied [3].

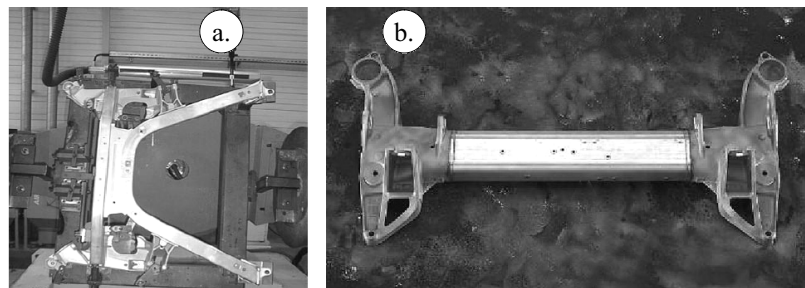
In general, the main problems and the high costs are associated with electrode wear, which is due to coated materials. Car bodies are often produced from zinc-coated steel sheets. Pure zinc melts at 419 °C and boils at 906 °C, which means that it boils at a much lower temperature than the steel and copper melt. During the welding, zinc penetrates the copper electrode, and produces a new alloy with a higher resistance, which changes the welding conditions. More recently, sintered electrodes of copper and aluminium oxide are used for the welding of zinc-coated sheets, due to improved endurance and a longer electrode life.

Other measures have to be taken regarding quality assurance in the running production. Besides destructive testing, the non-destructive testing of welds is frequently done. Generally, there is no test that can be widely used for the testing of all the welding spots on the car body in high series production [4].

1.2 Arc welding

In car-body manufacturing, arc welding is mainly used for precision mounting of the side doors, and for the sub-frames. Metal active gas (MAG) welding with a flat filler electrode was developed for the welding of car-body sub-frames. It enables welding speeds up to 2.0 m/min when welding with gas-shielding mixtures and flat electrodes of 3-to-5-mm thick ([5] and [6]).

VARILNI PARAMETRI WELDING PARAMETERS:
varilna žica/wire type G3S1 - SIST-EN-440
premer žice/wire diameter 1,0 mm
podajalna hitrost žice/wire feeding rate 4-5 m/min
plin/gas type 77Ar23CO ₂
pretok plina/gas flow ~15 l/min
napetost/voltage 18,25-19,25 V
hitrost varjenja/welding speed 0,42-0,48 m/min



Sl. 3. Utrijpno varjenje MIG aluminijastih komponent za sprednje podvozje avtomobila znamke BMW 7 (a) in za avtomobil znamke Citroen C5 (b) [2]

Fig. 3. Pulsed MIG welded aluminium components: a) front axle sub-frame, BMW 7-series and b) rear axle, Citroen C5 [2]

Na sliki 2 je prikazan potek klasičnega varjenja MAG z okroglo žico premera 1,2 mm za pritrdirditvi tečajev za vrata na karoserijo avtomobilov. Ta postopek še vedno uporabljo v različnih tovarnah za različne tipe avtomobilov (Renault - clio, Volvo - S40, Citroen - C5 itn.).

V večji meri se obločna tehnika varjenja uporablja pri izdelavi podvozij, obes in osi. Na sliki 3 je prikazano varjenje MIG z utriplnim varilnim tokom pri izdelavi komponent iz aluminija za avtomobil znamke BMW 7 (sl. 3a) in za avtomobil znamke Citroen C5 (sl. 3b).

1.3 Varjenje čepov

Varjenje čepov imenujemo postopek, s katerim pravokotno na površino privarimo element s poudarjeno eno izmero (vijaki, nosilni čepi, nosila za kable itn.). V avtomobilski izdelavi ta postopek uporabljamo za pritrdirtev nosil za kable, nosil za pritrdirtev izolacije in drugo.

Na sliki 4 je shematsko prikazan postopek za varjenje čepov, ki se uporablja v avtomobilski izdelavi [7].

1.4 Lasersko varjenje

V avtomobilski izdelavi se uporaba laserja močno povečuje. Uporabljamo ga za rezanje, varjenje, spajkanje in drugo (preoblikovanje, topotno obdelavo). Lasersko varjenje je močno povezano s tako imenovano

Fig. 2 shows the course of MAG welding, with a filler wire of 1.2 mm diameter, for the side-door-hinge welding on a car body. This is a generally used welding procedure for side-doors-hinge welding (Renault - Clio, Volvo - S40, Citroen - C5, etc.).

Generally, arc welding is used for the welding of sub-frames, axle sub-frames and axles. The Fig. 3 shows MIG pulsed welding of aluminium components for the BMW 7-series (Fig. 3a) and for the Citroen C5 (Fig. 3b).

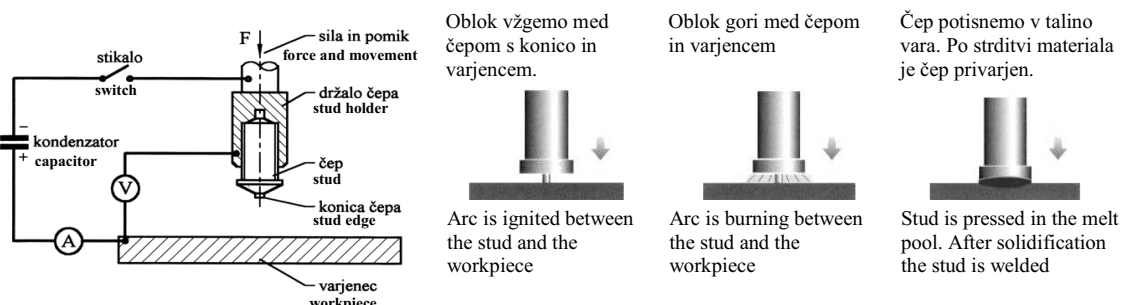
1.3 Stud welding

Stud welding is used for the perpendicular welding of components with one dimension expressed (screws, supporting studs, cable carriers, etc.). Generally, this procedure is used for the fastening of cable carriers, carriers for holding the isolation, etc.

Fig. 4 shows stud welding as used in the car-production industry [7].

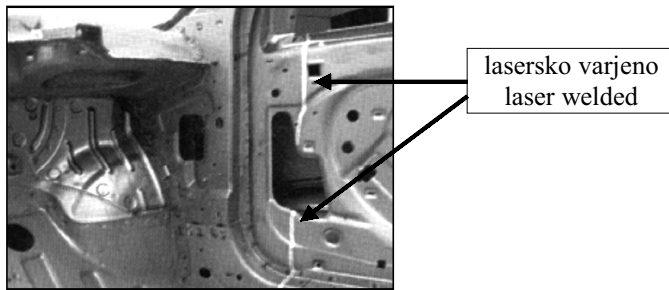
1.4 Laser welding

In general, the use of lasers in the automotive industry is on the increase. Lasers can be used for cutting, welding, brazing and other techniques (forming, heat treatment). Laser welding is closely

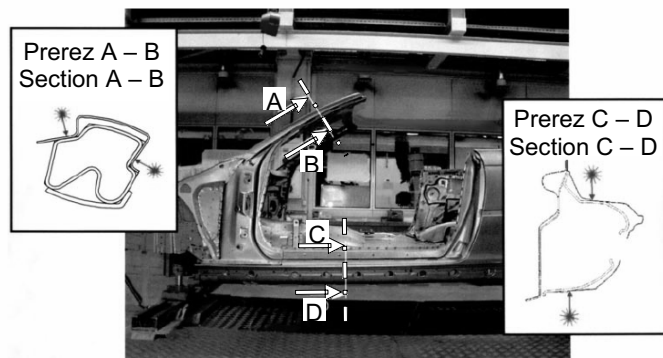


Sl. 4. Shematski prikaz varjenja čepov na karoserijo avtomobila [7]

Fig. 4. Stud welding on a car body [7]



Sl. 5. Lasersko varjeni krojeni deli za notranjo stran vrat za avto znamke Chrysler concorde [2]
Fig. 5. Chrysler concorde: laser-welded tailored blanks for the inner side-door structure [2]



Sl. 6. Uporaba laserskega varjenja pri izdelavi avtomobila znamke BMW 3 cabrio [10]
Fig. 6. Laser welding of the BMW 3-series cabrio [10]

proizvodnjo krojenih delov, kar pomeni, da z laserjem zvarimo polizdelke in nato te preoblikujemo v končne izdelke. Z uporabo te tehnike lahko prihranimo predvsem pri masi končnega izdelka, pri širini toplotno vplivnega področja in pri možnosti optimalne porazdelitve mehanskih napetosti v končnih izdelkih ([8] in [9]). Na sliki 5 je prikazana notranja stran stranskih vrat avtomobila znamke Chrysler concorde, ki je zvarjena po načelu krojenih delov. Tista dela notranje strani vrat, na katerih so tečaji vrat, in na drugi strani, kjer je ključavnica, sta izdelana iz debelejše pločevine kakor preostali deli. Med seboj pa so zvarjeni z laserjem in nato preoblikovani kakor prikazuje slika 5.

Veliko možnosti za uporabo laserskega varjenja sploh še ni izkorisčenih. Tu mislimo predvsem na zamenjavo uporavnega točkovnega varjenja z laserskim varjenjem in na številne možnosti pri konstrukcijskih rešitvah, ki naj bi bile prilagojene laserskemu varjenju.

Kot primer si oglejmo sliko 6, ki prikazuje dva dela nosilne konstrukcije avtomobila znamke BMW 3 cabrio, ki sta izdelana s hidropreoblikovanjem in nato varjena z laserjem. To je mogoče izvesti, če se zunanjii notranji del tesno stikata s hidropreoblikovanim nosilom. Prav zato je pomembno, da varilni strokovnjaki in konstrukterji sodelujejo že od samega začetka načrtovanja novega avtomobila [10].

V obeh primerih vidimo, da z laserjem varimo prekrivne spoje, ki sta iz aluminijaste pločevine. Uporabljen je bil CO₂ laser moči 8 kW. Celotna dolžina vseh neprekinjenih varov je bila 1,6 m.

connected to the tailored blanks technique, which consists of the laser welding of semi manufactures that are then formed in the finished product. With the use of this technique, the optimum material thickness and strength can be provided for different areas in a single component, the mass of the product can be reduced and the width of the heat-affected zone can be narrower ([8] and [9]). Fig. 5 shows the inner side-door structure of a Chrysler concorde that is produced using laser-welded tailored blanks. The thicker sections of the tailored blank provide the appropriate strength in the hinge and door-lock attachment area and are laser welded with the thinner area of the car doors. These parts are then formed as shown in Fig.5.

In general, only a few advantages of laser welding are exploited. Resistance spot welding can be replaced with laser welding and other parts, which have to be designed for laser welding.

For instance, Fig. 6 shows the joint geometries for the A-pillar and floor sill of the BMW 3-series cabrio, which are hydroformed and then laser welded. This can be made if the inner and outer sheets are in close contact. To produce such an application, welding experts and designers must co-operate from the beginning of the new car project [10].

In both the above-mentioned cases, the aluminium sheets in the lap joint are laser welded with an 8kW CO₂ laser. The overall weld length is 1.6 m.

2 SPAJKANJE

Spajkanje kot postopek spajanja se v avtomobilski industriji uporablja že od vsega začetka izdelave avtomobilov, toda tehnika spajkanja se je od takrat močno spremenila. Dandanes v največji meri uporabljamo le dva postopka, ki sta dokaj avtomatizirana in zelo učinkovita. Prvi je spajkanje MIG in drugi lasersko spajkanje.

V splošnem ima postopek spajkanja kar nekaj prednosti v primerjavi z varjenjem. Kot največjo prednost štejemo majhen vnos energije med spajkanjem in tem manjše zaostale napetosti in deformacije v celotnem spajkanem spoju.

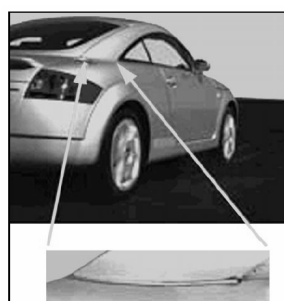
2.1 Spajkanje MIG

Spajkanje MIG se po opremi ne razlikuje od varjenja MIG, po postopku in dodajnem materialu pa ne od klasičnega spajkanja. Pri spajkanju MIG uporabljamo električni obrok kot vir toplote za taljenje spajke in za ogreto delov na delovno temperaturo. Dodajni material je v obliki žice, ki je navita na kolut in se med spajkanjem z nespremenljivo hitrostjo dovaja na mesto spajkanja. Za zaščito varilnega obloka, tekoče spajke in mesta spajkanja uporabljamo čisti argon. Najpogosteje spajkanje MIG uporabljamo za spajanje pocinkanih materialov, nerjavnih jekel in povsod tam, kjer je pomembna korozjska odpornost spoja. Pri spajkanju pocinkanih pločevin se cink veže z bakrom iz spajke in se na ta način prepreči njegov odgor.

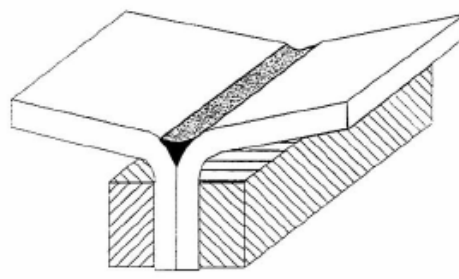
Vnos energije je pri spajkanju MIG v primerjavi z varjenjem MIG tudi do desetkrat manjši ([11] in [12]).

2.2 Lasersko spajkanje

Za lasersko spajkanje lahko zapišemo, da je nov postopek spajanja, saj je bil prvič uporabljen pri izdelavi avtomobila znamke Audi TT coupe, kar je prikazano na sl. 7. Z raziskavami je bilo ugotovljeno, da je mogoče le s spajkanjem doseči zaželeno obliko med streho in preostalim delom karoserije, ki sta izdelana iz pocinkane jeklene pločevine ([11] in [13]).



a)



b)

Sl. 7. Lasersko spajkanje karoserije avtomobila znamke Audi TT coupe: a) – prikaz spoja na avtomobilu, b) – shematski prikaz spajkanega spoja [2]

Fig. 7. Laser brazing of the Audi TT coupe: a) joint on the car; b) schematically shown brazed joint [2]

2 BRAZING

Brazing has been used in the car industry from the earliest days of car production. Since then it has undergone many changes. These days MIG brazing and laser brazing are widely used as a result of automation and high productivity.

In general, brazing has advantages over welding due to the lower heat input, which reduces the residual stresses and deformations in the brazed joint.

2.1 MIG brazing

MIG brazing has similarities with MIG welding, in terms of the equipment, and with classical brazing in terms of the procedure and filler material. In this case an electrical arc is used for melting the brazing wire and for heating the workpieces to the working temperature. The brazing wire is coiled on a disk and is brought to the work place at a constant speed. For the shielding of the arc, the liquid braze and the brazing workplace, pure argon gas is used. MIG brazing is used for brazing zinc-coated sheets, stainless steels and where corrosion resistance of the joint is required. When brazing zinc-coated sheets, zinc bonds with the copper and prevents its burn off.

The heat input during MIG brazing can be up to ten times smaller than during MIG welding ([11] and [12]).

2.2 Laser brazing

Laser-beam brazing is a new manufacturing process, developed and used for the first time in the production of the Audi TT coupe (see Fig. 7). Comparative investigations showed that only with this new process is it possible to achieve the sharp-edged transition from the roof dome to the wing in the area of the C-pillar, because zinc-coated material was used ([11] and [13]).

Uporabljena je bila spajka na osnovi srebra in cinka s tališčem pri temperaturi 650°C. Spajka je bila na mesto spajkanja dovajana v obliki tanke brezkončne žice s protitaktno napravo in se je talila v zaščiti inertnega plina argona. Uporabljen je bil YAG laser z močjo 1 kW. Celotna dolžina spajkanega spoja na eni karoseriji je bila 330 mm.

Drugi primer uporabe laserskega spajkanja je spajkanje pokrova prtljažnika pri avtomobilu znamke VW bora. Izdelan je iz dveh delov. Tudi v tem primeru je bila uporabljena spajka v obliki žice, brez talila in raztaljena v zaščiti nevtralnega (argon) plina.

Zaradi zelo ugodnih tehnoloških, trdnostnih in ekonomskih rezultatov laserskega spajkanja pri izdelavi avtomobilske karoserije se je podjetje VW odločilo, za širšo uporabo tega postopka v svoji proizvodnji pri izdelavi številnih različnih vrst avtomobilov.

2.3 Plazemsko spajkanje

Plazemsko spajkanje je v veliki meri podobno laserskemu spajkanju. Postopka se razlikujeta le v viru toplotne za ogrejite pločevin in za razdalitev spajke. Prednost plazemskega spajkanja je v cenejsi napravi in v nekoliko širšem toplotnem viru, kar je v določenih primerih prednost, ker ogrevamo širšo okolico z nekoliko nižjo intenzivnostjo. Plazemsko lahko spajkamo ročno v vseh položajih ali avtomatsko ali pa celo robotizirano ([14] in [15]).

3 LEPLJENJE

Pri izdelavi avtomobilskih karoserij smo do danes lepljenje uporabljali le kot pomožno tehnologijo spajanja. Večinoma se je lepljenje uporabljalo za polnitev in pečatenje raznih robov ali zaključkov.

Lepljenje pa se v zadnjem obdobju vedno bolj uporablja kot samostojna tehnologija spajanja ali pa kot del mešanega postopka spajanja; to je v kombinaciji z drugim postopkom varjenja (uporovno, lasersko itn.) ali mehanskega spajanja.

Primer uporabe lepljenja v avtomobilski industriji je Lotus elise. Avtomobilska karoserija tega avtomobila je izdelana z lepljenjem, z lepilom na podlagi epoksidnih smol, ki je bilo sušeno z zunanjim ogrevanjem. Posamezni lepljeni elementi so med seboj vijačeni. Na celotni karoseriji je bilo uporabljenih 155 vijakov [3].

Lepljenje ima številne prednosti pred drugimi postopki spajanja. Postopek je mogoče izvesti le z ene strani, spoj deluje prek celotne površine, kar poveča statično in dinamično togost in trdnost celotne karoserije. Največja prednost lepljenja je v zmožnosti spajanja različnih kovinskih (jeklo, aluminij) in nekovinskih (polimeri, keramika, kompoziti) materialov med seboj ([16] in [17]).

Z razvojem novih lepil na podlagi gume se je možnost lepljenja še povečala. Z uporabo različnih vrst lepil, oblike posameznih elementov bo mogoče izdelati poljubne in zaželene dele, ki bodo ustrezali sodobnim usmeritvam s trdnostnega, z varnostnega,

The brazing wire is silver based and has an extremely low processing temperature of 650 °C. Thin brazing wire is melted in the argon shielding gas and is brought to the brazing place with a push-pull system. The brazing cell is equipped with a 1kW Nd:YAG laser source. The total brazing length on a single car body is estimated to be 330 mm.

The second example of laser brazing is the brazing of the outer trunklid, which consists of an upper and a lower part. Even in this case, brazing wire is used with no flux and the brazing is conducted in an argon shielding gas.

Because of the good technological, strengthening and economic results of laser brazing, VW claims that all future trunklids will be made in this way.

2.3 Plasma brazing

Plasma brazing is a process similar to laser brazing. The difference between them is in the heat source for melting the braze and heating the workpiece. The advantage of plasma brazing is a cheaper device and a wider heating area, which heats a wider part of the workpiece with a lower intensity than the laser. Plasma brazing can be manual, automated or even robotised ([14] and [15]).

3 ADHESIVE BONDING

Until now, adhesives have been used to a limited extent in car-body manufacturing. They are mainly used as a combination of a sealant and a stiffening element for closures, such as hoods and trunk lids.

Adhesive bonding has recently been used as an independent joining technology or as part of hybrid joining, i.e. in combination with other welding procedures (resistance spot welding, laser welding, etc) or mechanical joining.

An example of an adhesive bonding application is the aluminium structure of a Lotus Elise, which features an interesting assembly philosophy consisting of a one-component curing epoxy adhesive combined with 155 flow-drill screws.

Adhesive technology offers many advantages, i.e. single-sided accessibility, and increased stiffness and strength as a result of continuous joints. Another big advantage of adhesive bonding is its ability to join different materials, such as aluminium to steel or polymers to metals ([16] and [17]).

The development of new, rubber-based adhesives will increase the possibilities of adhesive bonding. The use of different adhesives and element shapes will enable the production of specially designed products, which will respond to state-of-

okoljevarstvenega, ekonomskega in oblikovalskega vidika.

4 HIBRIDNO VARJENJE

Hibridno varjenje imenujemo postopek spajanja materialov, v katerem sta združena dva samostojna postopka varjenja. Najpogosteje sta to lasersko in obločno varjenje. Lahko uporabimo CO₂ ali YAG laser in pa enega od obločnih postopkov varjenja (MAG/MIG, TIG, plazma).

Medsebojni sinergetski učinek laserskega žarka in varilnega obloka prispeva kar nekaj prednosti varjenja, ki se izraža na različne načine. S hibridnim postopkom lahko povečamo hitrost varjenja, produktivnost, globino uvara, kakovost zvarnega spoja ter izkoristek varjenja in uporabljeni energije ([18] in [19]).

5 MEHANSKO SPAJANJE

K mehanskemu spajanju materialov štejemo klasično kovičenje, samokovičenje in robljenje. Pri klasičnem kovičenju uporabljamo kovice različnih oblik, različnih materialov in za različne načine pritrjevanja. Na sliki 8 je prikazan primer enostranskega kovičenja s posebej oblikovano dvokrako kovico, ki prebije obe pločevini in jih poveže v trajno zvezo.

Kovica mora biti izdelana iz kakovostnejšega materiala kakor sta pločevini, ki ju kovičimo. Kovica mora imeti določeno trdnost, togost in preoblikovalnost. Dobro preoblikovalne materiale pa lahko tudi samokovičimo, kar pomeni, da kovice sploh ne potrebujemo. V tem primeru mora imeti matrica (spodnji del orodja) posebno obliko, v kateri se preoblikujejo obe pločevini in s tem nastane neločljiva zveza.

Največje prednosti mehanskega spajanja so: tehnika spajanja je preprosta, zaostale napetosti v spoju so majhne, praktično brez deformacij, postopek je za okolje prijeten, orodje in oprema sta razmeroma poceni z dolgo dobo trajanja ter z majhnimi stroški vzdrževanja in zagotavljanje kakovosti del je razmeroma preprosto.

the-art trends of stiffness, safety, ecology, economics and design.

4 HYBRID WELDING

Hybrid welding consists of joining processes involving two independent welding procedures. Many times these include laser (CO₂ or the Nd:YAG) and arc-welding techniques (MAG/MIG, TIG, plasma).

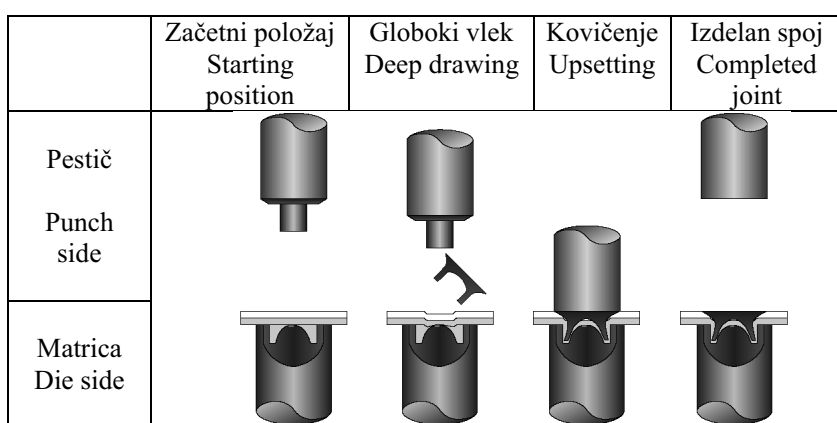
The synergetic effect of a laser beam and a welding arc enables higher welding speeds and productivity, as well as better weld depths, welding-joint quality and energy efficiency ([18] and [19]).

5 MECHANICAL JOINING APPLICATIONS

Mechanical joining applications consist of riveting, self-piercing riveting and clinch joining. When riveting rivets of different shapes and materials are used for divers joining applications. Fig. 8 shows one-side riveting with a specially shaped two-legged rivet that breaks through the sheets and fastens them together in a permanent connection.

The rivet must be of better quality than the riveting sheets. It must have a defined strength, stiffness and formability. Materials with good formability can be self-piercing riveted, which means that no additional rivets are needed when riveting. In this case, the matrices (the bottom part of the tool) must be of a special shape in which both sheets are formed into a permanent connection.

The advantage of mechanical joining techniques are: simplicity, low residual stresses in the joint, almost no deformations, environmentally friendly process, relatively cheap tools, and equipment with a long tool life. Maintenance costs are low and the quality assurance is done relatively easily.



Sl. 8. Enostransko kovičenje z dvokrako kovico [19]

Fig. 8. One-side riveting with a two-legged rivet [19]

6 SKLEPI

V prispevku je podan pregled postopkov spajanja, ki se uporabljajo pri izdelavi avtomobilov. Podanih je nekaj praktičnih primerov uporabe za več vrst različnih vrst osebnih avtomobilov in nakazan razvoj na tem področju za prihodnost.

Iz celotnega prispevka in iz podatkov omenjenih referenc lahko ugotovimo, da imamo dandanes v praksi; to je v industrijski avtomobilski izdelavi uporabljenih veliko število postopkov spajanja materialov, ki se med seboj zelo razlikujejo.

Poleg klasičnega talilnega in netalilnega varjenja uporabljamo spajkanje, lepljenje, mehansko spajanje in sestavljeni postopki iz več samostojnih postopkov, ki jih imenujemo hibridno spajanje. Prihodnji razvoj na tem področju lahko v grobem razdelimo v štiri smeri. Za talilno varjenje; to je za bolj obremenjene spoje, se bo v prihodnje v največji meri uporabljalo lasersko varjenje z dodajnim materialom in brez njega ali pa hibridno varjenje (laser + oblok), za trdnostno manj zahtevne spoje se bo uporabljalo spajkanje, ki pa se bo razvijalo v dveh smereh (laser ali spajkanje MIG), tretja smer razvoja bo lepljenje in četrta mehansko spajanje.

V največji meri pa bo razvoj spajanja materialov v avtomobilski industriji odvisen od vrste materialov, ki se bodo uporabljali pri izdelavi avtomobilskih delov.

6 CONCLUSIONS

This paper describes a survey of joining processes that are used in car-body manufacturing. A few practical examples are shown and a number of development trends are indicated.

From the paper and the references it can be concluded that car-body manufacturing facilities use a wide range of different joining techniques.

Besides classical non-melting and melting welding techniques, brazing, adhesive bonding, mechanical joining and hybrid joining processes are used. The development trends in the field of joining are going in four directions. Welding that involves melting will be used for highly loaded joints. For this, laser welding with or without the filler material or hybrid welding (laser + arc) will be used. Joints of lower stiffness will be produced with brazing, where the development will go in two directions, i.e. laser brazing and MIG brazing. The third development direction will be adhesive bonding, and the fourth will be mechanical joining.

Generally, the development directions of joining processes in car manufacturing will depend mainly on the materials that will be used for the car parts.

7 LITERATURA 7 REFERENCES

- [1] Schubert, J., K. Urlich, H. Scholler (1997) Schweißeignung ungleichartiger Verbindungen des Stahlgusses GX12CrMoWVNbN10 – 11 mit niedriglegierten Stählen, *Schweißen & Schneiden*, Vol. 49, 9, 672-676, ISSN 0036-7184.
- [2] Larsson, J. K. (2002) Overview of joining technologies in the automotive industry. Proceedings: Advanced Processes and technologies in welding and allied processes; IIW International Conference, Edited: J. K. Kristensen, Copenhagen.
- [3] Larsson, J.K., L. Bengtsson L. (2001) The joining of high- and extra-high-strength steels in the automotive industry – Pitfalls and Possibilities, *Proceeding DVM-Tag 2001 Fügetechnik im Automobilbau*, Berlin.
- [4] Tušek, J., T. Blatnik (2002) Ultrasonic detection of lack of fusion in spot welds, *Insight*, Vol. 44, No. 10, 684-688, ISSN 1354-2575.
- [5] Himmelbauer, K. (2002) Schutzgassschweißen mit Flachdrahtelektrode, *Schweiss- und Prüftechnik*, Vol. 56, No. 3, 34-35, ISSN 1027-3352.
- [6] N.N. (2001) Die nach Essen hat sich gelohnt (15. Internationale Fachmesse »Schweißen & Schneiden«), *Der Praktiker*, Vol. 53, No. 12, 474-514, ISSN 0554-9965.
- [7] Trillmich, R. (1999) Qualitätssicherung beim Bolzenschweißen, *Der Praktiker*, Vol. 51, 11, 454-460, ISSN 0554-9965.
- [8] Prange, W., C. Schneider, U. Jaroni (1994) Tailored blanks – contributions to an optimized steel body shell, *Proceeding of the LANE'94*, (Laser Assisted Net Shape Engineering), Edited by: M. Geiger, F. Vollertsen; 145-165, ISBN 3-87525-061-3.
- [9] Ahmetoglu, M., D. Brouwers, G. Kinzel (1994) Deep drawing of round cups from laser-tailored welded blanks, *Proceeding of the LANE'94*, (Laser Assisted Net Shape Engineering), Edited by: M. Geiger, F. Vollertsen; 167–176, ISBN 3-87525-061-3.
- [10] Hornig, J. (2001) Laserstrahlschweißen am 3er Cabrio, *Proceeding SLV Tagungsreihe Dünbblechverarbeitung »Fügen von Stahlwerkstoffen«*, München.

- [11] Henebuth, H., P. Hoffmann, M. Geiger (1994) Automated laser beam brazing for automobile body construction, *Proceeding of the LANE'94*, (Laser Assisted Net Shape Engineering), Edited by: M. Geiger, F. Vollertsen; 145-165, ISBN 3-87525-061-3.
- [12] Tušek, J. (2001) MIG spajkanje - obločno spajkanje v zaščiti inertnega plina: Obločno spajkanje, *Vzdrževalec*, št. 79, 18-20, ISSN 1318-2625.
- [13] Korte, M. (2000) Laserstrahllöten – ein Fügeverfahren mit Zukunft, *Proceedings European Automotive Laser Application (EALA)*, Bad Nauheim.
- [14] Walduk, B. (1999) Using plasmabraise in car body fabrication, *Welding & Fabrication*, August, 11-14.
- [15] Füssel, U., J. Zschetsche, U. Szieslo, L. Kriftel, J. Husner (2002) Plasmalöten mit strömführendem Zusatzwerkstoff. *Der Praktiker*, Vol. 54, 10, 336-340, ISSN 0554-9965.
- [16] Jost, R. (2002) Adhesive bonding in combination with mechanical joining, *Proceedings Joining in Automotive Lightweight Design*, Bad Nauheim.
- [17] Vollrath, K. (2002) Kleben für den Leichtbau bei Kraftfahrzeugen, *Der Praktiker*, Vol. 54, 7, 222-226, ISSN 0554-9965.
- [18] Dilthey, U., U. Reisgen, A. Wieschermann (1999) Hybrid technology laser beam – arc welding, *Proceeding of the Sheet Metal*, 399-406, ISBN 3-87525-110-5.
- [19] N.N. (2001) Entwicklungsstand und Forschungsergebnisse mit Praxisbezug, *Der Paktiker*; Vol. 53, No. 12, 522-535, ISSN 0554-9965.

Naslov avtorjev: prof.dr. Janez Tušek
mag. Damjan Klobčar
Univerza v Ljubljani
Fakulteta za strojništvo
Aškerčeva 6
1000 Ljubljana
janez.tusek@fs.uni-lj.si
damjan.klobcar@fs.uni-lj.si

Authors' Address: Prof.Dr. Janez Tušek
Mag. Damjan Klobčar
University of Ljubljana
Faculty of Mechanical Eng.
Aškerčeva 6
1000 Ljubljana
janez.tusek@fs.uni-lj.si
damjan.klobcar@fs.uni-lj.si

Prejeto: 29.9.2003
Received: 29.9.2003

Sprejeto: 8.4.2004
Accepted: 8.4.2004

Odprto za diskusijo: 1 leto
Open for discussion: 1 year

Numerično modeliranje hladilnega sistema na motorju z notranjim zgorevanjem

Numerical Modelling of an Engine-Cooling System

Tomislav Mrakovčić - Vladimir Medica - Nedjeljko Škifić

V prispevku je predstavljen simulacijski model za analizo prenosa toplote in snovi v hladilnem sistemu motorja v prehodnem režimu delovanja. Simulacijski model ima modularno sestavo in je sestavljen iz različnih podmodelov hladilnega sistema, ki so med seboj povezani s toplotnimi povezavami. Analizo je mogoče izvesti učinkovito le, če so povezave med posameznimi modeli upoštevane sočasno. V prispevku je zaradi svoje zahtevnosti in različnosti vgrajenih naprav predstavljen model hladilnega sistema za plovila, ki vsebuje dva ali več hladilnih krožnih tokov. Raven temperatur v posameznih delih hladilnega sistema se vzdržuje z uporabo termostatskih ventilov in z mešanjem različnih tokov hladilne tekočine. Različne oblike hladilnega sistema je mogoče doseči s spremjanjem toka skozi termostatske ventile, s spremjanjem toplotnih obremenitev ali s priklapljanjem in odklapljanjem različnih hladilnih naprav. Zaradi različnih možnih izvedb pomeni jedro simulacijskega modela prilagodljiv algoritem za izračun tokov in tlačnih padcev v hladilnem sistemu. Iz rezultatov ovrednotenja simulacijskega modela je mogoče ugotoviti dobro ujemanje numerično ocenjenih in izmerjenih vrednosti. Predstavljena je tudi uporaba tega modela na primeru motorja vozil.

© 2004 Strojniški vestnik. Vse pravice pridržane.

(Ključne besede: sistemi hladilni, motorji dizelski, modeliranje numerično, modeli simulacijski)

This paper presents a simulation model for a heat and mass transfer analysis applied to an engine-cooling system under transient conditions. The simulation model has a modular structure, composed of various cooling-system submodels that are interconnected by links. An efficient analysis is possible only when the interactions between the submodels are considered simultaneously. Because of its complexity and the variety of installed devices, a marine cooling system consisting of two or more interconnected cooling circuits is presented. The temperatures in particular parts of the cooling system are maintained through thermostatic valves by mixing or diverting streams of cooling fluid. Due to the change of flow rate through the thermostatic valves, by varying the heat load and connecting or disconnecting any cooled device, a different pipeline configuration occurs. For this reason, a self-adapting algorithm for the flow and pressure-drop calculation across the cooling system is the core of the simulation model. The validation of the presented simulation model indicates good matching of the numerical predictions with the measured values. The possible application of such a model to the cooling systems of vehicle engines is presented too.

© 2004 Journal of Mechanical Engineering. All rights reserved.

(Keywords: cooling systems, diesel engines, numerical modelling, simulation models)

0 UVOD

Namen hlajenja motorjev z notranjim zgorevanjem je ohranjanje ustreznegata temperaturnega stanja in s tem učinkovitega delovanja motorja. Glede na vedno večje zahteve tržišča po boljši gospodarnosti in zanesljivosti motorja postaja tudi hladilni sistem motorja tehnično vedno zahtevnejši. Pri zasnovi sodobnih hladilnih sistemov imajo načrtovalci v smislu izbire različnih konstrukcijskih rešitev široke možnosti.

Pri hladilnih sistemih ladijskih motorjev je zelo pomembno, da so cevovodi, skozi katere teče morska

0 INTRODUCTION

The purpose of an engine-cooling system is to keep the engine at its most efficient operating temperature. A consideration of the economic aspects and demands for better performance are leading to increasingly complex cooling systems. Engine-cooling systems have a variety of possible arrangements and devices, which leads to a demanding design task.

In marine cooling systems, the length of the pipeline and the number of components in contact

voda, čim krajsi, število krmilnih organov pa čim manjše. Sodobne hladilne naprave imajo zato zelo kratke cevi z morsko vodo in osrednji zelo učinkoviti in prostorsko prilagodljivi prenosnik toplote. Po drugi strani pa na strani hlajenja s sladko vodo običajno naletimo na vsaj dva ali več krožnih tokov, po katerih se pretaka voda z različnimi temperaturami. Temperature različnih krožnih tokov ohranjamо nespremenjene z mešanjem hladnejše ali toplejše vode z uporabo termostatskih ventilov. Obsežnost in konstrukcijske možnosti izbere sestavnih delov, npr. različne črpalkе in drugi gradniki obsežnega hladilnega sistema večjih ladijskih motorjev pomenijo za inženirja – oblikovalca velik izziv. Četudi je hladilni sistem ustrezno zasnovan in preverjen v razmerah ustaljenega delovanja, pa je njegovo delovanje v prehodnih, spremenljivih pogojih delovanja popolna neznanka. K temu znatno prispeva spremenljivo delovanje termostatskega ventila, ki v prehodnem režimu delovanja močno spreminja delovne parametre celotnega hladilnega sistema. Podoben učinek povzročata tudi vklop ali izklop katerekoli komponente hladilnega sistema.

Osnovo pri načrtovanju hladilnega sistema pomeni ustrezna določitev značilnosti cevovodov in tlačne črpalkе, ki mora zagotavljati ustrezen tok vode pri določeni tlačni višini. Če se povrnemo na osnovne zahteve omenjene v začetku, je treba na podlagi potrebnih tokovnih zahtev: masnih tokov, uporov itn. in vgradbenih – izmernih zahtev najprej določiti geometrijske izmere cevovodov in drugih sestavnih delov hladilnega sistema. Izračun izmernega in delovnega prilagajanja je iterativen in ga moramo ponavljati, dokler z rezultati nismo zadovoljni. Takšen način je zelo primeren za preproste cevne odseke, ni pa primeren za zahtevne, razvijane cevne sisteme. V razpoložljivi literaturi najdemo mnogo uporabnih metod, s katerimi lahko izračunamo zamotane cevne sisteme [1]. V prispevku opisan hladilni sistem je izračunan na podlagi Hardy-Crossove metode, ki je bila izboljšana z uporabo Newton-Raphsonove tehnike.

1 OPIS NUMERIČNEGA MODELA HLADILNEGA SISTEMA

Hladilni sistem motorja sestavljajo cevi, črpalkе, ventilи in porabniki toplote, ki jih moramo ohladiti. Vse omenjene sestavne dele lahko zložimo skupaj na različne načine, zato mora biti numerični model zelo gibek in prilagodljiv najrazličnejšim tehničnim izvedbam. Sestavne dele hladilnega sistema obravnavajo posebni, neodvisni modeli, ki jih lahko pri različnih izvedbah hladilnega sistema poljubno izberemo in med seboj povežemo. Vsak posamezni sestavni model obdeluje probleme prenosa snovi in toplote za obravnavano komponento, kot vhodni podatek pa je namenjen masni tok tekočine. Delovni parametri hladilnega sistema se stalno spremjamajo, zato je v raziskavah vpeljan algoritem masnega toka tekočine in kombiniran s posameznimi

with seawater are kept as low as possible. A modern cooling system has a very short seawater pipeline, using only one central heat exchanger, cooled with seawater, that offers good heat management combined with high flexibility. As parts of the freshwater cooling system are not operating within the same temperature range, at least two or more interconnected cooling circuits are used. The temperature in a particular cooling circuit is maintained by mixing the flow through a thermostatic valve. The complex structure and the variety of possible arrangements of the cooling-system pipeline represent design challenge in which appropriate pumps and other equipment have to be chosen. If that task is successfully completed for steady-state operation, system behaviour in the transients often remains unknown. In addition, it should be mentioned that the operation of thermostatic valves during transients constantly causes a change of the system's working point. The same happens when any unit is connected or disconnected from the cooling system.

The design of the cooling system involves a determination of the pipeline characteristics and the selection of the pump, which is able to satisfy the required flow rate and pressure specifications. Based on a previously established pipeline layout, the design process consists of defining the section dimensions, taking into account the recommended fluid velocities and the system constraints. This iterative process is repeated until the cooling system satisfies the design requirements. It is possible to apply the described process to a simple pipeline, but its application to the design of complex systems is impractical. Several methods for the analysis of complex pipe networks are described in [1]. The analysis of cooling system pipe network presented here is based on the Hardy-Cross approach, improved with the Newton-Raphson technique.

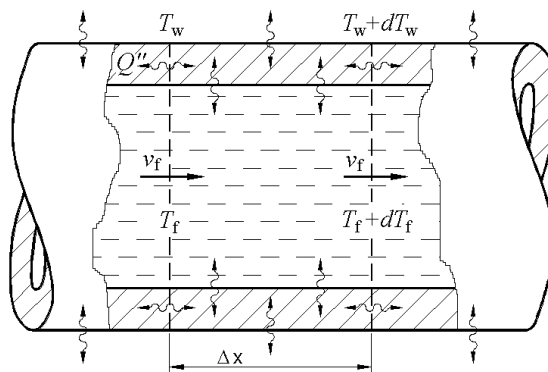
1 DESCRIPTION OF THE NUMERICAL MODEL OF THE COOLING SYSTEM

The engine-cooling system consists of pipes, heat exchangers, pumps, valves and units that need to be cooled. All these components can be arranged in many different ways, so the numerical model must be flexible in adapting to any possible cooling-system configuration. The above-mentioned components are represented through separate submodels, which are interconnected according to a given cooling-system layout. The component submodels are focused on heat and mass transfer within the component itself, taking flow rates as the input data. As the changes of the cooling system's working point occur constantly, an algorithm for

modeli gradnikov hladilnega sistema, ti pa so povezani v celotni numerični model hladilnega sistema. V prispevku so na kratko opisani numerični modeli – podsklopi celotnega numeričnega modela.

1.1 Cevovodi

Numerični model, ki opisuje cevovode, temelji na zakonih ohranitve snovi in energije. Pri tem je uporabljen enorazsežen model, ker je dolžina cevi znatno večja od njenega premera. Kinetična in potencialna energija sta v primerjavi s preneseno toploto neznačilni in ju zato v tem primeru zanemarimo, medtem ko so viskozne sile upoštevane pri izračunu tlačnih izgub. Predstavljeni model sestavlja sistem enačb, ki opisuje hladilno sredstvo oziroma steno cevovoda, skozi katerega se to sredstvo pretaka (sl. 1).



Sl. 1. Fizikalni model prenosa snovi in toplote v cevi
Fig. 1. Physical model for heat and mass transfer in a pipe

Enačbo, ki obravnava ohranitev energije v hladilu, lahko zapišemo v obliki:

$$\rho_f c_f A_f \frac{\partial T_f}{\partial t} + \rho_f c_f v_f A_f \frac{\partial T_f}{\partial x} = \lambda_f A_f \frac{\partial^2 T_f}{\partial x^2} + \alpha_f O_f (T_w - T_f) \quad (1),$$

medtem ko je ustrezni zapis zakona o ohranitvi snovi:

$$\frac{\partial}{\partial x} (\rho_f v_f) = 0 \quad (2).$$

Ravnotežna energijska enačba za cevno steno se glasi:

$$\rho_w A_w c_w \frac{\partial T_w}{\partial t} = \lambda_w A_w \frac{\partial^2 T_w}{\partial x^2} + \alpha_0 O_0 (T_0 - T_w) - \alpha_f O_f (T_w - T_f) \quad (3).$$

V enačbah (1) do (3) označujejo indeksi: f – hladilo, w – steno cevi in 0 – okolico. Spremenljivke so: gostota tekočine ρ , specifična toplota c , ploščina prečnega prereza cevi A , temperatura T , kinetična viskoznost v , toplotna prevodnost λ , toplotna prestopnost α in površina opazovanega mejnega elementa O .

1.2 Prenosnik topline

Pri sodobnih hladilnih sistemih motorjev z notranjim zgorevanjem najpogosteje srečamo ploščate

flow determination is combined with component submodels in a common numerical model. In the following text, numerical submodels are briefly presented.

1.1 Pipes

The numerical model of the pipes is based on equations of mass and energy conservation. As the length of the pipe is much larger than the cross-sectional diameter, a one-dimensional model is applied for the pipes. The potential and kinetic energies are neglected in comparison to the thermal energy, whereas viscous dissipation is taken into account during the calculation of the pressure drops. This model consists of an equations system related to a cooling fluid and an equations system related to a pipe wall (Fig.1).

The energy conservation for a coolant can be expressed as follows:

while mass conservation is:

The energy conservation for a pipe wall can be written as:

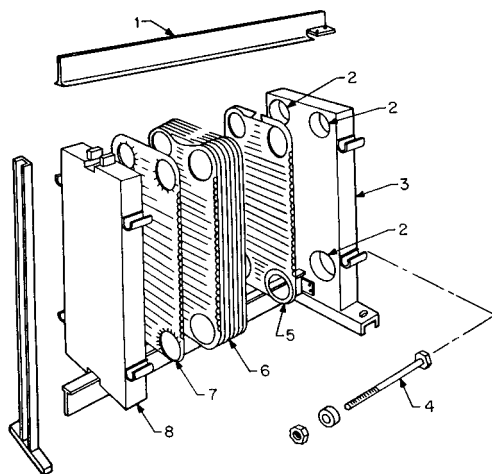
In Eq.(1-3) f is the index for the fluid, w for the pipe wall and 0 for the environment. The variables used in Eq.(1-3) are: ρ for the density, c for specific heat, A for the cross-sectional area, T for the temperature, v for the fluid velocity, λ for the conduction coefficient, α for the heat-transfer coefficient and O for the perimeter of the control volume boundary.

1.2 Heat exchanger

A plate heat exchanger (PHE) is the most frequently used heat exchanger in modern engine-

prenosnike toplote. Odlikuje jih zelo dober učinek prenosa toplote, poleg tega pa so v primerjavi s cevnimi prenosniki manj občutljivi na zamašitev z nečistočami. Zelo lahko jih očistimo, po zasnovi so zelo zgoščeni in prilagodljivi na spremembe delovanja. Žal pa je njihova uporaba zaradi uporabljenega gradiva tesnil temperaturno in glede na kemično sestavo hladivaomejena. Delovni tlak hladiva je omejen na 15 bar, tlache izgube – upori pa so sorazmerno veliki. V motorjih z notranjim zgorevanjem so tlaki hladiva navadno nižji od 15 bar, pa tudi sestava hladiva ni takšna, da bi ogrozila zanesljivost delovanja hladilnika; ploščati hladilniki so zato zelo primerna oblika hladilnikov za motorje (sl. 2).

cooling systems. PHEs have high heat-transfer rates and produce less fouling than shell-and-tube exchangers. They are easy to clean, require little space and they are very flexible if the process conditions are changed. However, the choice of fluids is limited by the chemical resistance and the temperature limits of the gaskets. The working pressures of PHEs are limited to 15 bar, and they produce a relatively high pressure drop. In normal conditions, the working pressures in engine cooling systems do not exceed 15 bar and the cooling fluids are not aggressive, so there are practically no limits for the applications of PHEs (Fig.2).



Sl. 2. Prikaz sestavnih delov ploščatega prenosnika toplote
Fig. 2. Exploded view of a plate heat exchanger

Zaradi sorazmerno zamotane oblike sestavnih delov in posebnosti v različnih razmerah delovanja ploščatih prenosnikov toplote, je bil razvit ustrezен prilagojen numerični model. V hladilniku hladivo teče skozi zaporedne ploščate prehode; numerični model obravnava le en prehod skozi ploščati kanal. Pri tem predpostavimo, da se tokovi hladiva v preostalih kanalih ne spremenijo in da se prenos toplote izvede le v dejavnih ploščah prenosnika (sl. 2, plošča 6).

Zaradi zgoraj omenjenih predpostavk lahko kanal ploščatega prenosnika (slika 3) obravnavamo kot model cevi:

$$\rho_f c_f A_f \frac{\partial T_f}{\partial t} + \rho_f c_f v_f A_f \frac{\partial T_f}{\partial x} = \lambda_f A_f \frac{\partial^2 T_f}{\partial x^2} + \alpha_f A_{pl} (T_{pl} - T_f) \quad (4)$$

kjer se indeks f nanaša na hladivo, indeks pl pa na dejavno ploščo prenosnika

Zaradi specifične oblike in sestave plošč prenosnika ima masni tok hladiva močan vpliv na učinek ploščatega hladilnika. Zato je v numeričnem modelu upoštevan vpliv masnega toka hladiva na toplotno prestopnost in tlache izgube in omogoča izračun obeh. Različne oblike površin prenosnikov toplote seveda določajo različne toplotne prestopnosti, zato, žal splošno veljavne odvisnosti med obliko prenosnih površin in prestopom toplote

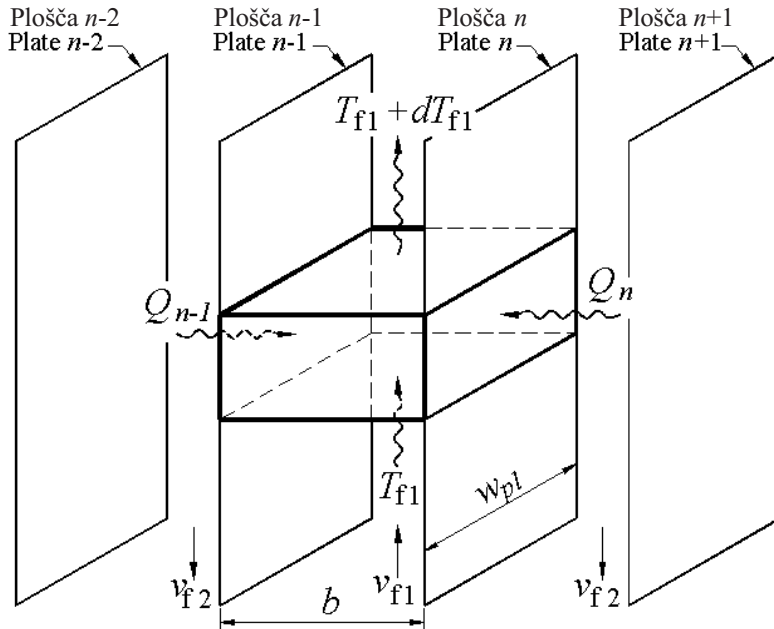
legenda:	legend:
1 – nosilna prečka	1 – carrying bar
2 – cevna povezava	2 – connection
3 – trdno ogrodje	3 – fixed frame
4 – sidrni vijaki	4 – tightening bolts
5 – sklepna plošča	5 – end plate
6 – plošča prenosnika	6 – channel plate
7 – sklepna plošča	7 – end plate
8 – pritisna plošča	8 – pressure plate

Due to the complexity of the geometry and the specific behaviour of the PHE in different operating conditions, a more detailed numerical model had to be developed. The fluids within a PHE flow in alternate spaces between the plates. The numerical model of a PHE can be reduced to a single channel between the plates, with the assumption that flows of the same fluid are equal in all channels. Also, it is assumed that the heat exchange is limited only to the plates.

With these assumptions, the physical model of a PHE channel (Fig.3) is similar to a pipe model:

where index f represents the cooling fluid and the index pl is the heat-exchanger plate.

Due to the specific geometry of the plates, the flow rate has a strong influence on the performance of a PHE. For this reason, the numerical model of the heat exchanger takes into account the flow rate, which is the basis for the heat-transfer coefficient and the pressure-drop calculation. Every type of plate has its own heat-transfer coefficient. There is no universal correlation for the calculation of the heat-transfer coefficient. An extensive



Sl. 3. Fizikalni model kanala v ploščatem prenosniku toplotne
Fig. 3. Physical model of a PHE channel

ne moremo določiti. Izčrpno razpravo o izrazih, ki popisujejo toplotno prestopnost, lahko najdemo v delu avtorjev Raja in Bensala [2]. V tem prispevku je uporabljen izračun toplotne prestopnosti v skladu z virom [3], medtem ko je koeficient tlačnih izgub izračunan z izrazom:

$$\frac{1}{\sqrt{\xi}} = \frac{\cos \varphi}{\sqrt{b \tan \varphi + c \sin \varphi + \xi_0 (\text{Re}) / \cos \varphi}} + \frac{1 - \cos \varphi}{\sqrt{a \xi_0 (\text{Re})}} \quad (5),$$

kjer pomenijo φ kot tokovnice delca toka na ploščo prenosnika, a, b in c pa so eksperimentalno določene stalnice z vrednostmi:

$$a = 1,6; b = 0,40; c = 0,36 \quad (6).$$

Koeficient trenja $\xi_0(\text{Re})$ se nanaša na kot tokovnice delca toka na ploščo prenosnika pri kotu $\varphi = 0$ in ga določimo z uporabo znanih izrazov:

$$\xi_0 = 53,39 / \text{Re} \text{ za/for } \text{Re} < 2000 \text{ (laminarni tok / laminar flow)} \quad (7)$$

$$\xi_0 = (1,8 \lg \text{Re} - 1,5)^2 \text{ za/for } \text{Re} \geq 2000 \text{ (turbulentni tok / turbulent flow)} \quad (8).$$

Toplotno prestopnost vsebuje Nusseltovo število, ki ga izračunamo z izrazom:

$$\text{Nu} = 0,122 \text{Pr}^{1/3} \left(\frac{\eta}{\eta_{st}} \right)^{1/6} \left[\xi \text{Re}^2 \sin(2\varphi) \right]^{0.374} \quad (9).$$

Diagrami na slikah 4 in 5 prikazujejo spremembo koeficiente trenja, vrednosti ξ , Nusseltovega števila in njegove odvisnosti od Reynoldsovega števila za različne vrednosti kota φ tokovnice delca toka na ploščo prenosnika. Veliki koti φ povzročajo večje tlačne izgube in zagotavljajo boljši prenos toplotne.

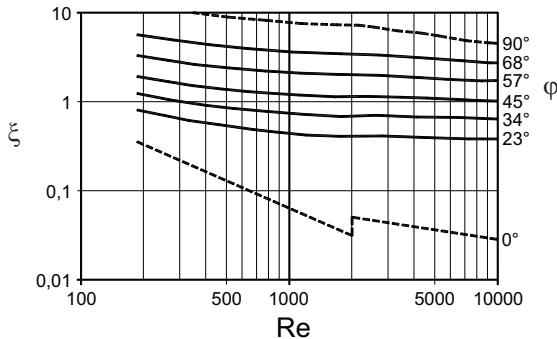
discussion of the equations for the heat-transfer coefficient is given in a paper by Raju and Bansal [2]. In this paper, a procedure for the heat-transfer coefficient calculation presented in [3] is used; the friction coefficient is calculated from the following equation:

where φ represents the angle of the chevron pattern on the plates, while a, b and c are experimentally determined constant whose values are:

The friction factor $\xi_0(\text{Re})$ refers to a chevron pattern with angle $\varphi = 0$, and is obtained from:

The heat-transfer coefficient is expressed with the Nusselt number calculated from the following equation:

The diagrams in Fig.4 and Fig.5 show the change of friction factor, ξ , and Nusselt number, Nu, depending on the Reynolds number and the angle of the chevron pattern, φ . It is obvious that a larger angle φ produces a higher pressure drop and a better heat-transfer coefficient.



Sl. 4. Koeficient tlačnih izgub v odvisnosti od Re števila in kota φ

Fig. 4. Friction factor as a function of Re and the chevron angle φ

1.3 Termostatski ventil

Termostatski ventil vzdržuje temperaturo tekočine v ozkem območju želene temperature. PI krmilnik uravnava – v odvisnosti od razlike med želeno in izmerjeno temperaturo – lego termostatskega ventila tako, da je nihanje temperatur okoli pričakovane vrednosti čim manjše. Vsako temperaturno zaznavalo, ki meri lastno temperaturo na različnih mestih toplotnega prenosnika, ima zaradi lastne mase določeno zakasnitev, ki jo opredeljuje časovna stalnica t_k . V predstavljenem numeričnem modelu termostatskega ventila je upoštevana časovna zakasnitev spremembe temperature v časovnem intervalu Δt z naslednjo eksponentialno odvisnostjo [4]:

$$T - T_0 = (T_f - T_0)(1 - e^{-\Delta t/t_k}) \quad (9).$$

V enačbi (9) se indeks 0 nanaša na začetno stanje, indeks f pa na zadnje dosegeno stanje.

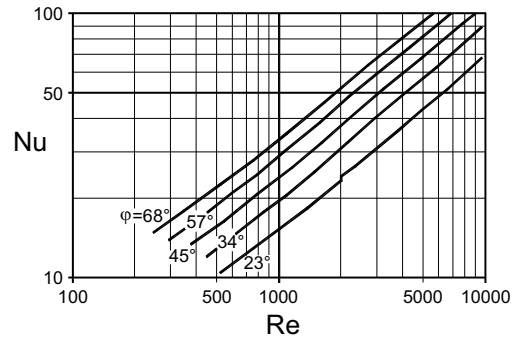
1.4 Določitev masnih tokov in tlačnih izgub

Rezultati izračunov vseh predloženih numeričnih modelov temeljijo na znanih masnih tokovih tekočin. Značilnici cevovoda in črpalk določata določeno skupno delovno točko. Izračun masnega toka tekočine temelji na upoštevanju zakonov o ohranitvi mase in energije. Kontinuitetna enačba mora biti izpolnjena v vsaki stični točki cevovoda, in sicer:

$$\sum_{k=1}^n \lambda_{j,k} Q_k = \sum_{k=1}^n \lambda_{j,k} A_k v_k = 0 \quad (10),$$

kjer koeficient λ nakazuje povezavo med k -to cevjo in j -tim spojem. Energijska enačba za ustaljen tok nestisljive tekočine v k -ti cevi lahko zapišemo v obliki:

$$(\Delta E)_k = (\Delta p)_k + \rho g (\Delta z)_k + \frac{1}{2} \rho (\Delta (v^2))_k + (\Delta p_{fr})_k - (\Delta p_P)_k = 0 \quad (11),$$



Sl. 5. Odvisnost vrednosti Nu števila od Re števila in kota φ

Fig. 5. Nu number as a function of Re and the chevron angle φ

1.3 Thermostatic valve

A thermostatic valve maintains the desired temperature within narrow limits for a particular cooling circuit. Depending on the difference between the measured and the desired temperature, a PI controller positions the thermostatic valve trying to eliminate temperature deviation. The temperature at which a particular point in the cooling system is measured by a temperature sensor that has time constant t_k . The numerical model of the thermostatic valve includes a transient response to temperature changes through time interval Δt according to the following exponential function [4]:

In Eq.(9), the index 0 represents the state before the change, whereas index f represents the last achieved state.

1.4 Flow rates and pressure drops

All the presented numerical models assume known flow rates through the cooling system. As mentioned before, the pipe characteristics associated with the selected pump will meet a certain working point. The flow-rate calculation is based on mass and heat conservation equations, too. The continuity equation must be satisfied at each junction, which can be written as:

where λ is an indicator representing the existence of the connection between pipe k and junction j . The energy equation for steady, incompressible fluid flow in pipe k can be written as:

kjer pomenijo: p vrednost statičnega tlaka, z višinsko razliko (lego) cevnega spoja, v hitrost tekočine, Δp_{fr} celotni padec tlaka, Δp_p pa tlačilki dovedeno energijo [5].

Celotni padec tlaka Δp_{fr} upošteva dolžinske in lokalne izgube tlaka v cevovodu. Dolžinske izgube so izračunane z uporabo znanih obrazcev za laminarni in turbulentni tok. Energija, ki je potrebna za pogon črpalke Δp_p , je izračunana na podlagi podatkov meritev, ki jih je podal izdelovalec črpalke. Podana je v obliki polinoma druge stopnje v odvisnosti od toka tekočine oziroma hitrosti tekočine:

$$p_p = f(Q) = a_0 + a_1 Q + a_2 Q^2$$

ali/or

$$p_p = f(v) = a_0 + a_1 v + a_2 v^2 \quad (12).$$

Nelinearni sistem enačb je rešljiv z Newton-Raphsonovo metodo, ki je zelo stabilna, hitro konvergira, rešitev pa ni odvisna od izbranih začetnih vrednosti ([1] in [6]).

V tem prispevku so glavni pogonski motor in pomožni motorji večjega postroja prikazani kot točkovni viri toplote. Ocenimo, da je dovod hladilne toplote motorja bodisi stalen, ali pa časovno odvisna funkcija. Podobno so obravnavani tudi drugi viri toplote: hladilnik polnilnega zraka, destilacijska naprava, kompresorji, generator električnega toka, hidravlični motorji, glavni ležaji itn. Hladilnik mazalnega olja je modeliran podobno kakor osrednji hladilnik motorske (sladke) hladilne vode, pri čemer so bili predpostavljeni podatki: stalni masni tok olja, vstopna temperatura mazalnega olja v hladilnik z izračunano gostoto in viskoznostjo.

2 RAČUNSKI PRIMER SIMULACIJE IN VREDNOTENJE REZULTATOV

Numerični model je bil uporabljen za določitev sedanjega ladijskega hladilnega sistema (sl. 6). Hladilni sistem sestoji iz dveh krožnih hladilnih tokov: visokotemperaturnega (oznaka VT), ki hladi glavni pogonski motor in nizkotemperaturnega (oznaka NT), ki hladi pomožne stroje in naprave. Pri hladilnem krogu VT vzdržujemo temperaturo vode pri 85 °C, medtem ko je temperatura vode na izstopu iz osrednjega hladilnika za sladko vodo omejena na 36 °C. Predpostavljeno je, da je vstopna temperatura hladilne morske vode pri delovanju v tropih omejena na 32 °C. Hladilni krožni tok VT ne teče skozi prenosnik toplote; želeno temperaturo vzdržujemo z neposrednim mešanjem s hladnejšo vodo iz hladilnega kroga NT. Izmerjena temperatura hladilne vode na izstopu iz motorja krmili termostatski ventil in določa delež primešane hladilne vode iz hladilnega kroga NT.

Podatki za izračun so dobljeni z meritvami na dejanskem ladijskem hladilnem sistemu. Rezultati izračunov se dobro ujemajo z izmerjenimi podatki; pri

where p is the static pressure, z is the height level of the junction, v is the flow velocity, Δp_{fr} is the total pressure drop and Δp_p is the energy added by the pump [5].

Total pressure drop Δp_{fr} consists of head loss for straight pipes and of local pressure drops. The head loss for straight pipes is calculated according to known relations for laminar or turbulent flow. The pressure energy, Δp_p , produced by the pump is calculated from characteristics obtained from the pump producer. The pump's characteristic curve is written in the form of a second-order polynomial as a function of flow rate or velocity:

$$p_p = f(v) = a_0 + a_1 v + a_2 v^2 \quad (12).$$

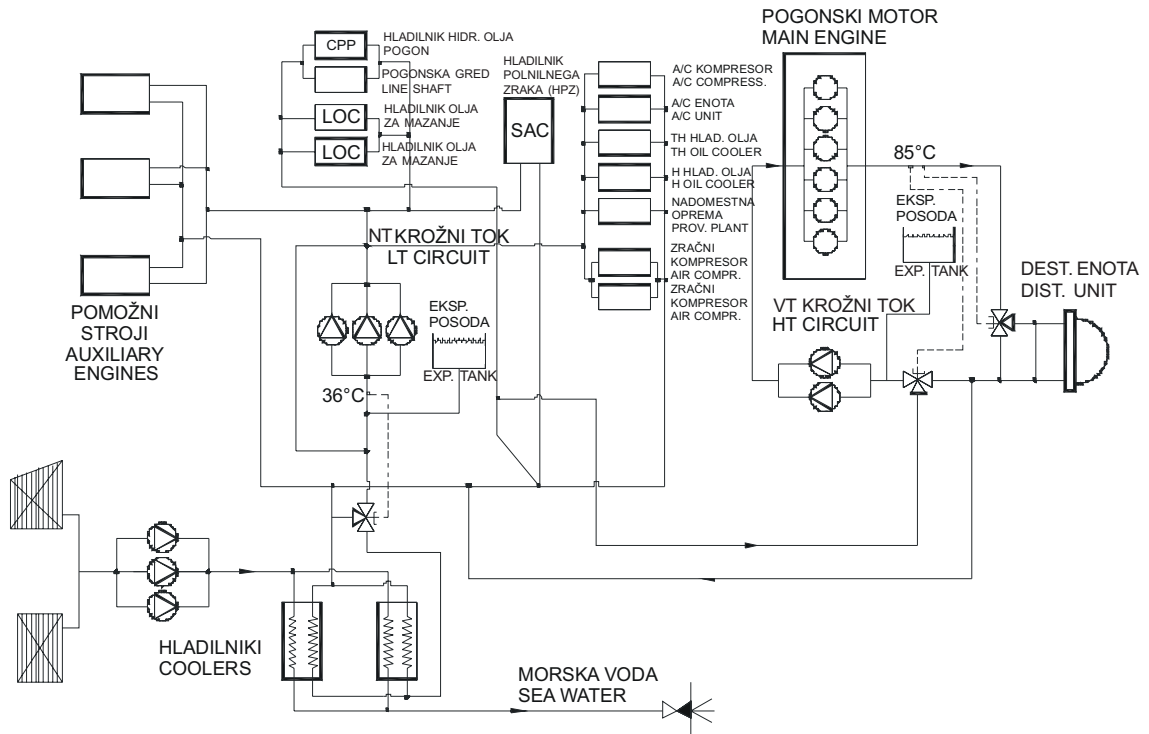
The obtained nonlinear system of equations is solved by the Newton-Raphson method. This method is very stable, it has a fast convergence and the solution is insensitive to the starting values ([1] and [6]).

In this study, the main engine and the auxiliary engines in a power plant are presented as nodal heat sources. The heat inflow can be assumed to be a constant value or as time-dependent function. The same method is used for the other units, like the scavenge air cooler, the distillation unit, the compressors, the A/C plant, the hydraulic plant, the line shaft bearing, etc. The lube-oil cooler is modelled in the same way as the fresh-water central cooler, with a constant lube-oil flow rate, given lube oil inlet temperature and corresponding viscosity and density values.

2 APPLICATION EXAMPLE AND RESULTS VALIDATION

The numerical model was applied to the prediction of an existing marine cooling system (Fig.6). This cooling system consists of a high-temperature (HT) circuit for the main engine cooling and a low-temperature (LT) circuit for auxiliary engines and other equipment. The high-temperature cooling circuit is maintained at 85°C on the main engine outlet, while the low-temperature cooling circuit should be 36°C on the fresh-water central cooler outlet. It is assumed that seawater cooling of the central cooler has an inlet temperature of 32°C (in tropical conditions). The high-temperature circuit has no heat exchanger or cooler. Its temperature is maintained by mixing with cooling fluid from the low-temperature circuit. According to the temperature measured at the engine outlet, a thermostatic valve determines the portion of fluid that has to be taken from the low-temperature circuit.

All the data for the cooling system are taken from an existing ship-propulsion plant. The results of the numerical simulation showed good matching with the measured data obtained during a sea trial. The measured values are the flow rate and pressure



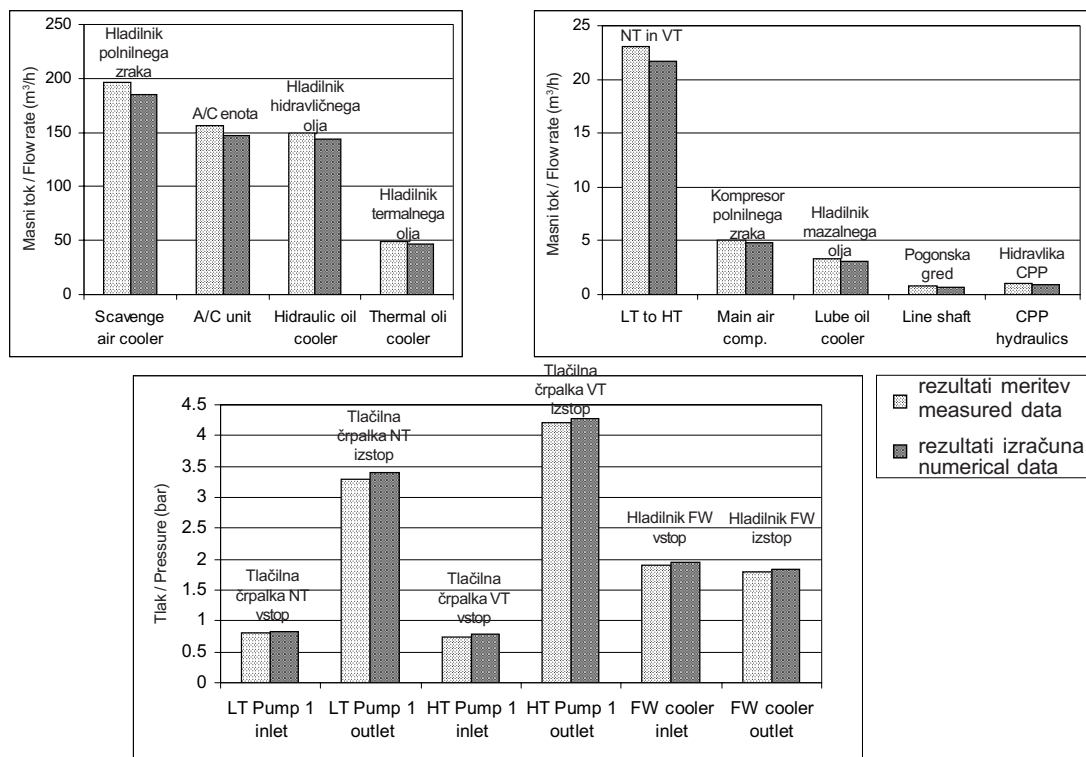
Sl. 6. Shema hladilnega sistema pogonskega sistema na ladji
Fig. 6. Example of the layout of a marine cooling system

tem mislimo predvsem na vrednosti masnih tokov in ustreznih tlakov v nadzornih točkah hladilnega sistema. Na sliki 7 so prikazani rezultati primerjavi med izračunanimi in izmerjenimi rezultati preizkusov na ladji. Pri preizkušanjih so bili podatki zajeti šele, ko je bilo doseženo ustaljeno temperaturno stanje pri določeni izbrani moči pogonskega motorja oziroma celotnega postroja.

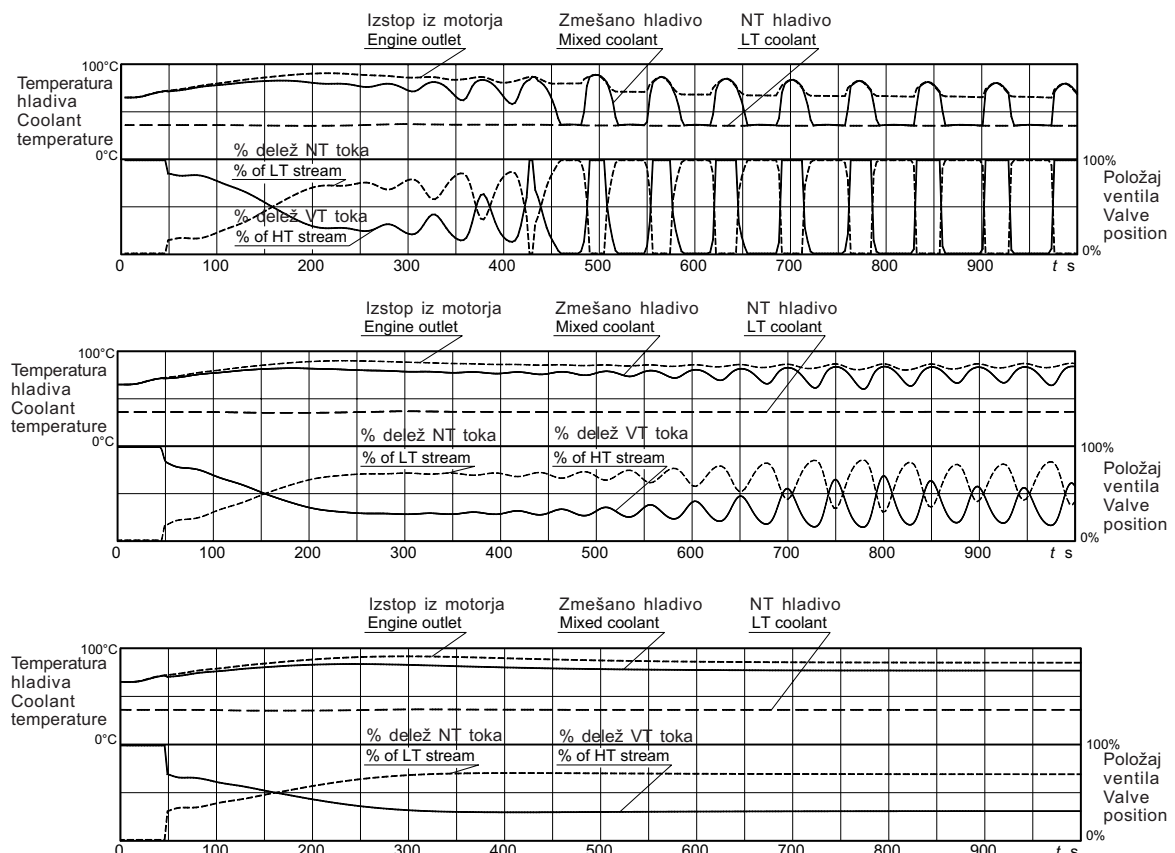
Med delovanjem motorja je bilo opazovano tudi nihanje masnih tokov vode v ceveh, ki povezujejo oba hladilna kroga. Posebej težavna naloga je bila določitev časovnega poteka lege povezovalnih členov med obema hladilnima krogoma, še posebej zaradi različnih tlačnih ravni obeh krogov. Zato je zelo pomembno, da je tlačna razlika na obeh koncih povezovalnega voda ustreza, saj tako zagotavlja ustrezen tok hladilne vode in s tem tudi ustrezen količino odvedene toplotne. Rezultati numeričnega modeliranja so pokazali, da je lega cevne povezave med obema hladilnima krožnima tokovoma pravilno izbrana, da pa je za izrazita prenihanja kriva predvsem nastavitev krmilnika, ki upravlja termostatski ventil. Opravljeni so bili še različni primeri izračunov za različne nastavitev krmilnika termostatskega ventila, rezultati pa so prikazani na sliki 8. Izbira - nastavitev temperatur v obeh hladilnih krogih je bila enaka tisti, ki smo jo navedli v prvem primeru. Začetek simulacije upošteva hladni zagon pogonskega motorja in temperaturo "vroeče vode" (VT) 65 °C. Zgornji diagram prikazuje premočni vpliv sorazmernega in prešibek vpliv integracijskega člena krmilnika termostatskega ventila. Spodnji in tretji diagram kažeta vpliv popravka krmilnih parametrov in doseganje želenega stanja v hladilnem krogu VT.

in the characteristic points of the cooling system. Fig.7 shows a comparison between the numerical model results and the measured data during one sea trial. During the sea trial the values are measured after the temperatures and other parameters have reached steady values for a given power output of the main engine, or in other words, for steady-state conditions of the propulsion plant.

A fluctuation of the flow rates in the pipes that connect two cooling circuits was observed during the measurement. It is not an easy task to determine the right positions for the connections between two cooling circuits, especially when they work at different pressure levels. It is essential that the pressure difference between two points of the connecting pipe must be sufficient to provide adequate fluid exchange between the two cooling circuits. In this case, the numerical model showed that the connecting pipes are well positioned and that the cause of the fluctuations was in the controller adjustments, which is responsible for the thermostatic valve behaviour. Further analysis with different controller parameters was performed and the obtained results are shown in Fig.8. The temperatures of the cooling circuits are set as described earlier. The simulation started with a cold engine and the high-temperature (HT) coolant at 65°C. The first diagram shows a too strong proportional and a weak integral component of the HT thermostatic valve controller. The second and third diagrams show a correction of the controller parameters and achieving the desired behaviour of the HT cooling circuit.



Sl. 7. Primerjava med izračunanimi in izmerjenimi rezultati
Fig. 7. Comparison of numerical and measured data



Sl. 8. Vpliv krmilnih parametrov na odzivnost hladilnega sistema
Fig. 8. Influence of controller parameters on cooling-system behaviour

3 UPORABA NUMERIČNEGA MODELJA ZA DOLOČITEV HLADELNIH SISTEMOV CESTNIH VOZIL

Prilagodljivost predstavljenega numeričnega modela omogoča uspešno uporabo tudi pri določanju hladilnih sistemov cestnih vozil. Seveda je treba uvesti določene značilnosti in razviti ustrezne dodatne sestavne modele, npr.:

- model prenosnika toplotne zrak - voda
- model obtočne, mehansko gnane črpalk za vodo
- model termostata

Cevi, ki povezujejo osnovne dele hladilnega sistema vozil, so opazno krajše, tokovi hladilne tekočine so majhni, zato je odzivnost takšnega sistema na spremembe sorazmerno hitra. Sistem ima tudi manjšo toplotno vztrajnost, zato je treba določiti bolj podroben sistem odvoda toplotne iz motorja. Način določanja masnih tokov, tlačnih izgub v cevovodih ostaja nespremenjen, dodatno pa je treba upoštevati še dejstvo, da sta motor in hladilnik glavna vira toplotnih izgub.

Na podlagi zgoraj opisanih dejstev lahko povzamemo, da lahko opisani numerični model uspešno uporabimo pri določitvi ladijskih in drugih hladilnih sistemov za hlajenje motorjev, le ustrezne dodatne modele je treba dodati osnovnemu modelu.

4 SKLEPI

Brez predhodne uporabe rezultatov numeričnega modeliranja v začetni fazi načrtovanja hladilnega sistema motorja bi za določitev sestavnih delov in njihovega skupnega delovanja porabili zelo veliko časa. Zaradi varnosti se v približnih rešitvah pogosto uporabi prevelike agregate, ki sicer zagotavljajo varno delovanje, vendar se kasneje v fazi prilaganja dejanskim razmeram s postopki dušenja in dodatnih obvodov vnašajo nepotrebne velike izgube energije.

Prednost predstavljeni metode je v natančni določitvi masnih tokov in tlačnih padcev v vsaki točki hladilnega sistema za ustaljene in prehodne načine delovanja. Zelo preprosto je tudi mogoče ugotoviti vpliv posameznih komponent in njihovih parametrov na delovanje celotnega hladilnega sistema. To je zelo pomembno v primerih, ko je treba določiti delovanje hladilnega sistema pri hitrem izklapljanju obtočne črpalki, hladilnika, ali celo pri ustavitvi motorja.

Z uporabo predstavljenega numeričnega modela lahko spremljamo časovno spremembo hladilnih parametrov tudi v prehodnih režimih delovanja. V prispevku obravnavani računski primer je pokazal, da je mogoče s pomočjo izračunov izbrati in optimirati celo krmilne parametre termostatskega ventila.

Prikazani model je skratka vsestransko uporaben za snovanje in preverjanje različnih hladilnih sistemov, ki so povezani z motorji z notranjim zgorevanjem.

3 APPLICATION OF THE DEVELOPED NUMERICAL MODEL TO THE COOLING SYSTEMS OF VEHICLE ENGINES

The flexibility of the presented numerical model allows it to be applied to the cooling systems of vehicle engines. However, there are some differences that require minor changes to the presented model and require the creation of additional numerical submodels for the following components:

- air-to-fluid heat exchangers,
- engine-driven centrifugal pump,
- thermostat.

The pipes between the vehicle's cooling-system components are short and there is less cooling fluid than in a marine cooling system, so the response of such a system is relatively fast. Due to the smaller thermal inertia of the whole cooling system, a more detailed engine-heat release model should be used. The method and the principle of the flow rate and pressure drop calculations in the pipeline remain the same, but in this case the engine and the radiator generate the majority of the heat losses.

From these facts it can be concluded that the developed numerical model can be applied to marine, vehicle or any other engine-cooling system, including adequate numerical submodels of the system components.

4 CONCLUSION

If the initial design of a cooling system is performed without the help of an appropriate numerical model and computer, a lot of time will be spent for extensive calculations due to iterative nature of this problem. As a result, an approximate solution is obtained and the designer usually chooses over-dimensioned pumps to satisfy design requirements with a safety margin. In this case, the required flow rates and pressures are obtained with some damping device or bypass giving high energy losses.

The advantage of the presented numerical model is the precise determination of flow rates and pressure drops at any desired point of the cooling system during steady-state and transient operation. This is very helpful in primary designs. Also, it is easy to investigate how the change of any design parameter influences the behaviour of the whole cooling system. This is especially important for simulation of emergency situations when pump, heat exchanger or even the main engine must be shut down.

Transients that occur during any change of stationary working point are easily monitored. It was shown in the paper that such a numerical model can even be used for setting the thermostatic valve controller.

The presented numerical model can also be used for different optimisations of the cooling system.

5 LITERATURA
5 REFERENCES

- [1] Teixeira, A. (2002) Marine pumping system design based on pipe network analysis methods, *Congress Proceedings IMAM 2002*, Rethymnon Crete, Greece.
- [2] Raju, K.S.N., J.C. Bansal (1983) Design of plate heat exchangers, *Hemisphere Publishing*, Washington, DC, 913–932.
- [3] Holger, M. (1996) A theoretical approach to predict the performance of chevron-type plate heat exchangers, *Chemical Engineering and Processing*, Vol 35, 301-310.
- [4] Recknagel, H., E. Sprenger, V. Hönnemann (1985) Taschenbuch für Heizung und Klimatechnik, *R. Oldenbourg Verlag*, München.
- [5] Streeter, W.L. (1985) Fluid mechanics, *McGraw-Hill*.
- [6] Stoecker, W.F. (1989) Design of thermal systems, *McGraw-Hill*, 3rd edition.

Naslov avtorjev: Tomislav Mrakovčić
prof.dr. Vladimir Medica
dr. Nedjeljko Škifić
Sveučilište u Rijeci
Tehnički fakultet
Vukovarska 58
51000 Rijeka, Hrvatska
tomica@riteh.hr

Authors' Address: Tomislav Mrakovčić
Prof.Dr. Vladimir Medica
Dr. Nedjeljko Škifić
University of Rijeka
Faculty of Engineering
Vukovarska 58
51000 Rijeka, Croatia
tomica@riteh.hr

Prejeto: 11.11.2003
Received: 11.11.2003

Sprejeto: 8.4.2004
Accepted: 8.4.2004

Odprto za diskusijo: 1 leto
Open for discussion: 1 year

Metoda robnih elementov v akustiki - primer ovrednotenja zvočnega polja enosmernega elektromotorja

The Boundary-Element Method in Acoustics - an Example of Evaluating the Sound Field of a DC Electric Motor

Martin Furlan · Miha Boltežar

V prispevku so predstavljeni osnovni prijemi za reševanje zunanjih akustičnih problemov z metodo robnih elementov (MRE) ter njena izvedba v programu za reševanje trirazsežnih problemov. Prikazana je tudi integracija programa v komercialni programske paket metode končnih elementov (MKE), ki osnovno rabi kot orodje za določitev strukturnega odziva oz. vzroka za zvočno polje, drugotno pa za pripravo in kasnejšo obdelavo akustičnega modela. Program MRE je ovrednoten na akustičnem problemu, pri katerem je poznana analitična rešitev. Sama ovrednotitev je izvedena s poudarkom na raziskavi vpliva gostote diskretizacije na natančnost izračuna zvočnega polja. Poleg tega je zaradi narave numeričnega problema oz. sistema linearnih enačb, ki pri tem nastane, ovrednotena tudi hitrost reševanja problema glede na izbiro postopka reševanja sistema linearnih enačb. Prikazana je tudi uporaba izvedenega programa MRE na dejanskem primeru. Na podlagi strukturnega odziva enosmernega elektromotorja, ki smo ga dobili kot posledico harmoniskega vzbujanja magnetnih sil z MKE, smo ovrednotili zvočno polje v okolini enosmernega elektromotorja.

© 2004 Strojniški vestnik. Vse pravice pridržane.

(Ključne besede: akustika, metode robnih elementov, hrup, dinamika struktur)

This paper presents a basic approach to solving exterior acoustic problems using the boundary-element method (BEM) and the development of a BEM program for solving three-dimensional (3D) problems. It also shows the integration of the developed BEM program into a finite-element method (FEM) program, which is primarily used to evaluate the structural response that generates a sound field, but can also be used to pre-process and post-process the acoustic model. The program was verified by using an acoustic problem for which the analytical solution was already known. The verification was performed by researching the influence of the discretization density on the accuracy of the numerically defined sound field. In addition to this, we also evaluated the time necessary to solve the problem and its system of linear equations, and related it to the method chosen for solving this system of linear equations. The program was applied to a real case where the sound field of a DC electric motor was calculated using the BEM. Based on the structural response of the DC electric motor that is the result of the harmonic excitation of magnetic forces, and was calculated with the FEM, we evaluated the sound field surrounding the DC electric motor.

© 2004 Journal of Mechanical Engineering. All rights reserved.

(Keywords: acoustics, boundary-element method, noise, structural dynamics)

0 UVOD

Metoda robnih elementov (MRE) je orodje, ki se lahko uporablja tudi za ovrednotenje zvočnega polja kot posledice gibanja kompaktnih teles ali vibracij na njihovi površini. MRE je posebej učinkovita pri reševanju tako imenovanih zunanjih akustičnih problemov, to je sevanju zvoka v neomejenem zvočnem polju oz./ali prostem zvočnem polju. V takem primeru so druge metode, npr. metoda

0 INTRODUCTION

The boundary-element method (BEM) is a numerical tool that can be used for evaluating the sound field that results from the movement of compact bodies or due to the vibrations on their surfaces. The BEM is especially effective for solving so-called exterior acoustic problems, where the unbounded acoustic domain or free field is considered. In this case the finite-element method

končnih elementov (MKE) ali metoda končnih razlik (MKR) zaradi potrebe po diskretizaciji celotnega obravnavanega območja numerično bistveno bolj zahtevne od MRE in zato manj primerne ali celo neuporabne. Poleg tega omenjene metode zahtevajo posebej pazljivo obravnavo vpliva neomejenosti zvočnega polja. Nasprotro pa se pri obravnavi takih problemov MRE ponuja sama po sebi, saj že v temelju odpravlja omenjeni problem in zahteva diskretizacijo le na površini telesa, kar zelo zmanjša čas za pripravo modela in za njegovo numerično reševanje.

V nadaljevanju so opisani osnovni prijemi za reševanje zunanjih akustičnih problemov z uporabo MRE ter izvedba MRE v programu za reševanje trirazsežnih problemov. Prikazana je tudi integracija izvedenega programa v programske paket MKE ANSYS, ki je namenjena za pripravo izhodnih podatkov in kasnejšo obdelavo rezultatov akustičnega modela. Izveden program je ovrednoten na akustičnem problemu, pri katerem je poznana analitična rešitev. Sama verifikacija je izvedena s poudarkom na raziskavi vpliva gostote diskretizacije na natančnost izračuna spremenljivk zvočnega polja.

1 DEFINICIJA PROBLEMA AKUSTIKE

Širjenje zvočnega valovanja skozi tekočino opisuje valovna enačba (1). Le-ta vsebuje eno samo akustično spremenljivko, zvočni tlak p , in velja za širjenje valovanja skozi poljuben posrednik, pri čemer je c hitrost širjenja valovanja v posredniku.

$$\nabla^2 p(\mathbf{r}, t) - \frac{1}{c^2} \ddot{p}(\mathbf{r}, t) = 0 \quad (1).$$

Valovna enačba (1) ima lahko različne rešitve, ki so odvisne od oblike valovnih čel v prostoru oz. oblike in karakteristike meje tekočine in porazdelitve vira zvoka. V večini primerov ne poznamo analitičnih rešitev zanjo, ker so viri in njegove meje pogosto zapletenih oblik ali celo neznane. Analitične rešitve obstajajo le za nekatere zelo preproste oblike zvočnih valov, to so ravni, krogelni ali cilindrični val. Če predpostavimo, da se zvočni tlak in hitrost gibanja delcev v posredniku spreminja s časom harmonično:

$$p = \hat{p} e^{i\omega t}, \mathbf{v} = \hat{\mathbf{v}} e^{i\omega t} \quad (2),$$

lahko valovno enačbo (1) zapišemo v skrčeni obliki,

$$\nabla^2 \hat{p} + k^2 \hat{p} = 0 \quad (3),$$

ki ne vsebuje več odvoda po času. Enačbo (3) imenujemo tudi Helmholtzova valovna enačba, kjer je k akustično valovno število in velja $k^2 = \omega^2/c^2$. Z namenom poenostavitev pri numerični obravnavi akustičnih problemov vpeljemo pojmom hitrostnega potenciala ϕ . Ta omogoča, da tako zvočni tlak kakor

(FEM), the difference method (DM) and other similar methods are numerically more demanding, due to the need for a discretization of the whole domain under consideration. In some cases these methods can also prove to be ineffective; moreover, they need special consideration because of the effect of the unbounded acoustic field. In contrast, the BEM itself solves this problem, meaning that only the boundary needs to be discretized, and this shortens the time necessary for preparing the model and solving the problem.

This paper describes the BEM for solving exterior acoustic problems and the development of the BEM program for solving three-dimensional (3D) problems. The integration of the developed BEM program into the FEM software ANSYS, which is used for pre-processing and post-processing of the acoustic BEM models, is also presented. The developed program is verified and the verification is based on an acoustic problem with a known exact solution. The verification gives special emphasis to the influence of the discretization on the accuracy.

1 DEFINITION OF THE ACOUSTIC PROBLEM

The sound radiation through a fluid medium is described by the wave equation (1), which includes only one acoustic variable, the sound pressure p . The wave equation is valid for any acoustic medium, where c is the speed of sound in this medium.

The solution of the wave equation (1) depends on the distribution of the sound source and on the shape and the characteristics of the boundary of the acoustic medium, which all together define the acoustic waves. In most cases the exact analytical solution is unknown as both the source and the boundary have complicated or even unknown shapes. The exact analytical solution exists only for very simple sound waves, like planar, cylindrical or spherical waves. If we assume that the sound pressure and the velocity in the medium change harmonically with time:

the wave equation (1) can be formulated in a reduced form,

that does not include a time derivative. Equation (3) is also known as the Helmholtz wave equation, where k is the acoustic wave number defined as $k^2 = \omega^2/c^2$. When a numerical approach to the sound field is needed, the introduction of the velocity potential ϕ is convenient, as both the sound pressure and the

hitrost izračunamo neposredno iz hitrostnega potenciala ϕ , ki je definiran z:

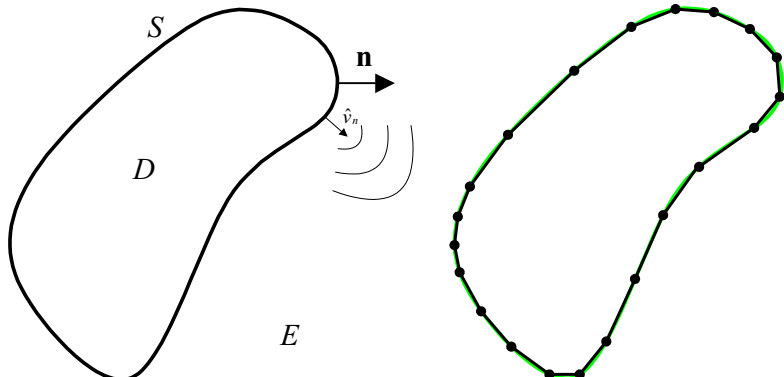
$$\hat{p} = i\omega\rho\phi, \text{ kar da/that gives } \hat{\mathbf{v}} = \nabla\phi \quad (4).$$

Z uporabo hitrostnega potenciala lahko Helmholtzovo valovno enačbo zapišemo v obliki:

$$\nabla^2\phi + k^2\phi = 0 \quad (5).$$

1.1 Reševanje Helmholtzove valovne enačbe

V splošnem lahko razdelimo akustične probleme kakor tudi reševanje akustične valovne enačbe na: *notranji akustični problem, zunanj akustični problem ter problem lastnih vrednosti*. V našem primeru se bomo omejili na reševanje zunanjega akustičnega problema. Slika 1 prikazuje osnovno obliko, ki je potrebna za definiranje takega problema. Na njej je prikazano neomejeno zunanje območje E , ki objema površino S z zunanj normalo \mathbf{n} , ter omejeno notranje območje D .



S. 1. Oblika zunanjega akustičnega problema (na levi) in njegova diskretizacija (na desni)
Fig. 1. Definition of the exterior acoustic problem (on the left) and its discretization (on the right)

Ker gre v omenjenem problemu za akustično analizo neomejenega zvočnega polja, mora v oddaljenem zvočnem polju veljati Sommerfeldov sevalni pogoj ([1] do [4]), ki opisuje zmanjševanje zvočnega tlaka z oddaljenostjo od vira. Posledica Sommerfeldovega pogoja je, da v fizikalni rešitvi za oddaljeno zvočno polje dopušča le tako valovanje, ki se od vira oddaljuje:

$$\lim_{r \rightarrow \infty} r \left(\frac{\partial \hat{p}}{\partial r} - ik\hat{p} \right) = 0 \quad (6).$$

Rešitev Helmholtzove valovne enačbe je v našem primeru opredeljena z le Neumannovim robnim pogojem, ki opisuje gibanje delcev tekočine tik ob površini:

$$\frac{\partial \phi}{\partial n} = \hat{v}_n, \quad \hat{v}_n = \mathbf{n} \cdot \hat{\mathbf{v}} \quad (7),$$

velocity can be calculated from it directly. The velocity potential ϕ is defined as:

With the use of the velocity potential ϕ the Helmholtz wave equation can be reformulated as:

1.1 Solving the Helmholtz wave equation

In general, acoustic problems and the solution of the wave equation can be divided into the following: *an interior acoustic problem, an exterior acoustic problem and an eigenvalue problem*. In our case we are limited to the exterior acoustic problems only. Figure 1 shows a definition of the acoustic problem for an object with an infinite exterior domain E that surrounds surface S with an outward normal \mathbf{n} and an interior domain D .

The exterior acoustic problem is related to the unbounded medium and therefore the Sommerfeld radiation condition, which describes the relation between the sound pressure and the distance from the source, should be applied in the far field ([1] to [4]). The consequence of the Sommerfeld radiation condition is a physical solution to the sound field that is limited to a wave that travels away from the source:

The solution of the Helmholtz wave equation of the investigated problem is in our case defined only by the Newmann boundary condition, which describes the velocity in the medium at the surface S :

kjer je \hat{v}_n hitrost točke na površini v smeri normale \mathbf{n} . Osnovna rešitev skrčene oblike valovne enačbe (5), ki zadostuje Sommerfeldovemu sevalnemu pogoju, je Greenova funkcija:

$$G_k(P, Q) = \frac{e^{ikr}}{4\pi r}, \quad r = |P - Q|, \quad \nabla^2 G_k(P, Q) + k^2 G_k(P, Q) = -\delta(P, Q) \quad (8)$$

kjer sta $\delta(P, Q)$ Diracova funkcija in r evklidska razdalja med točkama P in Q v zvočnem polju, tako v območju E kakor tudi na površini S .

1.2 Helmholtzovi integralski operatorji

V enačbah (9) do (12) so zapisane definicije integralskih operatorjev Helmholtzove valovne enačbe. Vsi navedeni operatorji so rešitve valovne enačbe (5) ob predpostavki zvezne porazdelitve vira z amplitudo $\phi(Q)$ na sevalni površini S ([2] in [3]).

where \hat{v}_n is the velocity of the surface S in the direction of the surface's outward normal \mathbf{n} . The fundamental solution of the reduced form of the wave equation (5) that satisfies the Sommerfeld radiation condition is the Green's function:

where $\delta(P, Q)$ is the Dirac delta function, r is Euclidian distance between the points P and Q in the exterior domain E or on the surface S .

1.2 Helmholtz integral operators

The equations (9) to (12) define the Helmholtz integral operators. All the presented operators are the solution of the Helmholtz wave equation (5), where the distribution of the source on the surface S , with the amplitude of $\phi(Q)$, is considered to be continuous ([2] and [3]):

$$L_k[\phi](P) = \int_S G_k(P, Q) \phi(Q) dS \quad (9)$$

$$M_k[\phi](P) = \int_S \frac{\partial G_k(P, Q)}{\partial n_Q} \phi(Q) dS \quad (10)$$

$$M_k^T[\phi](P) = \int_S \frac{\partial G_k(P, Q)}{\partial n_P} \phi(Q) dS \quad (11)$$

$$N_k[\phi](P) = \int_S \frac{\partial G_k(P, Q)}{\partial n_P \partial n_Q} \phi(Q) dS \quad (12)$$

in operator istovetnosti:

and the identity operator:

$$I[\phi](P) = \phi(P) \quad (13)$$

1.3 Integralska oblika Helmholtzove valovne enačbe

Z upoštevanjem prvega Greenovega izreka na prostorninskem integralu Helmholtzove valovne enačbe po širšem zunanjem območju E , ki objema zvočni vir D , dobimo zapis enačbe kot integral na površini S , imenovan tudi *površinska Helmholtzova integralska enačba* ([2] in [3]):

$$\int_S \left(\phi(Q) \frac{\partial G_k(P, Q)}{\partial n_Q} - \frac{\partial \phi(P, Q)}{\partial n_Q} G_k(P, Q) \right) dS = c(P) \phi(P) \quad (14)$$

kjer je $c(P)$ faktor lege točke P , določen tudi z enačbo (15) ([2] in [3]):

$$c(P) = \begin{cases} 1 & P \in E \\ \frac{1}{2} & P \in S \\ 0 & P \in D \end{cases} \quad (15)$$

Za enačbo (15) mora veljati, da je površina S v točki P gladka. Površinsko Helmholtzovo integralsko enačbo (14) lahko zapišemo tudi v obliki z integralskimi operatorji ([2] in [3]):

1.3 Integral formulation of the Helmholtz wave equation

Considering the Green's formula, the volume integral of the Helmholtz wave equation over an extended exterior domain E , that completely surrounds the sound source D , a new formulation, the so-called *surface Helmholtz integral equation*, is introduced as a surface integral on the surface S ([2] and [3]):

where $c(P)$ is a jump term, which is defined by the position of the point P , see equation (15) ([2] and [3]).

Equation (15) should be valid if the surface S is to be smooth at the point P . In terms of the integral operators the surface Helmholtz integral equation (14) can be given by ([2] and [3]):

$$L_k \frac{\partial \phi}{\partial n} = [-c(P)I + M_k] \phi \quad (16).$$

Odvod površinske Helmholtzove integralske enačbe (14) po normali na površini S da nov izraz, enačba (17), imenovan *diferencirana površinska Helmholtzova integralska enačba*, ki ga uporabljamo pri upoštevanju robnih pogojev ([2] in [3]):

$$\int_S \left(\phi(Q) \frac{\partial^2 G_k(P, Q)}{\partial n_Q \partial n_P} - \frac{\partial \phi(P, Q)}{\partial n_Q} \frac{\partial G_k(P, Q)}{\partial n_P} \right) dS = c(P) \frac{\partial \phi(P)}{\partial n_P} \quad (17).$$

Tako kakor osnovno obliko površinske Helmholtzove integralske enačbe (14) lahko tudi njeno diferencirano obliko zapišemo z integralskimi operatorji ([2] in [3]):

$$N_k \phi = [-c(P)I + M_k^T] \frac{\partial \phi}{\partial n} \quad (18).$$

Ker obe formulaciji Helmholtzove integralne enačbe (16) in (18) nimata enolične rešitve za določena akustična valovna števila, sta Burton in Miller vpeljala nov zapis ([1] in [3]), njuno linearno kombinacijo, ki izloči vpliv nestabilnih akustičnih valovnih števil:

$$\langle \alpha [-c(P)I + M_k] + \beta N_k \rangle \phi = \left\{ \alpha L_k + \beta [c(P)I + M_k^T] \right\} \frac{\partial \phi}{\partial n} \quad (19),$$

kjer je vrednost faktorjev α in β odvisna od valovnega števila, in sicer $\alpha=1$ ter $\beta=i/k$ za vrednosti $k \geq 1$ in ter $\beta=i$ za vrednosti $k < 1$ ([1] in [3]).

1.4 Zapis problema MRE

Burton–Millerjev zapis Helmholtzove integralske enačbe (19) z integralskimi operatorji je osnova za postavitev MRE za reševanje zunanjih akustičnih problemov. Sprememba problema v zapis MRE temelji na diskretizaciji površine S z robnimi elementi (sl. 1). Površino S poenostavimo z diskretizirano površino, ki je sestavljena iz n površin robnih elementov. Podobno je treba diskretizirati tudi funkcijo hitrostnega potenciala ϕ z interpolacijsko funkcijo, ki pomeni njen ustrezek na diskretiziranem območju. V našem primeru je interpolacijska funkcija konstanta in ima po celotnem elementu vrednost 1. Ob vseh zgoraj navedenih predpostavkah lahko določimo približno vrednosti za integralske operatorje.

Reševanje zunanjega akustičnega problema je v splošnem sestavljeno iz dveh delov. Prvi del vključuje reševanje integralne enačbe (19) na območju S , kjer je roben pogoj definiran kot $\partial \phi(P)/\partial n_Q = \hat{v}_n(P)$ pri pogoju $P \in S$. Rešitev je hitrostni potencial $\phi(P)$ za točke P na površini S . Drugi del vključuje določitev hitrostnega potenciala $\phi(P)$ za točke P , ki ležijo v zunanjem območju E , in temelji na uporabi površinske Helmholtzove integralske enačbe (16).

With the differentiation of the surface Helmholtz integral equation (14) with respect to the normal to the surface S , we get a new formulation, Equation (17), the so-called *differentiated surface Helmholtz integral equation*, which is used when boundary conditions need to be taken into account ([2] and [3]):

Like the surface Helmholtz integral equation, its differentiated formulation, Equation (17), can also be written with the Helmholtz integral operators ([2] and [3]):

$$N_k \phi = [-c(P)I + M_k^T] \frac{\partial \phi}{\partial n} \quad (18).$$

As both formulations of the Helmholtz integral equations (16) and (18) do not have unique solutions for specific wave numbers, Burton and Miller introduced a new formulation ([1] and [3]). Their linear combination that eliminates the effect of instable wave numbers is:

$$\langle \alpha [-c(P)I + M_k] + \beta [c(P)I + M_k^T] \rangle \phi = \left\{ \alpha L_k + \beta [c(P)I + M_k^T] \right\} \frac{\partial \phi}{\partial n} \quad (19),$$

where the values of the factors α and β depend on the wave number: $\alpha=1$ and $\beta=i/k$ for wave numbers $k \geq 1$ and $\beta=i$ for wave numbers $k < 1$ ([1] and [3]).

1.4 Formulation of the BEM problem

The Burton–Miller formulation of the Helmholtz integral equation (19), written by integral operators, represents a basis for the BEM formulation for solving exterior acoustic problems. Its transformation into the BEM formulation is based on the discretization of the surface S with boundary elements, see Figure 1. The surface S is approximated by a discretized surface that consists of n boundary elements. Consequently, it is also necessary to discretize the velocity potential function ϕ by an interpolation function that represents its equivalent on the discretized surface. In our case a constant interpolation function that has a constant value of one over the entire boundary element was chosen. Taking into account all the above-mentioned assumptions, the approximation of the integral operators can be completed.

Generally, the solution of an exterior acoustic problem can be divided into two steps. The first step includes the solution of the integral equation (19) on the boundary S , where the boundary condition is defined as $\partial \phi(P)/\partial n_Q = \hat{v}_n(P)$ where $P \in S$. Its solution is the velocity potential $\phi(P)$ for points P on the surface S . The second step includes the calculation of the velocity potential $\phi(P)$ for points P that lie in the exterior domain E and is based on the usage of the surface Helmholtz integral equation (16).

Z uporabo kolokacijske metode in diskretizacije območja lahko diskretizirane Helmholtzove integralske operatorje, kot interakcije med i -to kolokacijsko točko z j -tim elementom, zapišemo v obliki matrik \mathbf{L}_k , \mathbf{M}_k , \mathbf{M}_k^T in \mathbf{N}_k z izmero $n \times n$. Podobno lahko v vektorski obliki zapišemo tudi aproksimacijsko funkcijo za hitrostni potencial v kolokacijskih točkah robnih elementov Φ .

Z uvedbo kolokacijske metode na Burton-Millerjevem zapisu Helmholtzove integralske enačbe (19) dobimo matrično enačbo za rešitev akustičnega problema z MRE:

$$\{\alpha[\mathbf{M}_k - \frac{1}{2}\mathbf{I}] + \beta\mathbf{N}_k\}\Phi = \{\alpha\mathbf{L}_k + \beta[\mathbf{M}_k^T + \frac{1}{2}\mathbf{I}]\}\mathbf{v} \quad (20),$$

kjer je \mathbf{v} vektorski zapis robnih pogojev – normalnih hitrosti v kolokacijskih točkah robnih elementov, $\mathbf{v}=[\hat{v}_n(P_1), \dots, \hat{v}_n(P_n)]^T$. Rešitev matrične enačbe vodi k aproksimativni določitvi hitrostnega potenciala v kolokacijskih točkah robnih elementov, $\Phi=[\phi(P_1), \dots, \phi(P_n)]$, in pomeni prvi del reševanja zunanjega akustičnega problema. Fizikalna interpretacija tako dobljenega hitrostnega potenciala je zvočni tlak tik ob površini S , $\mathbf{p}=[(1/i\omega\rho)\phi(P_1), \dots, (1/i\omega\rho)\phi(P_n)]^T=(1/i\omega\rho)\Phi$. V drugem delu reševanja zunanjega akustičnega problema z MRE, ko imamo znano aproksimativno rešitev hitrostnega potenciala na diskretizirani površini, določimo aproksimativno rešitev hitrostnega potenciala zunanjih točk $\phi(P)$ za $P \in E$. Rešitev lahko izvedemo za poljubno število točk P , ki ležijo v zunanjem območju E . V ta namen uporabimo diskretiziran zapis enačbe (16) pri pogoju, da točke P ležijo v zunanjem območju E . Določitev hitrosti v točkah zunanjega območja lahko izvedemo z numeričnim odvajanjem hitrostnega potenciala ali pa neposredno z izračunom parcialnega odvoda hitrostnega potenciala po želenem smernem vektorju \mathbf{n} . V slednjem primeru uporabimo diskretizirano obliko diferencirane površinske Helmholtzove integralske enačbe (18).

2 IZVEDBA MRE

Za reševanje splošnih trirazsežnih zunanjih akustičnih problemov z MRE smo v programskem paketu *DIGITAL Visual Fortran 6.0* razvili program, ki omogoča integracijo v programske pakete MKE za reševanje problemov iz strukturne dinamike, kakršen je npr. *ANSYS* ipd. Pri izračunu diskretnih Helmholtzovih integralskih operatorjev smo izhajali iz že izvedenih podprogramov avtorja Kirkupa [2]. Za diskretizacijo trirazsežnega problema smo uporabili trikotne elemente. Reševanje problema smo razdelili v dva dela.

V prvem delu reševanja problema MRE se opravi izračun diskretnih Helmholtzovih integralskih operatorjev, čemur sledi sestavljanje matrične enačbe (20) in nazadnje njen reševanje. Z upoštevanjem razmerja

Using the collocation method, the discretized Helmholtz integral operators, as the interaction between the collocation point with an index i and the boundary element with an index j , can be written with the matrices \mathbf{L}_k , \mathbf{M}_k , \mathbf{M}_k^T and \mathbf{N}_k that have the dimensions $n \times n$. Similarly, the velocity potential approximation can also be written as a vector Φ in the collocation points of the boundary elements.

Applying the collocation method to the Burton-Miller formulation of the Helmholtz integral formulation (19) we get a matrix equation that describes the BEM formulation of the acoustic problem:

$$\{\alpha[\mathbf{M}_k - \frac{1}{2}\mathbf{I}] + \beta\mathbf{N}_k\}\Phi = \{\alpha\mathbf{L}_k + \beta[\mathbf{M}_k^T + \frac{1}{2}\mathbf{I}]\}\mathbf{v} \quad (20),$$

where \mathbf{v} is the vector of the boundary conditions – normal velocities in the collocation points of the boundary elements, $\mathbf{v}=[\hat{v}_n(P_1), \dots, \hat{v}_n(P_n)]^T$. The solution of this equation gives the approximation of the velocity potential in the collocation points of the boundary elements and represents the first step in the solution of the exterior acoustic problem. The physical interpretation of the calculated velocity potential is the sound pressure at the surface S , $\mathbf{p}=[(1/i\omega\rho)\phi(P_1), \dots, (1/i\omega\rho)\phi(P_n)]^T=(1/i\omega\rho)\Phi$. In the second step of the solution to the exterior acoustic problem with the BEM, the velocity potential $\phi(P)$, where $P \in E$, is calculated. This calculation is based on the previously calculated velocity potential on the discretized surface. The calculation of the velocity potential can be made for any number of points P that lie in the exterior domain E , using the discretized formulation of Equation (16), for which it is assumed that the point P lies in the exterior domain E . The velocities at the points of the exterior domain can be calculated either by numerical differentiation, or directly, by using the discretized formulation of the differentiated surface Helmholtz integral Equation (18), where the partial differentiation of the velocity potential with respect to the desired directional vector \mathbf{n} is considered.

2 DEVELOPMENT OF THE BEM PROGRAM

To solve the 3D exterior acoustic problems with the BEM we developed a computer program, using *DIGITAL Visual Fortran 6.0*, that can be integrated into any FEM software, e.g. *ANSYS*, intended for solving structural dynamic problems. The evaluation of the discretized Helmholtz integral operators is made with Kirkup's [2] subroutines. The discretization of the 3D problem is made with triangular elements. The problem's solution procedure is divided into two steps.

In the first step the discrete Helmholtz integral operators are calculated, this is followed by the composition of the matrix equation (20), and finally the matrix equation is solved. Regarding the relation between the velocity potential and the sound

med hitrostnim potencialom in zvočnim tlakom v enačbi (2) lahko enačbo (20) zapišemo v poenostavljeni obliki:

$$\mathbf{H} \cdot \mathbf{p} = i\omega\rho \mathbf{G} \cdot \mathbf{v} \quad (21).$$

Rešitev matrične enačbe (21) je zvočni tlak \mathbf{p} na robu diskretizirane površine oz. v kolokacijskih točkah robnih elementov. V drugem delu reševanja se na podlagi poznavanja zvočnega tlaka \mathbf{p} in robnih pogojev – normalnih hitrosti \mathbf{v} na robu diskretizirane površine z diskretiziranimi oblikami Helmholtzovih integralnih enačb (16) in (18) določi zvočni tlak $\mathbf{p}_E = [(1/i\omega\rho)\phi(P_1), \dots, (1/i\omega\rho)\phi(P_m)]^T = (1/i\omega\rho)\Phi_E$ in hitrosti $\mathbf{v}_E = [\hat{v}_n(P_1), \dots, \hat{v}_n(P_m)]^T$ za množico točk zunanjega območja, ki ležijo v zunanjem območju E . Poenostavljen matrični zapis omenjenih enačb za določitev rešitev v zunanjem območju se tako glasi:

$$\mathbf{p}_E = \mathbf{h}^T \cdot \mathbf{p} - i\omega\rho \mathbf{g}^T \cdot \mathbf{v} \quad (22),$$

$$\mathbf{v}_E = \mathbf{h}_v^T \cdot \mathbf{p} - i\omega\rho \mathbf{g}_v^T \cdot \mathbf{v} \quad (23).$$

V nasprotju s prvim delom reševanja, pri katerem gre za iskanje rešitve na robu in je treba rešiti sistem linearnih enačb (21), je drugi del reševanja numerično manj zahteven, če ne gre za veliko število točk zunanjega območja. Tu imamo opraviti le z množenjem matrik in vektorjev, glej enačbi (22) in (23).

2.1 Reševanje problema MRE

Glede na numerično zahtevnost tako zastavljenega zunanjega akustičnega problema MRE lahko njegovo reševanje, v smislu časa, potrebnega za izračun, razdelimo v tri sklope. Prva dva sklopa izhajata iz iskanja rešitve na robu, pri čemer prvi sklop vključuje ovrednotenje diskretnih Helmholtzovih integralnih operatorjev in sestavljanje matrične enačbe (20) oz. (21), drugi pa pomeni reševanje omenjene matrične enačbe. V zadnjem, tretjem sklopu reševanja problema MRE, se izvede ovrednotenje zvočnega polja za zunanje točke.

Sistem linearnih enačb, ki nastane pri sestavu matrične enačbe (21), lahko postane iz več vidikov numerično izredno zahteven, predvsem pa takrat, ko se število robnih elementov poveča prek določene meje. Vzrok za to je matrika \mathbf{H} , ki se pojavi v enačbi (21) in ima lastnost, da je polna in nesimetrična – vsi njeni elementi so različni od nič in so kompleksna števila. Pri reševanju nastalega sistema linearnih enačb so običajne metode, ki se uporabljajo pri MKE, praktično neuporabne. Zato smo za reševanje problema MRE uporabili iterativne metode, izhajajoč iz fortranske knjižnice *PIM 2.2* [5]. Tako smo poleg osnovne Gaussove izločilne metode v izvedeni program MRE vključili še štiri iteracijske

pressure, Equation (2), Equation (20) can be simplified in the following way:

The solution of the matrix Equation (21) is the sound pressure \mathbf{p} on the boundary of the discretized surface, exactly in the collocation points of the boundary elements. In the second step, the sound pressure $\mathbf{p}_E = [(1/i\omega\rho)\phi(P_1), \dots, (1/i\omega\rho)\phi(P_m)]^T = (1/i\omega\rho)\Phi_E$ and the velocity $\mathbf{v}_E = [\hat{v}_n(P_1), \dots, \hat{v}_n(P_m)]^T$ are calculated for the group of points that lie in the exterior domain E . This calculation is based on the previously calculated sound pressure \mathbf{p} , on the boundary conditions – velocities \mathbf{v} on the boundary – and on the formulation of the discretized Helmholtz integral Equations (16) and (18). The simplified formulation for the calculation of the sound field in the exterior domain is given by:

$$\mathbf{p}_E = \mathbf{h}^T \cdot \mathbf{p} - i\omega\rho \mathbf{g}^T \cdot \mathbf{v} \quad (22),$$

$$\mathbf{v}_E = \mathbf{h}_v^T \cdot \mathbf{p} - i\omega\rho \mathbf{g}_v^T \cdot \mathbf{v} \quad (23).$$

The first step, where a system of linear equations (21) is to be solved, is numerically more demanding than the second step, except if we have an enormous number of exterior points. However, the second step is numerically less demanding, as we only have to multiply matrices and vectors, see Equations (22) and (23).

2.1 Solution of the BEM problem

Considering the numerical pretentiousness of the presented exterior acoustic BEM problem its solution can be divided into three parts with regard to the time needed for the computation of the whole problem. The first two parts represent the solution on the boundary, where the first part includes the calculation of the discrete Helmholtz integral operators and their composition into the matrix Equation (20) or (21), while the second part represents the solution of the matrix equation. The third, and last, part includes the computation of the sound field for the points that lie in the exterior domain.

The system of linear equations that results from the composition of the matrix equation (21) can become very numerically demanding, especially when the number of boundary elements exceeds certain limits. The reason for this is the matrix \mathbf{H} , which is presented in Equation (21). This matrix is typically unsymmetrical and dense – all its elements are non-zero complex values. When solving such a system of linear equations, classical methods, which are normally convenient for the FEM, are not practical. To solve our BEM problem we applied iterative methods, using the Fortran library *PIM 2.2* [5]. So, besides the Gauss elimination method the developed BEM program has

metode [5], t.i. metoda konjugiranih gradientov z raznimi izpeljankami ter metoda posplošenih najmanjših residuumov (CGS, Bi-CGSTAB, RBi-CGSTAB in GMRES).

Čas, ki je bil potreben za reševanje sistema linearnih enačb, v odvisnosti od izbrane metode in obsežnosti problema, odvisnega od števila robnih elementov, je prikazan v preglednici 1. Poleg tega omenjena preglednica ponuja tudi primerjavo časa, potrebnega za sestavo matrične enačbe in za izračun zvočnega polja v 148 zunanjih točkah. Število zunanjih točk je bilo za različne obsežnosti problemov vedno enako. Primerjalna analiza je bila izvedena na osebnem računalniku s procesorjem Celeron 900MHz in pomnilnikom 384MB DRAM. Analizo smo izvedli na trirazsežnem problemu, ki je v nadaljevanju natančneje opisan.

Preglednica 1. Analiza porabe časa za reševanje problema MRE (v sekundah)

Table 1. Time needed for the solution of the BEM problem analysis (in seconds)

Postopek / Method	Število robnih elementov / Number of boundary elements									
	36	144	224	480	642	1028	1228	1736	2654	3788
Gauss	0,070	0,070	0,401	7,951	11,09	58,72	105,6	575,4	2245,	7657,
CGS	0,000	0,070	0,180	0,851	1,592	4,587	7,120	16,59	42,80	128,9
Bi-CGSTAB	0,000	0,070	0,180	1,032	1,963	5,558	8,632	12,65	54,42	134,0
RBi-CGSTAB	0,010	0,300	0,951	5,638	10,45	34,30	53,98	124,2	354,2	1053,
GMRES	0,000	0,170	0,651	2,704	5,908	17,87	20,42	76,16	254,1	548,1
Sestav matrike / Matrix composit.	0,080	1,302	3,135	14,33	25,69	65,33	93,36	186,9	404,3	774,9
Zunanje reševanje / External solution	1,282	5,177	8,022	17,26	22,95	36,80	44,02	62,21	87,09	116,8

Iz podatkov v preglednici 1 lahko ugotovimo, da je čas, potreben za reševanje obsežnejših problemov, močno odvisen od izbire postopka reševanja sistema linearnih enačb. Pri reševanju problemov večjega obsega so iterativne metode tudi 60-krat in več hitrejše od običajne Gaussove izločilne metode, ki je za obsežnejše probleme praktično neuporabna. Za najhitrejšo izmed vseh metod se je izkazala metoda CGS.

Reševanje problema je še dodatno oteževalo dejstvo, da je matrika, ki je opisovala problem MRE, zasedala precejšen del pomnilnika. Elementi matrike so namreč kompleksna števila, določena z dvojno natančnostjo (COMPLEX*16), kar je k temu še dodatno pripomoglo. Npr. matrika reda 3788, ki v predstavljeni analizi opisuje najobsežnejši problem z enakim številom robnih elementov, zaseda v pomnilniku 224MB. Zaradi omejitve, ki izhaja iz operacijskih sistemov *Windows* in dovoljuje največjo uporabo pomnilnika 2GB, je reševanje problemov omejeno do približno desetisoč robnih elementov.

four iterative methods included, the so-called »Conjugate-Gradients Squared«(CGS), »Stabilised Bi-Conjugate-Gradients« (Bi-CGSTAB), »Restarted Stabilised Bi-Conjugate-Gradients«(RBi-CGSTAB) and »Generalised Minimal Residual (GMRES)«.

The time needed to solve the system of linear equations regarding the solution method and the size of the problem, defined by the number of boundary elements, is given in Table 1. This table also shows the time needed, both for the composition of the matrix equation and for the calculation of the integral operator, and the time needed for the calculation of the sound field in 148 exterior points. The number of exterior points is the same for all the problem sizes. The analysis was performed on a personal computer with a Celeron 900MHz processor and 384MB of DRAM. The problem that was investigated is precisely described in the text that follows.

From Table 1 it is clear that the time needed to solve extensive problems mainly depends on the chosen method for solving the system of linear equations. When dealing with such problems, iterative methods can be up to 60 times faster than the classical Gauss elimination method, which is practically useless for problems that are more extensive. From among all four iterative methods, the fastest one was the CGS method.

Additional difficulties with solving BEM problems occur because of the reality that the matrix describing the BEM problem takes up a considerable amount of computer memory. The fact is that the matrix is dense and its elements are complex numbers, defined with double precision (COMPLEX*16). For example, a matrix with the size 3788, which in our case represents the biggest BEM problem with the same number of boundary elements, takes up 228MB of computer memory. Due to the limitation relating to the computer's operating system, *Windows*, which allows a 2GB-maximum memory, the solution of the BEM problem is limited to a maximum of approximately ten thousand boundary elements.

2.2 Vhodno-izhodni podatki

Podatke, ki se pojavljajo v interakciji z izvedenim programom MRE, delimo na vhodne in izhodne. Med prve uvrščamo informacije o položaju vozlišč, povezljivosti vozlišč v elemente, zunanjih normalah elementov in vektorjih hitrosti v vozliščih ter informacije o materialnih lastnostih posrednika, frekvenci ter obsežnosti problema. Drugi del vhodnih podatkov vsebuje informacije o mreži zunanjih točk, pri katerih je zajet zapis njihovih koordinat in povezljivost v končne elemente ter informacija o obsegu mreže zunanjih točk. Izhodni podatki vsebujejo rešitev problema na robu in v zunanjih točkah. Prvi del vsebuje informacije o vrednostih tlaka na robnih elementih ter vrednosti zvočne moči in sevalne učinkovitosti. Drugi del izhodnih podatkov vsebuje informacije o vrednostih tlaka in vektorjih hitrosti v zunanjih točkah. Vsi podatki so urejeno zapisani v ustreznih datotekah.

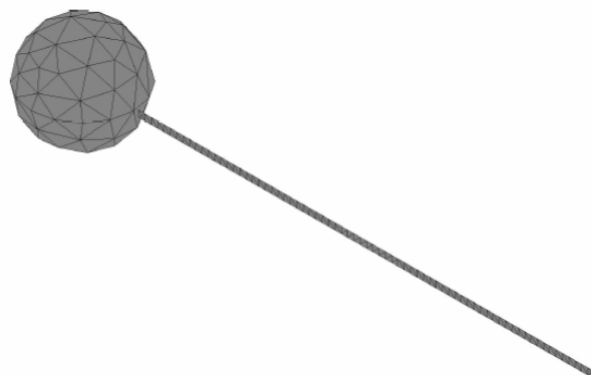
2.3 Verifikacija programa MRE

Za verifikacijo programa MRE smo pripravili trirazsežni verifikacijski model, za katerega je znana analitična rešitev. V našem primeru smo izbrali problem sevanja utripajoče krogle, ki ga lahko enakovredno opišemo z monopolnim točkastim virom. Valovna čela, ki pri takem valovanju nastajajo, imajo obliko krogel in se zvočno hitrostjo enakomerno odmikajo od vira. Enačbi (24) in (25) sta matematični opis take oblike zvočnega valovanja za časovno spremenjanje zvočnega tlaka p in hitrosti v v prostoru:

$$p(r,t) = (i\omega\rho/r)e^{i(\omega t+kr)} \quad (24)$$

$$v(r,t) = (ik - 1/r)e^{i(\omega t+kr)} \quad (25).$$

Za izvedbo verifikacijskega modela je bilo treba problem krogelnega valovanja natančneje opredeliti. Predpostavili smo, da gre za zvočno valovanje, ki se širi s hitrostjo 344m/s skozi zrak



Sl. 2. Trirazsežni verifikacijski model
Fig. 2. 3D verification model

2.2 Input–output data

All the data that interact with the developed BEM program can be divided into input and output data. The input data include information about the nodes, their coordinates and connectivity into the elements, element outward normals, velocity vectors in the nodes, material data, frequency and information about the size of the problem. The second part of the input data contains information about the mesh of exterior points, nodes with their coordinates, and connectivity into finite elements, and information about the size of the exterior mesh. On the other hand, the output data contain information about the solution on the boundary and exterior points. The first part of the data includes the calculated complex values of the sound pressure for boundary elements, the sound power and the sound radiation factor. The second part of the output data contains information about the sound pressure and the velocity at exterior points. All data are available in formatted data files.

2.3 Verification of the BEM program

For the verification of the developed BEM program a 3D verification model, which has a known analytical solution, was prepared. In our case we chose the problem of a pulsating sphere. This kind of sound source can be described with a monopole point source that produces spherical waves travelling away from the source with the speed of sound. These sound waves are defined by the Equations (24) and (25), which represent the exact analytical solution of the sound pressure p and velocity v in time and space:

$$p(r,t) = (i\omega\rho/r)e^{i(\omega t+kr)} \quad (24)$$

$$v(r,t) = (ik - 1/r)e^{i(\omega t+kr)} \quad (25).$$

To prepare the verification model it was necessary to define its parameters more precisely. We assumed that we were dealing with sound radiation in the air at a frequency of 688 Hz, with the

gostote $1,22 \text{ kg/m}^3$ pri frekvenci 688 Hz in ga oddaja krogla s polmerom $0,1 \text{ m}$. Valovno število k , ki izhaja iz navedenih predpostavk, znaša $12,5664$. Robne pogoje oz. hitrost v na površini krogle določimo iz enačbe (25). Njena vrednost pomeni amplitudo hitrosti nihanja površine krogle in je kompleksno število z vrednostjo $(150,4 - 56,27i) \text{ m/s}$.

Za analizo vpliva gostote diskretizacije je bilo pripravljenih več različnih izvedenih verifikacijskega modela, tako da je bila dolžina robnega elementa določena na podlagi valovne dolžine, in sicer od največje priporočene velikosti robnega elementa [2] $\lambda/6$, padajoče v korakih, $\lambda/10$, $\lambda/15$ do $\lambda/40$. Na sliki 2 je prikazana izvedenka modela z robnimi elementi velikosti $\lambda/10$. V zunanjih okolicih krogle je definirano območje končnih elementov v obliki pasnice, namenjene za opazovanje rešitve zvočnega polja. Velikost končnih elementov je tu opredeljena z $\lambda/40$, kar omogoča bolj natančno opazovanje akustičnih parametrov v odvisnosti od oddaljenosti od zvočnega vira. Iz primerjave med analitično in numerično izračunanimi vrednostmi zvočnega tlaka in hitrosti v odvisnosti od razdalje do zvočnega vira (sl. 3) lahko ugotovimo, da so odstopanja v oddaljenem polju skoraj neopazna.

Pri analizi vpliva gostote diskretizacije smo opazovali nekaj osnovnih vrednosti zvočnega polja, ki smo jih primerjali z analitično izračunanimi vrednostmi in nato ocenili njihovo napako. Med opazovane vrednosti smo uvrstili zvočno moč ter zvočni tlak in hitrost v točki, oddaljeni 1 m od središča krogle. Pri vrednostih zvočnega tlaka in hitrosti smo opazovali napako amplitude in faze. Rezultati analize so prikazani v preglednici 2, kjer poleg napak lahko opazujemo tudi število robnih elementov, potrebnih za diskretizacijo obravnavanega zvočnega vira, krogle s polmerom $0,1 \text{ m}$.

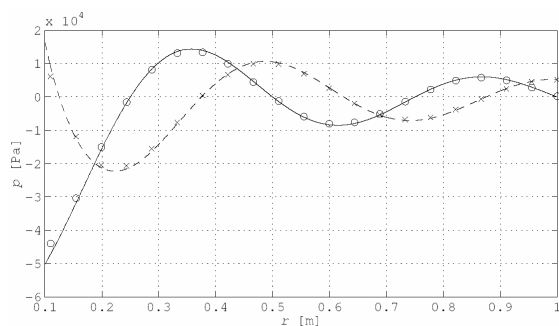
Napake, ki nastanejo pri numeričnem izračunu zvočnega polja z MRE, imajo tri glavne vire [3], v formulaciji zapisa MRE, numeričnem izračunu in diskretizaciji. Kljub temu, da izvedena

sound speed equal to 344 m/s and with an air density of 1.22 kg/m^3 . The radius of the pulsating sphere is 0.1 m . Thus, the wave number k is 12.5664 . The boundary conditions – velocity v is calculated directly from Equation (25). Its value represents the amplitude on the surface of the pulsating sphere and it is a complex value of $(150.4 - 56.27i) \text{ m/s}$.

To analyse the influence of the discretization it was necessary to prepare more derivatives of the verification model, where each derivative had a different discretization or size of the boundary element. The size of the boundary element for each derivative is related to the wavelength, starting from the biggest recommended size of a boundary element of $\lambda/6$ [2] to smaller sizes of $\lambda/10$, $\lambda/15$ to $\lambda/40$, decreasing in steps. Figure 2 shows the derivative verification model with an element size of $\lambda/10$. In the exterior domain of the sphere there is also a strip-shaped mesh of finite elements that are intended for observing the solution of the sound field. The size of the exterior finite elements is defined by $\lambda/40$, which allows precise control of the numerically calculated acoustic parameters in terms of the distance from the sound source. From Figure 3 it is evident that the differences between the analytically and numerically calculated values are hardly noticeable in the far field.

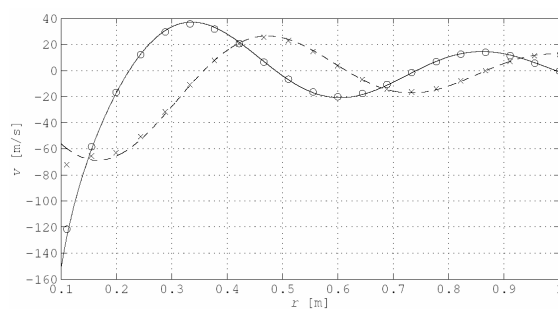
In the analysis of the influence of the discretization only a few parameters of the sound field were controlled, and their errors are compared to the exact analytical values. Those acoustic parameters are the sound power, the sound pressure and the velocity at a distance of 1 m from the centre of the sphere. For the sound pressure and the velocity, both the phase and the amplitude errors were estimated. The results of the analysis are given in Table 2, where one can also find the number of boundary elements needed for the discretization of the sound source, i.e. the sphere with the radius of 0.1 m .

The errors that occur in the sound field, calculated by using the developed BEM program, have three major sources [3]: the formulation of the BEM, the numerical calculation and the discretization. Although this analysis



Sl. 3. Primerjava analitično (— Re, --- Im) in numerično (○ Re, × Im) izračunanih vrednosti zvočnega tlaka in hitrosti v odvisnosti od razdalje do zvočnega vira

Fig. 3. Comparison between analytically (— Re, --- Im) and numerically (○ Re, × Im) calculated sound pressure and velocity as function of the distance from the sound source



Preglednica 2. Analiza napak pri izračunu akustičnih spremenljivk s programom MRE

Table 2. Error analysis of the acoustic parameters calculated by the BEM program

Velikost elementov Element size	Število elementov Number of elements	Napaka moči Power error %	Napaka tlaka Sound pressure error		Napaka hitrosti Velocity error	
			Ampl. %	Faza / Phase °	Ampl. %	Faza / Phase °
$\lambda/6$	36	-29,740	-20,047	-1,912	-20,034	-1,886
$\lambda/10$	144	-2,724	-2,903	-2,445	-2,901	-2,434
$\lambda/15$	224	1,329	-0,563	-3,174	-0,556	-3,161
$\lambda/20$	480	4,749	2,282	-3,687	2,284	-3,667
$\lambda/25$	642	5,836	3,231	-3,677	3,233	-3,657
$\lambda/30$	1028	7,367	4,689	-3,626	4,691	-3,607
$\lambda/35$	1228	7,920	5,289	-3,623	5,292	-3,603
$\lambda/40$	1763	8,833	6,461	-3,536	6,462	-3,543

analiza napak ne opredeljuje virov, lahko ob podrobnejšem pogledu v preglednico 2 sklepamo o njihovem viru. Pri velikosti robnih elementov $\lambda/6$ ali blizu tej vrednosti prevladuje napaka diskretizacije z negativnimi vrednostmi. Z zmanjševanjem velikosti elementov se napaka manjša in pri $\lambda/15$ ali več spremeni predznak ter postane pozitivna vendar manjša kot prej. Pozitivna vrednost napake se zvečuje neodvisno od numeričnega obsega oz. števila robnih elementov problema, vendar počasneje. Zaradi omenjenega sklepamo, da je v tem primeru vir napake v oblikovanju zapisa MRE in/ali numeričnem izračunu. Pri analizi napak je pomembno tudi spoznanje o vplivu frekvence. Ugotovili smo tudi, da se pri enaki gostoti diskretizacije in velikosti zvočnega vira napaka zmanjšuje z večanjem frekvence. To pomeni, da diskretizacija problema z velikostjo elementov $\lambda/6$ zagotavlja dovolj natančno reševanje problemov pri višjih frekvencah.

2.4 Integracija MRE v programske paket MKE

ANSYS je eden izmed programskih paketov za reševanje fizikalnih problemov z uporabo MKE. Odprtost omenjenega programa omogoča, da ga lahko izkoristimo tudi kot orodje za pripravo in obdelavo splošnih fizikalnih problemov, pri katerih diskretizacija modela temelji na mreženju (MKE, MRE, MKR idr.). Ker smo se v našem primeru pri reševanju akustičnih problemov omejili na tiste, ki izhajajo iz strukturnih nihanj, je bilo smiseln izkoristiti možnost reševanja problemov strukturne dinamike v programu *ANSYS* ter vanj integrirati izvedeno MRE za reševanje akustičnih problemov, ki je bistveno hitrejša od MKE.

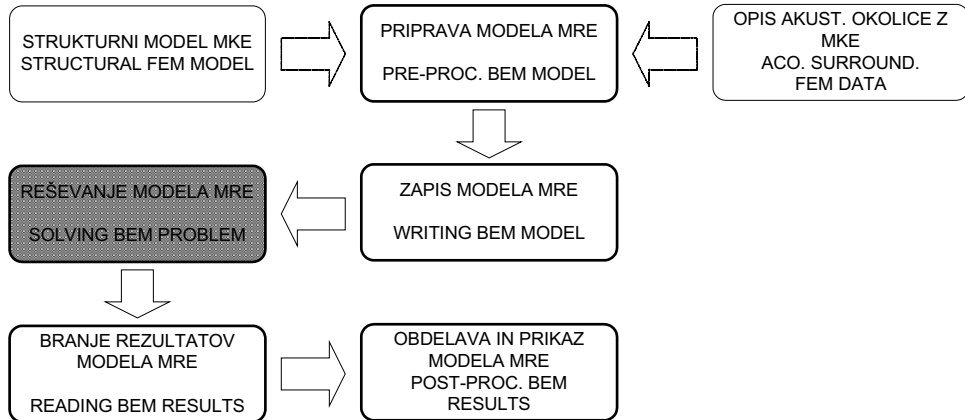
Za program MRE smo v *ANSYS*-ovem programskem okolju pripravili knjižnjico makro ukazov, ki so namenjeni za pripravo in obdelavo izhodno-vhodnih podatkov ter njihovo obdelavo.

does not specially define the source of the errors, closer inspection of the data in Table 2 can lead to the correct conclusion about the sources of the errors. As the size of the boundary element gets bigger or closer to $\lambda/6$, it is obvious that the error due to the discretization dominates with negative values. When decreasing the size of the boundary elements or increasing the discretization density, the error reduces, and at an element size of approximately $\lambda/15$ the error changes sign. A further reduction in the element size leads to an increase of the positive error, but its value is relatively small. For the error that occurs at smaller element sizes we cannot say if it is related to the discretization. On the contrary, this error has its source in the formulation of the BEM or/and in the numerical calculation. Analysing the error we came to an important conclusion about the frequency's influence on the accuracy. When we increase the frequency and keep the same discretization and the same size of the sound source, the error decreases. This means that the discretization that is defined with an element size of $\lambda/6$ also ensures sufficient accuracy for solving problems at higher frequencies.

2.4 Integration of the BEM program into the FEM software

ANSYS is one of the FEM software packages intended for solving general physical problems, and it can also be used as a tool for pre-processing and/or post-processing general physical models where the discretization is based on meshing (FEM, BEM, DM, etc.). In our case we limited the study to acoustic problems related to structural vibrations. Therefore, it was reasonable to use one of the FEM software packages, in our case *ANSYS*, to solve the structural dynamic problem and later on to integrate the developed BEM program into *ANSYS*. The fact is that the BEM is much faster for solving exterior acoustic problems than the FEM.

To allow the interaction between the BEM program and *ANSYS* it was necessary to develop a library of macro commands that allow one to pre-process, post-process and analyse the BEM input



Sl. 4. Postopek izdelave in reševanja modela MRE

Fig. 4. Pre-processing, solving and post-processing the BEM model

Omogočen je tudi prikaz in animacija akustičnih spremenljivk, kakor so zvočni tlak, vektorsko polje hitrosti in vektorsko polje zvočne intenzivnosti, kakor tudi prikaz ravni zvočnega tlaka ter zvočne intenzivnosti. Celoten postopek izdelave in reševanja modela MRE v okolju ANSYS je prikazan na sliki 4. Praktičen primer reševanja akustičnega problema z MRE pa je opisan v nadaljevanju za primer enosmernega elektromotorja.

3 OVREDNOTENJE ZVOČNEGA POLJA ELEKTROMOTORJA Z MRE

Prvi korak v pripravi modela MRE je bila izdelava diskretizirane zunanje površine, to je mreže robnih elementov. V našem primeru smo izhajali iz ANSYS-ovega strukturnega modela MKE enosmernega elektromotorja (sl. 5) in poznavanja njegovega harmonskega odziva, kot posledice vzbujanja z magnetnimi silami ([6] in [7]) (sl. 6). Na celotni zunani površini strukturnega modela MKE smo izdelali mrežo trikotnih elementov, pri čemer je leta imela sklenjeno površino (sl. 7).

Zaradi poenostavitev prenosa robnih pogojev – hitrosti oz. vibracij iz strukturnega modela

and output data in the ANSYS environment. With the so-prepared macro commands it is also possible to animate the acoustic parameters, such as the instantaneous sound pressure and the velocity vector field and to display the sound pressure and the sound intensity level. Figure 4 shows the complete process of pre-processing, solving and post-processing of the BEM model in the ANSYS environment. A practical example of the acoustic BEM problem study is presented in the next paragraph.

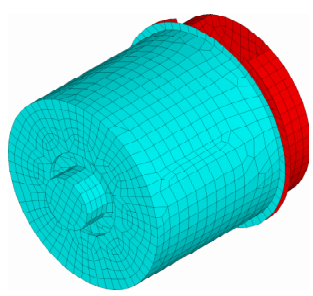
3 SOUND-FIELD CALCULATION OF AN ELECTRIC MOTOR USING THE BEM

Building a mesh of boundary elements that covers the outer surface of the DC electric motor, shown in Fig. 5, was the first step in the procedure of the BEM model set-up. In our case we started from the ANSYS structural FEM model of the investigated electric motor, see Fig. 6, and from the previously FEM-calculated harmonic response due to the harmonic excitation of the magnetic forces. To build up a boundary-element mesh, the complete surface of the structural FEM model was covered by triangular elements that all together represented a closed surface, see Fig. 7.

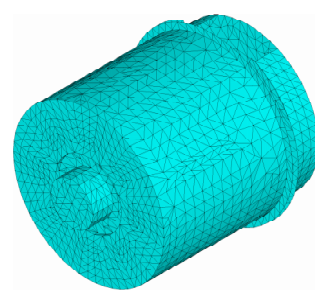
Due to the simplification of the transfer of boundary conditions, velocities or vibrations from the



Sl. 5. Trirazsežni model
Fig. 5. 3D model

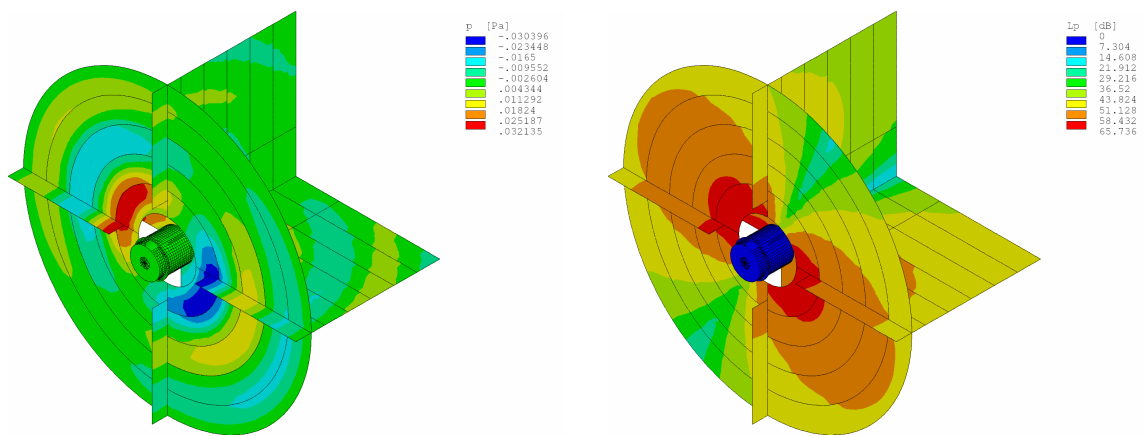


Sl. 6. Strukturni model MKE
Fig. 6. Structural FEM model



Sl. 7. Model MRE
Fig. 7. BEM model

na robne elemente, smo pri nastajanju mreže robnih elementov uporabili vozlišča in/ali elemente, ki določajo zunanjou površino strukturnega modela MKE. Ker pa je natančnost rešitve akustičnega problema odvisna od velikosti robnih elementov v celotni mreži, je treba pri snovanju strukturnega modela MKE že vnaprej upoštevati dejstvo, da morajo biti elementi na zunanjji površini dovolj majhni. Drugi korak priprave modela MRE je izdelava mreže zunanjih točk. Za izdelavo mreže smo uporabili trikotne elemente, s katerimi smo zmrežili površine, na katerih smo želeli opazovati zvočno polje elektromotorja. Na podlagi pripravljenega modela MRE smo z izvedenim programom MRE poiskali njegovo rešitev in ovrednotili zvočno polje v okolini elektromotorja. Na sliki 8 so prikazane nekatere akustične spremenljivke, ki opisujejo zvočno polje v okolini enosmernega elektromotorja in so posledica strukturnega odziva osnovnega harmonika magnetnih sil. Prikazano zvočno polje, ki ga elektromotor oddaja in nastane zaradi delovanja osnovne harmonike komponente magnetnih sil, približno ustreza zvočnemu polju dipola [4].

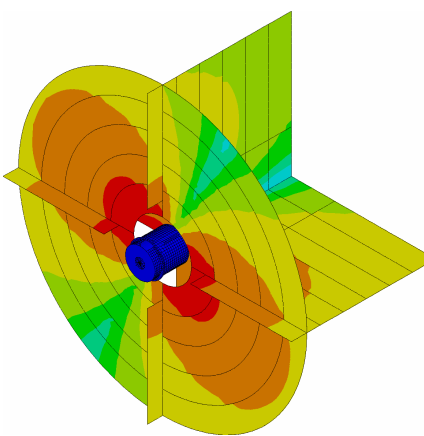


Sl. 8. Trenutni zvočni tlak (levo) ter raven zvočnega tlaka (desno)
Fig. 8. Instantaneous sound pressure (on the left) and sound pressure level (on the right)

4 SKLEP

Prispevek opisuje reševanje zunanjih akustičnih problemov z MRE ter primer uporabe MRE za ovrednotenje zvočnega polja enosmernega elektromotorja, nastalega zaradi delovanja magnetnih sil. Predstavljena je tudi izvedba programa MRE za reševanje trirazsežnih problemov ter težave, na katere smo naleteli pri svojem delu ter integracija MRE v programske pakete MKE – ANSYS. Izvedeni program smo ovrednotili s poudarkom na raziskavi vpliva gostote diskretizacije in identificirali vire napak. Glede na težave, ki se pojavijo pri reševanju problema MRE

structural FEM model into the BEM model, we used the nodes of the structural FEM model that lie on the exterior surfaces to define the boundary-element mesh. As the accuracy of the acoustical model depends on the size of the boundary elements, it was necessary to consider the mesh density of the structural FEM model in advance. Therefore, the finite elements of the structural model should be small enough. The second step in the process of the BEM model set-up was to prepare the mesh of the exterior points. The exterior mesh was built using triangular finite elements on the surfaces, where the sound field of the electric motor was to be controlled. Based on the so-prepared BEM model, the developed BEM program was used to calculate the sound field of the DC electric motor. Figure 8 shows two acoustic parameters that describe the sound field in the surroundings of the DC electric motor and that are the result of the structural response due to the basic harmonic component of the magnetic forces' excitation. The presented sound field radiated by the electric motor, due to the basic harmonic component of the magnetic forces, is similar to the acoustic dipole sound field [4].



4 CONCLUSION

This paper shows a basic approach to solving exterior acoustic problems using the BEM and a practical example of the calculation of an electric motor's sound field resulting from magnetic forces. Also presented is the development of the BEM program for solving 3D problems and its integration into a commercial FEM software package called ANSYS, with all the encountered difficulties. The developed BEM program was verified and a special emphasis was given to the influence of the discretization on the error. In addition, the sources of error were identified. Due to the difficulties that we came across when solving the system of linear equations

oz. sistema linearih enačb, ki pri tem nastane, smo raziskali vpliv izbire postopka reševanja sistema linearih enačb glede na porobljeni čas.

of the BEM problem, different iterative methods were implemented into the BEM program and tested with regard to the time needed for the solution.

5 LITERATURA 5 REFERENCES

- [1] Amini, S., P.J. Harris, D.T. Wilton (1992) Coupled boundary and finite element methods for the solution of the dynamic fluid-structure interaction problem. Lecture notes in engineering, *Springer-Verlag*, Berlin, NewYork.
- [2] Kirkup, S. (1998) The boundary element method in acoustics: A development in Fortran. Integral equation methods in engineering. Integrated Sound Software, Hebdon Bridge.
- [3] Newhouse, S. (1995) Adaptive error analysis with hierarchical shape function for three dimensional rigid acoustic scattering. PhD thesis, *Imperial College of Science, Technology and Medicine*, London.
- [4] Rschevkin, S.N. (1963) The theory of sound. *Pergamon Press*, Oxford.
- [5] da Cunha R.D., T. Hopkins (1996) The parallel siterative methods package for systems of linear equations, User's guide (Fortran 90 version). Mathematics Institute and National Supercomputing Centre Universidade Federal do Rio Grande do Sul Brasil; Computing Laboratory University of Kent at Canterbury, United Kingdom.
- [6] Furlan, M., M. Boltežar, A. Černigoj (2002) Modeling the magnetic noise of a permanent magnet DC electric motor. 15th International conference on electrical machines, Brugge, Belgium.
- [7] Furlan, M. (2003) Karakterizacija magnetnega hrupa enosmernega elektromotorja. Doktorsko delo, *Fakulteta za strojništvo*, Ljubljana.

Naslova avtorjev: dr. Martin Furlan
ISKRA Avtoelektrika d.d.
Razvojni center
Polje 15
5290 Šempeter pri Gorici
martin.furlan@iskra-ae.com

prof.dr. Miha Boltežar
Univerza v Ljubljani
Fakulteta za strojništvo
Aškerčeva 6
1000 Ljubljana
miha.boltezar@fs.uni-lj.si

Authors' Addresses: Dr. Martin Furlan
ISKRA Avtoelektrika d.d.
R & D
Polje 15
SI-5290 Šempeter pri Gorici
martin.furlan@iskra-ae.com

Prof.Dr. Miha Boltežar
University of Ljubljana
Faculty of Mechanical Eng.
Aškerčeva 6
SI-1000 Ljubljana
miha.boltezar@fs.uni-lj.si

Prejeto:
Received: 26.11.2003

Sprejeto:
Accepted: 8.4.2004

Odperto za diskusijo: 1 leto
Open for discussion: 1 year

Izboljšanje dinamične karakteristike tlačno polnjenega motorja z uporabo električnih podpornih naprav

Improving the Transient Response of a Turbocharged Diesel Engine by using Electrical Assisting Systems

Tomaž Katrašnik - Ferdinand Trenc - Vladimir Medica -
Samuel Rodman Oprešnik - Frančišek Bizjan

Za tlačno polnjene dizelske motorje je značilen daljši čas, potreben za odziv na nenadno povečanje obremenitve, v primerjavi s sesalnimi motorji, kar je posledica načina izmenjave energije med motorjem in turbopolnilnikom. Odzivnost tlačno polnjenega motorja je, z uporabo dodatnih električnih virov energije, mogoče izboljšati z neposrednim dovajanjem energije na ročično gred motorja z integriranim zaganjalnikom-generatorjem, ki je pritrjen na vztrajnik motorja in deluje kot dodatni elektromotor; ali s posrednim dovajanjem energije z uporabo elektromotorja, pritrjenega na gred turbopolnilnika. Za analizo vpliva obeh konceptov je bila uporabljena doslej večkrat preverjena brezrazsežna simulacijska metoda modeliranja pojavov v motorju, ki omogoča hitro in razmeroma natančno ovrednotenje dinamičnih karakteristik motorja. Eksperimentalno določene karakteristike elektromotorjev smo uporabili kot vhodne podatke simulacije, kar, povezano z natančnostjo simulacije, zagotavlja verodostojnost prikazanih rezultatov. V prispevku je analizirana interakcija motorja z električnimi podpornimi sistemi in nakazane so zahteve, ki jih morajo izpolnjevati električni motorji za učinkovito izboljšanje dinamične karakteristike motorja. Predstavljeni so rezultati simulacij različnih režimov vožnje vozila, ki nazorno prikazujejo značilnosti in razlike med obema zasnovama električne podpore.

© 2004 Strojniški vestnik. Vse pravice pridržane.

(Ključne besede: motorji dizelski, polnjenje tlačno, simuliranje numerično, karakteristike dinamične)

It is a well-known fact that turbocharged Diesel engines suffer from inadequate response to sudden load increases, which is a consequence of the nature of the energy exchange between the engine and the turbocharger. The dynamic response of a turbocharged Diesel engine could be improved by the use of electrical assisting systems, either by direct energy supply with an integrated starter-generator mounted on the engine's flywheel or indirect energy supply with an electrically assisted turbocharger. A previously verified zero-dimensional computer-simulation method was used for the analysis of both concepts of electrical assistance. The reliability of the presented data is additionally ensured by the experimentally determined characteristics of the electric motors used as input parameters for the simulation. The paper offers an analysis of the interaction between the turbocharged Diesel engine and the electrical assisting systems as well as the requirements for electric motors that are suitable for the improvement of an engine's dynamic response in a vehicle. The presented results of vehicle dynamics indicate the features and differences of both concepts of electrical assistance.

© 2004 Journal of Mechanical Engineering. All rights reserved.

(Keywords: Diesel engines, turbocharging, numerical simulations, dynamic response)

0 UVOD

Povečanje delovne sposobnosti sodobnih dizelskih motorjev je predvsem posledica tlačnega polnjenja in naknadnega hlajenja polnilnega zraka, saj se tako poveča masa svežega zraka v valju in tem največja dovoljena količina vbrizganega goriva. Za takšne motorje je značilen slabši odziv na nenadno

0 INTRODUCTION

Turbocharging and subsequent charge cooling of the working medium causes an increase in the brake mean effective pressure (bmeep) in a Diesel engine due to the increased in-cylinder mass of fresh air and, therefore, the maximum quantity of injected fuel. Poor performance during the engine load

povečanje obremenitve kakor za sesalne motorje. Tlačno polnjeni motorji v fazi nenadnega povečanja obremenitve, zaradi prenizkega začetnega tlaka polnilnega zraka, z zakasnitvijo dosežejo največjo stacionarno vrednost srednjega efektivnega tlaka motorja. Doseganje največje stacionarne vrednosti srednjega efektivnega tlaka motorja je povezano z zagotovitvijo zadostne mase polnilnega zraka, ki omogoča popolno zgorevanje največje količine vbrizganega goriva. Masa svežega zraka v valju je neposredno povezana s tlakom v polnilnem zbiralniku. Na hitrost naraščanja tlaka v polnilnem zbiralniku imajo največji vpliv vztrajnostni moment rotorja turbopolnilnika ter karakteristike turbine in kompresorja. Večina sodobnih tlačno polnjenih dizelskih motorjev je opremljenih s sistemom za krmiljenje količine vbrizganega goriva v odvisnosti od tlaka polnilnega zraka – pnevmatski omejevalnik dobave goriva (PODG - LDA). Glavna naloga sistema je zagotavljanje popolnega zgorevanja v prehodnem režimu delovanja motorja ter posledično zmanjševanje emisije škodljivih snovi v izpušnih plinih, predvsem saj. PODG je nujen za doseganje strogih okoljevarstvenih norm. Emisija saj se bistveno poveča že pred nastopom nepopolnega zgorevanja, zato PODG običajno dopuščajo dobavo manjše količine goriva od količine, ki bi še lahko popolno zgorela. Zaradi omenjenega dejstva je odziv motorja, opremljenega s PODG, slabši od motorja brez PODG, saj je zaradi manjše količine vbrizganega goriva moč motorja manjša (neposredno zmanjšanje), hkrati pa je manjša tudi entalpija izpušnih plinov, kar vpliva na slabše pospeševanje turbopolnilnika ter posredno prek tlaka polnilnega zraka in PODG ponovno na zmanjšanje moči motorja v prehodnem režimu. Zahteve po izpolnjevanju strogih okoljevarstvenih norm, ki pa ne predstavljajo predmet raziskav tega prispevka, in izboljšanju dinamičnega odziva tlačno polnjenega motorja je mogoče izpolniti z uporabo električnih podpornih naprav. V nadaljevanju je predstavljen njihov vpliv na pospeševanje cestnega vozila in razložena interakcija z motorjem, ki poskuša osvetliti še neraziskano področje ter ponuditi temelj za nadaljnji razvoj električnih podpornih naprav.

1 SISTEM ZA DOBAVO GORIVA IN ELEKTRIČNE PODPORNE NAPRAVE

Motor MAN D826 LOH15, ki je predmet raziskav, je opremljen z vrstno visokotlačno tlačilko za gorivo ter PODG. Na sliki 1 je izrisana izmerjena karakteristika delovanja PODG pri različnih vrtljajih motorja v odvisnosti od nadtlaka v polnilnem zbiralniku (dp_2). Predstavljena karakteristika, ki je bila nespremenjena uporabljena v vseh prikazanih raziskanih primerih, določa najmanjši razmernik zraka, s katerim je, v istem motorju in ob podobnih delovnih pogojih, v prvem približku povezana emisija saj. Slike

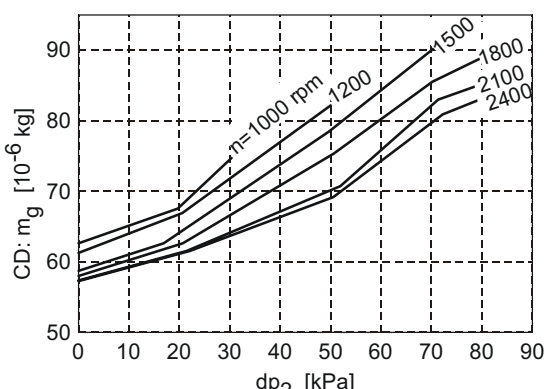
increase, when compared with naturally aspirated engines, is attributed to the nature of the energy exchange between the engine and the turbocharger. The maximum stationary bmep is reached with a delay, since it depends on there being a sufficient mass of fresh air in the cylinders to allow the complete combustion of a maximum amount of injected fuel. The mass of fresh air in the cylinder is directly proportional to the boost pressure, the increase rate of which is primarily influenced by the turbocharger's mass moment of inertia and the characteristics of the applied turbine and compressor. Advanced, turbocharged Diesel engines are usually equipped with a boost-pressure-controlled fuel-limiting system, called an LDA. The purpose of the LDA is to ensure complete combustion during engine-transient operating conditions, thereby reducing exhaust gas emissions, in particular, of black soot. Thus, the LDA is indispensable for meeting strict environmental regulations. Black-soot emission increases significantly before incomplete combustion occurs; the LDA therefore generally dictates the injection of a lower maximum fuel quantity than that which could have burned completely. The dynamic response of turbocharged Diesel engines equipped with an LDA is therefore slower than that of those without one. This phenomenon is firstly the consequence of direct engine-power reduction due to the lower quantity of fuel injected and secondly, the consequence of indirect engine-power reduction: the lower specific enthalpy of exhaust gases reduces turbocharger acceleration, resulting in a lower boost pressure and, via the LDA, in a reduced amount of fuel being injected. Meeting strict environmental regulations, on the one hand, which is not the subject of this paper, and improving the baseline engine dynamic response, on the other, is enabled by the application of electrical assistance systems. In this paper, the influence of electrical assisting systems on the dynamic-response improvement of a turbocharged Diesel engine propelling a truck is investigated. A variety of electrical assisting systems combined with the operation of the engine under various loading conditions should reveal an improvement in the dynamic response of a turbocharged Diesel engine equipped with electrical assisting systems, their interaction with the Diesel engine, as well as the demands placed on them.

1 FUEL-INJECTION EQUIPMENT AND ELECTRICAL ASSISTING SYSTEMS

A simulated MAN engine (D0826 LOH 15) was equipped with a Bosch high-pressure fuel-injection pump linked with a pneumatically controlled LDA. Fig. 1 shows the influence of the gauge pressure (dp_2) on the cyclic fuel delivery (CD) for various engine speeds. The same LDA characteristics was used in all investigated cases, which results in nearly equal minimum air-fuel ratio that is, in the same engine and under similar operating conditions, in

1 je razvidno, da je karakteristika PODG za majhne nadtlake nekoliko položnejša, kar gre najverjetneje pripisati pnevmatskemu krmiljenju, nato pa narašča skoraj linearno. Z naraščajočimi vrtljaji se količina vbrizganega goriva pri nespremenljivem nadtlaku zmanjšuje, kar je, zaradi nespremenljivih krmilnih časov ventilov, posledica nižjega volumetričnega izkoristka motorja pri višjih vrtljajih, saj je tako zagotovljen približno enak najmanjši razmernik zraka pri različnih vrtljajih. Na sliki 2 je prikazana izmerjena največja ciklična dobava goriva (maks. m_g) ter ciklična dobava goriva pri okoliškem tlaku, pritisnjeno na PODG ($m_g (dp_2=0)$), v odvisnosti od vrtljajev. Zraven točk največje ciklične dobave goriva so vpisane vrednosti (v odstotkih) razmerja tlaka, pri katerem PODG dopušča dobavo največje količine goriva proti stacionarnem tlaku pri tej vbrizgani količini goriva. Iz prikazanega je razvidno, da pri 1000 in 1200 min⁻¹ največje količine goriva ne omejuje karakteristika tlačilke za gorivo, ampak nastavitev PODG. Omenjeno dejstvo je predvsem posledica nelinearne naravne pretočne karakteristike turbine, ki v povezavi s kompresorjem pri nizkih vrtljajih motorja ne omogoča doseganja visokih polnilnih tlakov, kar, pri določeni najmanjši vrednosti razmernika zraka, rezultira v zmanjšano količino dobavljenega goriva. Od 1400 min⁻¹ naprej PODG ne omejuje največje ciklične dobave goriva. Med 1400 min⁻¹ in 2400 min⁻¹ se največja ciklična dobava goriva zmanjšuje, s čimer je zagotovljen približno enak največji tlak v valjih in zmerne toploste obremenitve motorja. Iz vrednosti razmerja tlakov je tudi razvidno, da je z večanjem vrtljajev motorja največja količina goriva dobavljena pri razmeroma nižjem tlaku. To razmerje se zmanjšuje hitreje od največje ciklične dobave goriva, kar je posledica prej omenjene nelinearne pretočne karakteristike turbopolnilnika.

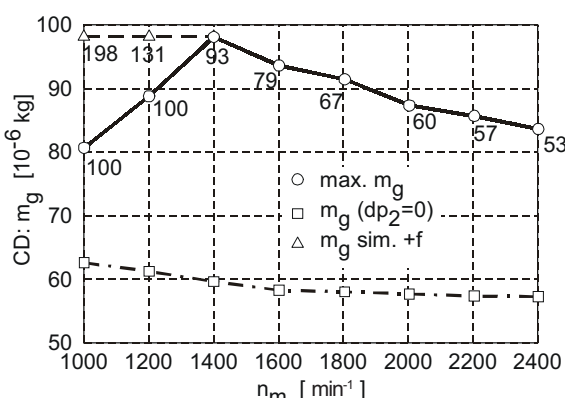
Zaradi opisane interakcije med tlačilko za gorivo in PODG pri 1000 in 1200 min⁻¹ je bila v primeru posrednega dovajanja energije z elektromotorjem, pritrjenim na gred turbopolnilnika, ki omogoča doseganje polnilnih tlakov nad ustaljeno vrednostjo, največja količina dobavljenega goriva pri omenjenih



Sl. 1. Karakteristika LDA
Fig. 1. LDA characteristics

relatively strong relation to the emission of black soot. The quantity of injected fuel decreases with increasing engine speed at a constant boost pressure, thus enabling an almost constant in-cylinder air-fuel ratio due to a lower volumetric efficiency of the engine at higher engine speeds. Fig. 2 shows the maximum measured CD (max. m_g) and the CD for ambient pressure applied on the LDA ($m_g (dp_2=0)$) as functions of the engine speed. The ratio (in percentages) of the LDA full-fueling gauge pressure to stationary gauge pressure for the same quantity of injected fuel are plotted along the 'max. m_g ' curve. It is obvious that at 1000 and 1200 rpm the CD is limited by the LDA setting rather than by the characteristics of the fuel-injection pump. This phenomenon is generally the consequence of the free-floating turbine flow characteristics, which in connection with the compressor produces a low boost pressure at low engine speeds, thus resulting in a low CD at the set minimum air-fuel ratio. Above 1400 rpm, the LDA no longer influences the stationary maximum CD . From 1400 to 2400 rpm the CD decreases, maintaining an almost constant maximum cylinder pressure and thermal loads of the engine. The relative pressure at which the LDA enables full fuel delivery decreases with increasing engine speed (Fig. 2); this ratio decreases faster than the maximum cyclic fuel delivery, due to the previously discussed turbocharger characteristics.

Because the maximum CD is limited by the operation of the LDA below 1400 rpm, the maximum CD will rise if the boost pressure is increased, as in the case when using an electrically assisted turbocharger. For the simulation of an engine with an electrically assisted turbocharger, a maximum CD below 1400 rpm was, in addition to the measured one, also set to a value equal to that at 1400 rpm. This is supposed to be an acceptable value when the peak cylinder pressure and the thermal loadings are



Sl. 2. Karakteristika tlačilke za gorivo
Fig. 2. Fuel injection pump characteristics

vrtljajih v simulaciji, poleg izmerjene, postavljena (izbrana) tudi na vrednost dovedenega goriva pri 1400 min^{-1} (slika 2: m_g sim. +f).

V simulaciji je kot neposredni dodatni vir energije uporabljen integriran in na vztrajnik motorja pritrjen zaganjalnik generator (ISG), izdelan v podjetju ISKRA Avtoelektrika. Uporabljena je karakteristika ISG s 36-voltnim napajanjem; največji navor 70 Nm ISG doseže pod 1200 min^{-1} , nato pa se navor zmanjša skoraj linearno do 10 Nm pri 2200 min^{-1} , ki predstavlja zgornjo mejo delovanja ISG. ISG naj bi delno kompenziral razliko med močjo v prehodnem režimu in največjo stacionarno močjo ter tako izboljšal odziv motorja.

Kot posredni vir energije sta bila uporabljena dva elektromotorja z namenom, da čim hitreje zagotovita tlak v polnilnem zbiralniku, ki že omogoča vbrizgavanje največje količine goriva ter posledično doseganje največjega stacionarnega srednjega efektivnega tlaka motorja. Zgornja meja delovanja obeh elektromotorjev je 85000 min^{-1} , kar za simulirani motor predstavlja ekvivalent največjega polnilnega tlaka pri določenih vrtljajih motorja, pri katerih PODG šeomejuje dobavo goriva [1]. Prvi elektromotor (EM2), ki je podrobno predstavljen v [1] do [3], razvije največji navor $0,2 \text{ Nm}$ in ima masni vztrajnostni moment $6 \cdot 10^{-5} \text{ kgm}^2$. Zaradi stvarnejše primerljivosti je v analizi uporabljen tudi elektromotor, izdelan v družbi za uporabno mestno okoljevarstvo (Gesellschaft für angewandte Stadtökologie - GfAS mbH), s karakteristikami, ki so predstavljene v [4]; največji navor znaša $0,57 \text{ Nm}$ ob masnem vztrajnostnem momentu $2.87 \cdot 10^{-5} \text{ kgm}^2$.

2 SIMULACIJSKI PROGRAM

Uporabljena je bila brezrazsežna simulacijska metoda, katere zasnova je predstavljena v [5], dopolnjena in razširjena trenutno uporabljena verzija pa v [1] do [3]. Za simulacijo, ki je uporabljena v tem prispevku je bil dodan podprogram za spreminjanje kota začetka vbrizgavanja goriva, ki omogoča doseganje natančnosti pod 4% med izmerjenimi in simuliranimi parametri po celotni zunanjki karakteristiki motorja. Osnova simulacije cestne vožnje je bila povzeta po [6] ter razširjena za potrebe simulacije.

3 REZULTATI

V rezultatih so prikazana tri različna povečanja obremenitve motorja, vgrajenega v tovorno vozilo, ki simulirajo obnašanje vozila na cesti ter prikazujejo značilnosti in vpliv električnih podpornih naprav. Tovorno vozilo MAN 8.225 LC z največjo dovoljeno skupno maso 7490 kg je opremljeno s šeststopenjskim menjalnikom S6-850. Vanj je vgrajen 6-valjni tlačno polnjeni motor MAN 826D LOH15 s hladilnikom polnilnega zraka ter turbopolnilnikom HOLSET H1E-8264BF/H16WA8. Motor z delovno prostornino $6,87 \text{ dm}^3$, vrtino/gibom

concerned. This modified CD was labeled with ' m_g sim. +f' in Fig. 2 and denoted by the maximum added CD.

An integrated starter generator (ISG) produced and tested by ISKRA "Avtoelektrika" was used in the simulation as a direct energy-supply source. This ISG develops 70 Nm below 1200 rpm, decreasing almost linearly to 10 Nm at a maximum operating speed of 2200 rpm (at a voltage of 36 V). The ISG partially compensates the difference between the transient and stationary bmep, and therefore improves the dynamic behavior of the turbocharged engine.

Two electric motors mounted on the turbocharger shaft were used as an indirect energy supply, with the aim of ensuring faster boost pressure build-up to enable the simultaneous injection of a larger amount of fuel. Both electric motors operate up to a maximum of 85000 rpm, representing the equivalent to the maximum boost pressure still limiting full fuelling via an LDA [1]. A prototype asynchronous electric motor produced by ISKRA Avtoelektrika, labeled EM2, and presented in detail in [1] to [3], develops a maximum torque of 0.2 Nm and has a mass moment of inertia of $6 \cdot 10^{-5} \text{ kgm}^2$. Another high-performance electric motor, denoted EMG, developing 0.57 Nm at 20000 rpm with $2.87 \cdot 10^{-5} \text{ kgm}^2$ mass moment of inertia (produced by Gesellschaft für angewandte Stadtökologie - GfAS mbH [4]) was used in the simulations for better comparisons.

2 SIMULATION PROGRAM

The simulation program is based on the zero-dimensional filling and emptying method. The basis of the simulation method is presented in [5], whereas the extended code used here is described in detail in [1] to [3]. The recent version of the simulation program automatically adapts the start of fuel injection to the engine load and speed, enabling agreement between the experimental and simulated results of within 4% for the whole engine maximum-load characteristics. The vehicle dynamics simulation subroutine was developed according to [6].

3 RESULTS

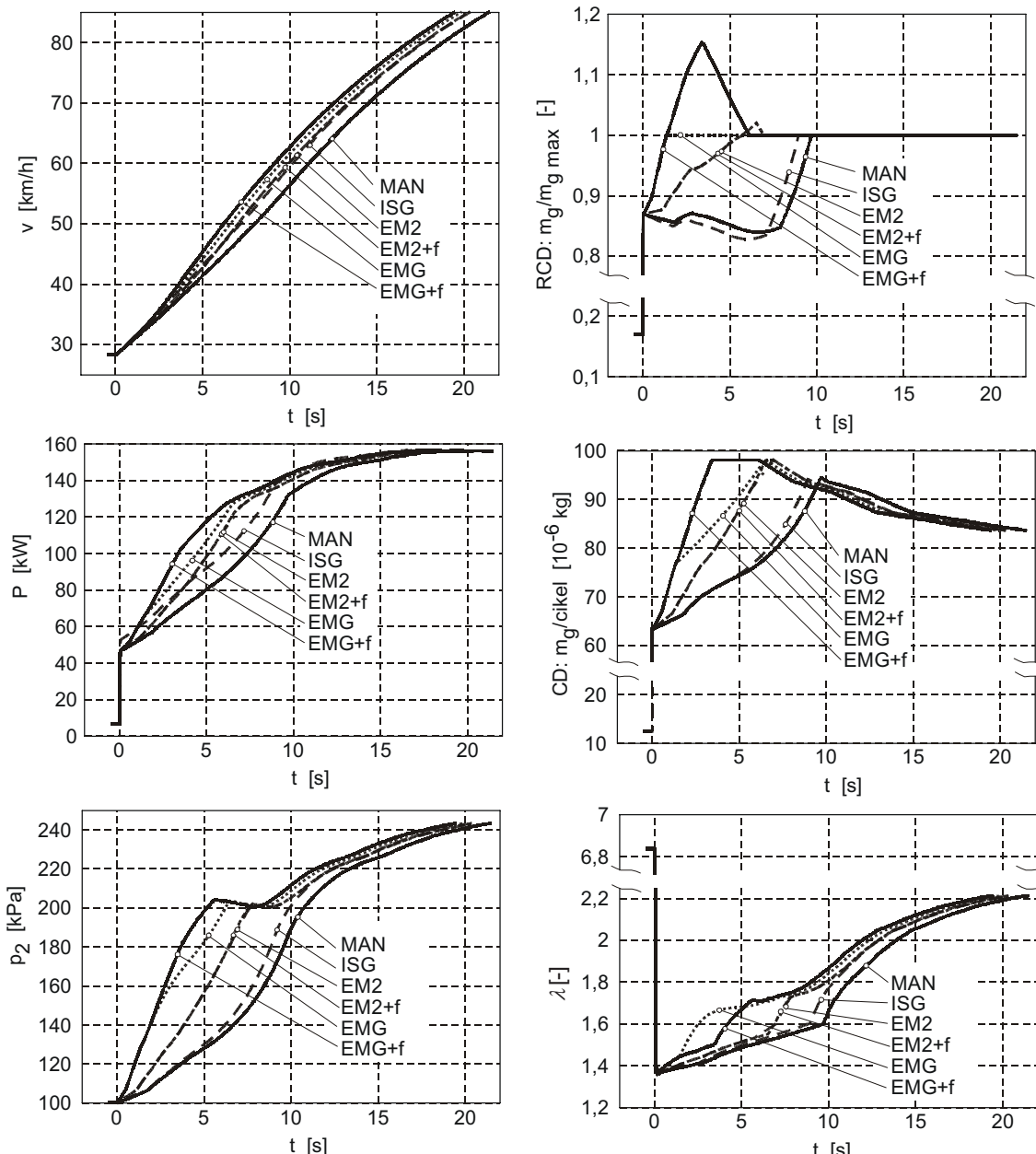
The results of three different loading cases of the engine powering a MAN 8.225 LC truck with a maximum gross weight of 7490 kg, equipped with an S6-850 gearbox, are presented. These results should reveal only improvement in the dynamic response of the turbocharged Diesel engine by electrical assisting systems and their characteristics. A 6.87 dm^3 six-cylinder MAN D0826 LOH 15 engine with a bore/stroke of 108/125 mm, a compression ratio of 18:1, which develops 162kW at 2400 rpm is equipped with a

108/125 mm ter kompresijskim razmerjem 18:1 razvije 162kW pri 2400 min^{-1} .

Prvi primer obremenitve ustreza preizkusu prožnosti motorja; pri vrtilni frekvenci motorja 800 min^{-1} v peti prestavi pri polno obteženem vozilu v času nič na ravni cesti dodamo polni plin. Z izboljšanjem dinamičnega odziva motorja se zmanjša potreba po pretikanju, posledica pa je boljše pospeševanje vozila ali možno podaljšanje prestavnih razmerij ob enaki odzivnosti vozila. Na sliki 3 so predstavljeni hitrost vozila (v), moč motorja (P), polnilni tlak (p_2), ciklična dobava goriva (CD), razmernik zraka (λ) in relativna ciklična dobava goriva (RCD) za opisano obremenitev. RCD predstavlja razmerje med trenutno dobavljenim maso goriva in

charge air cooler and a HOLSET H1E-8264BF/H16WA8 turbocharger.

First, the fully loaded vehicle was running at a constant speed of 30 km/h (800 rpm) in fifth gear on a flat road. At time $t=0$ the fuel rack was pushed to its maximum. The use of electrical assisting systems enables better vehicle dynamics, or allows the introduction of gearboxes with fewer gears. Fig. 3 shows the vehicle speed (v), the engine power (P), the boost pressure (p_2), the cyclic fuel delivery (CD), the air-fuel ratio (λ) and the relative cyclic fuel delivery (RCD) for the described acceleration. The RCD represents the ratio of instant injected-fuel quantity to the maximum cyclic fuel delivery (Fig. 2 max. m_g), and thus the ratio of the instant to the maximum



Sl. 3. Pospeševanje od 800 do 2400 min^{-1} v peti prestavi
Fig. 3. Vehicle acceleration from 800 to 2400 min^{-1} in fifth gear

največjo ciklično dobavo goriva (sl. 2: maks. m_g) ter neposredno razmerje med trenutnim in največjim stacionarnim srednjim efektivnim tlakom motorja pri določenih vrtlajah (zanemarjene razlike zaradi dela izmenjave delovnega medija). V primeru uporabe elektromotorja, pritrjenega na gred turbopolnilnika, je za vrtljaje motorja, manjše od 1400 min^{-1} in dodatno količino vbrizganega goriva (sl. 2: m_g sim. +f), to razmerje lahko tudi večje od 1.

Slike 3 je nazorno razvidno obnašanje tlačno polnjenega motorja, opremljenega s PODG v prehodnem režimu delovanja. Motor MAN (osnovna inačica motorja) v začetku dobavi 87% največje količine goriva. Zaradi povečane entalpije izpušnih plinov začne naraščati tlak v polnilnem zbiralniku, kar posledično, prek PODG, vpliva na povečanje CD. Kljub povečanju CD pa se RCD zmanjšuje, saj v tem času vozilo pospešuje (zvečanje vrtlajev motorja), največja ciklična dobava goriva pa se proti 1400 min^{-1} zvečuje. Za motor MAN se začne RCD zvečevati po 7,9 s, ko motor doseže 1400 min^{-1} (ekstrem CD; sl.2), saj se tlak p_2 še zvišuje, največja ciklična dobava goriva pa se začne zmanjševati. Največjo ciklično dobavo goriva ($RCD=1$) motor MAN doseže po 9,8 s, kar je povezano s prenehanjem omejevanja dobave goriva s PODG. Tlak p_2 se je zvišal nad vrednost, pri kateri, pri 1570 min^{-1} , PODG še omejuje gorivo. Opisani pojav je lepo viden tudi kot vrh na sliki 3-CD, kot sprememba strmine krivulje moči (sl. 3-P) in razmernika zraka (sl. 3-λ).

Motor, opremljen z ISG, ki se vklopi v trenutku dodajanja pedala za plin, brez zakasnitve poveča moč motorja, kar je razvidno iz poteka moči motorja (sl. 3-P). Ker ISG dodaja moč neposredno na gred motorja, s tem ne povečuje polnilnega tlaka. Polnilni tlak se zvišuje le nekoliko hitreje kakor pri motorju MAN, kar je posledica večjega masnega toka skozi motor, povezanega z višjo vrtilno frekvenco motorja, saj motor z ISG pospešuje hitreje. Manjša vrednost RCD kakor pri motorju MAN do 7 s je posledica še večjega zaostajanja polnilnega tlaka za vrtljaji motorja, saj ISG dovaja moč na gred motorja in ne turbopolnilniku. Po 7 s motor z ISG doseže 1400 min^{-1} in RCD se začne zviševati zaradi že opisanega dejstva.

Slike 3: p_2 , CD in RCD je razvidno, da zaradi višjega polnilnega tlaka motor z EM2, zaradi karakteristike PODG, dobiva več goriva, kar vpliva na večjo CD, RCD in moč motorja. Na hitrost zviševanja tlaka motorja z EM2 poleg navora elektromotorja (EM) vpliva tudi večji navor turbine, ki je posledica večje CD. Opisana pojava sta aditivna, kar pomeni, da se razlika v p_2 med motorjem z EM2 in motorjem MAN povečuje prenosorazmerno s časom do časa največje ciklične dobave goriva motorja z EM2, ki znaša 5,9 s, kar je bistveno manj kakor v obeh prejšnjih primerih. Moč motorja z ISG

stationary bmep, ignoring the influence of the medium exchange bmep. The maximum cyclic fuel delivery of the baseline engine was used as a reference value to form a realistic base for evaluating the improvements. The use of an electrically assisted turbocharger and the injection of an added fuel quantity (Fig. 2: m_g sim. +f) could raise the RCD above 1 below 1400 rpm due to the facts previously discussed.

The acceleration of the baseline MAN engine represents typical behavior of turbocharged engine operating under transient conditions (Fig. 3). Only 87% of the maximum CD is injected immediately as a consequence of the LDA operation. p_2 increases due to the larger enthalpy of the exhaust gasses, enabling greater CD via the LDA. The RCD decreases, despite the increasing CD, because at the same time the vehicle and, therefore the engine, is accelerating; 'max. m_g ' increases up to 1400 rpm. After 7.9 seconds the engine reaches 1400 rpm and the RCD starts to rise due to decreasing 'max. m_g ' and the growing boost pressure. The maximum cyclic fuel delivery ($RCD=1$) is reached after 9.8 seconds. At this point the engine is running at 1570 rpm and the boost pressure has just reached the value at which the LDA allows full fueling at this speed. The phenomenon is clearly seen as a peak of the CD in Fig. 3-CD, as well as the curve slope change in the engine power (Fig. 3-P) and the air-fuel ratio (Fig. 3-λ).

Turning on the ISG at the time of fuel rack change (increase) increases the engine power with no delay (Fig. 3-P). The ISG adds power directly to the crankshaft and therefore does not directly affect the boost pressure. The boost pressure of the engine with the ISG rises only slightly faster than that of the MAN engine, due to a greater mass flow through the engine, as a consequence of higher vehicle speed, and therefore higher engine speed. The lower value of the RCD compared to that of the MAN up to 7 seconds is the consequence of a still greater boost-pressure delay vs. engine speed, resulting from the energy addition to the crankshaft and not to the turbocharger. After 7 seconds the engine equipped with the ISG reaches 1400 rpm, and the RCD increases for the reasons already mentioned.

The electrically assisted turbocharger enables (via the LDA), due to the higher boost pressure, the injection of a larger quantity of fuel in comparison to the baseline engine, resulting in a higher RCD and a higher engine power. The faster boost-pressure build-up of the engine with the electrically assisted turbocharger is the consequence of additional electric-motor (EM) torque and a higher turbine torque due to the higher CD and therefore a higher enthalpy of exhaust gasses. Both phenomena are additive, resulting in a time-proportional increase of the boost-pressure difference between the MAN and the EM engines until the full fueling is reached (Fig. 3-p, and CD). The engine with the EM2 reaches $RCD=1$ at 1270 rpm after 5.9 seconds, being a

je do 3,9 s večja od moči motorja z EM2, saj je v primeru motorja z EM2 potreben določen čas, da EM zagotovi zadosten polnilni tlak, ki omogoča vbrizganje dodatne količine goriva, ki je ustreznata moči ISG. V območju 3,9 do 8,9 s je motor z EM2 močnejši od motorja z ISG, saj je razlika v moči zaradi večje CD večja od moči ISG. Od 8,9 s je ponovno močnejši motor z ISG, saj se ta čas za motor z ISG ujemata z $RCD=1$, kar pomeni, da se v oba motorja vbrizga največja količina goriva; v primeru motorja z ISG pa je na voljo še dodatni navor ISG. Moči motorjev z ISG in EM2 je smiselno primerjati, ker je zaradi skoraj enake hitrosti vozila primerljiva tudi vrtilna frekvence motorja. Iz primera motorja z EM2+f, pri katerem je pod 1400 min⁻¹ dovoljena dodatna CD (sl. 2: m_g sim. +f), je razvidno, da je največja ciklična dobava goriva, enako kakor pri motorju z EM2, dosežena po 5,9 s, v tem času se motor vrta s frekvenco 1300 min⁻¹. Dodatna količina goriva se tako vbrizgava le v času od 5,9 do 7 s, ko motor doseže 1400 min⁻¹. Pojav je viden kot vrh (vrednosti nad 1) na sliki 3-RCD ter kot razlika med masama goriva (sl.3-CD) in razmernikoma zraka (sl. 3-λ) za motorja z EM2+f in EM2. Razlika v moči motorja pa je zaradi majhne razlike v CD majhna, prav tako pa je majhna razlika v hitrosti vozila in p_2 . Slike 3-CD je razvidno, da se največja dodatna količina goriva (m_g sim. +f) vbrizgava le od 6,6 do 7 s. Iz opisanega izhaja, da je EM2 prešibek, da bi v teh delovnih razmerah omogočil vbrizgavanje znatne količine dodatnega goriva.

Motor z EMG že po 1,35 s in pri 900 min⁻¹ doseže največjo ciklično dobavo goriva ter v primeru EMG+f do 6,2 s (ustreza 1400 min⁻¹) omogoča dobavo dodatne količine goriva. Zaradi velikega navora EM oba motorja z EMG in EMG+f dosežeta moč motorja z ISG že po 0,9s. V primeru uporabe EMG je dovod dodatne količine goriva smiseln, saj motorju z EMG sistem LDA omejuje količino dobavljenega goriva le 1,35 s, v nadaljevanju pa, zaradi omejene največje količine goriva, ostaja vpliv višjega polnilnega tlaka neizkorisčen. Zaradi dodatne količine goriva, ki se vbrizga od 1,35 do 6,2 s, je moč motorja z EMG+f znatno večja od moči motorja z EMG, posledica tega je občutna razlika pri hitrosti vozila ter tudi višji tlak p_2 . Največja dodatna količina goriva se v primeru uporabe motorja z EMG+f vbrizga od 3,5 do 6,2 s, kar nakazuje, da bi močnejši EM še dodatno izboljšal pospeševanje vozila v teh delovnih razmerah. Od 4,1 do 5,7 s EM deluje z vmesnim izklapljanjem ter zagotavlja vrtilno frekvenco 85000 min⁻¹. Po 5,7 s se EM popolnoma izklopi, saj motor pospeši turbopolnilnik nad 85000 1/min. Opisan pojav je viden kot pojemanje polnilnega tlaka na sliki 3- p_2 , kar je posledica počasnega pospeševanja turbopolnilnika ter karakteristike kompresorja pri nespremenljivih vrtljajih ob povečanju masnega toka.

substantially shorter time than that required by both previous versions. The power of the engine with the ISG is greater than that of the engine with the EM2 up to 3.9 seconds, because of the time required for the boost pressure to reach a value enabling the injection of an additional fuel quantity, equivalent to the power of the ISG. The power of the engine with the EM2 is then greater from 3.9 to 8.9 seconds, as the power gain due to a larger CD is higher than the power of the ISG. After 8.9 seconds the power of the engine with the ISG is higher again, since at that time the engine with the ISG reaches $RCD=1$, indicating that both engines are supplied with 'max. m_g ', while the engine with the ISG still has the ISG power benefit. A comparison of the instant power of the engines with the ISG and the EM2 is justified by an almost equal vehicle speed and, therefore, a similar engine speed. Both the engine with the EM2 and the engine EM2+f reach maximum CD after 5.9 seconds, when the engine is running at 1300 rpm. From Fig. 3-RCD it is clear that the use of the EM2+f enables the injection of an added fuel quantity ($RCD>1$) only between 5.9 and 7 seconds, corresponding to engine speeds of 1300 to 1400 rpm. The difference in the engine power and, therefore, in the vehicle speed is low, due to the small difference in CD. From Fig. 3-CD it is clear that the maximum added fuel quantity is injected only between 6.6 and 7 seconds. It is obvious that the EM2 is not powerful enough to make possible the injection of a significant amount of added fuel under these operating conditions.

An engine equipped with the EMG reaches $RCD=1$ after only 1.35 seconds at 900 rpm, and enables the injection of added fuel up to 6.2 seconds with the EMG+f, reaching 1400 rpm (Fig. 3-RCD). The power of the engine with the ISG is reached after only 0.9 seconds. The injection of an added fuel quantity is reasonable when using the EMG, since the LDA restricts the injected quantity of fuel only for first 1.35 seconds; the potential of a higher boost pressure remain unused thereafter. An added fuel quantity injected from 1.35 to 6.2 seconds results in a larger engine-power output and, therefore, higher vehicle speeds and p_2 when comparing engines with EMG+f and EMG. The maximum added CD is injected from 3.5 to 6.2 seconds (Fig. 3-CD) for the engine with EMG+f, indicating that an even more powerful electric motor would still have the potential to improve the acceleration of the vehicle under these loading conditions. The EMG operates with intermediate switching off between 4.1 and 5.7 seconds, maintaining a constant turbocharger speed of 85000 rpm; the slope of the boost-pressure curve changes at 4.1 seconds (Fig. 3- p_2). After 5.7 seconds the EMG switches off completely, while the engine speeds up the turbocharger beyond 85000 rpm. This phenomenon can be clearly seen as the boost pressure decreases (Fig. 3- p_2) due to the slow turbocharger acceleration and the compressor characteristics at constant turbocharger speed, while increasing the mass flow by engine acceleration.

Stvarno oceno podpornih sistemov kaže potek hitrosti vozila. Do 1,9 s je največja hitrost vozila, opremljenega z ISG, kar je posledica njegovega takojšnjega odziva. Pri 6,2 s motor z EM2 preseže hitrost motorja z ISG, kar je posledica večje moči od 3,9 s naprej, saj hitrost približno predstavlja integral moči motorja. Razlika v hitrosti vozil z motorjem z EM2 in EM2+f je zanemarljiva zaradi majhne dodatne količine dobavljenega goriva. Leta pa ima velik vpliv pri uporabi EMG, ki omogoča vbrizgavanje znatne količine dodatnega goriva, kar je tudi razvidno iz hitrosti vozila (sl.3-v). Največje vrtljaje (2400 min^{-1}) oz. hitrost vozila 85 km/h dosežejo motorji z ISG, EM2 in EM2+f 5,4%, EMG 7,5% ter EMG+f 9,3% hitreje kakor osnovna različica MAN. Za pospeševanje vozila do hitrosti 56 km/h (1600 min^{-1}) pa potrebujemo motor z ISG 8,8%, EM2 in EM2+f 11,3%, EMG 16% ter EMG+f 20,8% manj časa kakor osnovni motor MAN. Za opisano pospeševanje so električne podporne naprave potrebovale: ISG 106,4 kJ (0,7 Ah), EM2 in EM2+f 13,3 kJ (0,09 Ah), EMG 17,8 kJ (0,12 Ah) ter EMG+f 16,5 kJ (0,11 Ah) električne energije oziroma naboja pri 42 V.

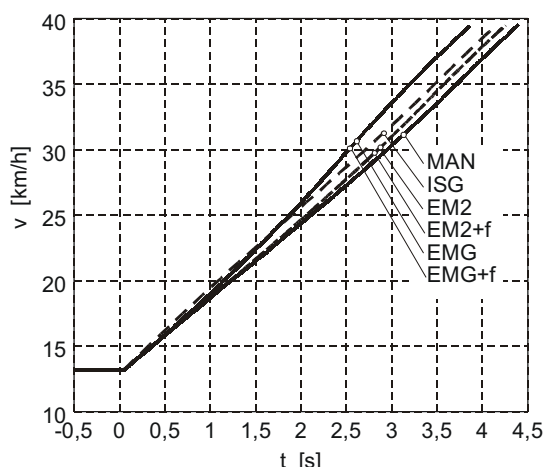
Na sliki 4 in 5 sta predstavljena pospeševanje v tretji prestavi in pospeševanje v šesti prestavi v klanec s strmino 1° , vsi drugi pogoji pa so enaki kot pri pospeševanju v peti prestavi. Ta dva primera sta bila izbrana, ker skupaj s sliko 3 podajata celostno razumevanje delovanja električnih podpornih naprav.

Na sliki 4 je predstavljeno pospeševanje od 800 do 2400 min^{-1} v tretji prestavi, ki traja bistveno krajši čas kakor enako pospeševanje v peti prestavi. Pri motorju MAN RCD ponovno skoči na 87%, vendar nato bolj strmo pada do 1,8 s (1400 min^{-1}), saj je na voljo manj časa za povišanje tlaka p_2 , kar, zaradi PODG, rezultira v nižjo CD. Največjo ciklično dobavo goriva motor doseže po 3,7 s pri 2100 min^{-1} ,

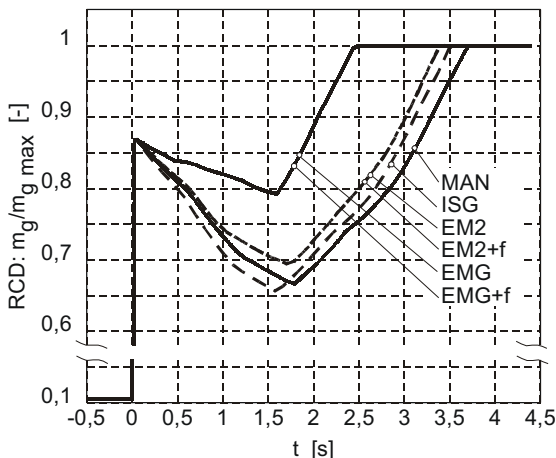
The realistic judgment of electrical assisting systems is reflected in the variation of vehicle velocity, as it is the only parameter perceptible to the driver. The velocity of a vehicle equipped with the ISG is higher than that of an engine with the EMG up to 1.9 seconds, and up to 6.2 seconds considering the engine with EM2: this being the consequence of the ISG's immediate power addition. The above-mentioned times are greater than those for engines with an EM, reaching the power output of the engine with the ISG, since the velocity can be seen as a kind of integral of the power output. The difference in vehicle speed for engines with EM2 and EM2+f is very small due to the minimum difference in CD. On the other hand, the EMG ensures faster acceleration due to the injection of a significant amount of added fuel quantity. A maximum engine speed of 2400 rpm, corresponding to 85km/h, is reached faster for the engine with the ISG, EM2 and EM2+f by 5.4%, EMG by 7.5% and EMG+f by 9.3% than with the MAN engine, whereas 1600 rpm is correspondingly reached faster by 8.8% for the engine with ISG, 11.3% with EM2 and EM2+f, 16% with EMG and 20.8% for the engine with the EMG+f than with the MAN engine. The electrical assisting systems consumed: ISG 106.4 kJ (0.7 Ah), EM2 in EM2+f 13.3 kJ (0.09 Ah), EMG 17.8 kJ (0.12 Ah) and EMG+f 16.5 kJ (0.11 Ah) of electrical energy or electric charge at 42 V respectively.

Fig. 4 and 5 show the vehicle acceleration in third gear and in sixth gear on a road inclined at 1° , with all other conditions identical to the case explained in Fig. 3. These two loading cases were chosen since they allow a deeper insight into the interaction between the electrical assisting systems and the TC Diesel engine.

The acceleration in third gear (Fig. 4) is the representative case of fast engine acceleration. The RCD of the MAN engine again rises up to 87%, but then decreases faster until 1.8 seconds (1400 rpm), due to a still larger boost-pressure lag behind the engine speed compared to acceleration in fifth gear, resulting in a lower CD. The maximum CD (RCD=1) is



Sl. 4. Pospeševanje od 800 do 2400 min^{-1} v tretji prestavi
Fig. 4. Vehicle acceleration from 800 to 2400 rpm in third gear



kar je bistveno več od 1570 min^{-1} pri pospeševanju v peti prestavi. Omenjeno dejstvo je posledica zelo kratkega časa, potrebnega za pospeševanje motorja, le-ta pa, zaradi vztrajnognega momenta turbopolnilnika in končne prostornine polnilnega in izpušnega zbiralnika, povzroča še večje zaostajanje polnilnega tlaka za vrtljaji motorja. Vpliv ISG je v tem režimu pospeševanja večji, saj je razmerje moči ISG proti moči motorja, zaradi manjše CD , večje. Iz enakega poteka krivulj motorjev z EM2 in EM2+f je razvidno, da EM2 ni zmožen zagotoviti polnilnega tlaka, potrebnega za dobavo dodatne količine goriva. S slike 4-RCD je razvidno, da je CD motorja z EM2 le nekoliko večja od motorja MAN, saj doseže največjo ciklično dobavo šele po 3,4 s (pri 2050 min^{-1}). Omenjeno dejstvo je posledica dinamike turbopolnilnika. EM poleg dodatnega navora prispeva tudi k povečanju masnega vztrajnognega momenta rotorja turbopolnilnika in izboljša pospeševanje le v primeru, ko je razmerje vsote navorov turbine kompresorja in EM proti skupnemu vztrajnostnemu momentu večje od razmerja vsote navorov turbine in kompresorja proti vztrajnostnemu momentu osnovnega turbopolnilnika ([1] do [3]). V analiziranem primeru se zaradi hitrega povečanja vrtlajev motorja hitro zveča tudi masni tok skozi motor, posledica česar je hiter odziv turbopolnilnika. Dinamika turbopolnilnika, opremljenega z EM2, je v tem primeru le nekoliko boljša od dinamike osnovnega turbopolnilnika. Pri enakem pospeševanju v drugi prestavi, ki traja še krajši čas, je dinamika obeh turbopolnilnikov enaka, v primeru pospeševanja v prvi prestavi, ki je še krajše, pa EM2 povzroča slabšo dinamiko turbopolnilnika. Tako kakor EM2 tudi uporaba EMG ne omogoča dobave dodatne količine goriva (sl.4-RCD), vendar pa zaradi boljše dinamike turbopolnilnika (zaradi boljših karakteristik EMG v primerjavi z EM2) omogoča večjo CD , kar je lepo razvidno s slike 4-RCD ter posledično tudi iz hitrosti vozila (sl. 4-v). Za izboljšanje dinamične karakteristike motorja pri hitrem pospeševanju (v nizkih prestavah) so primerni EM z velikim navorom na enoto vztrajnognega momenta, ki pa hkrati razvijajo razmeroma velik navor.

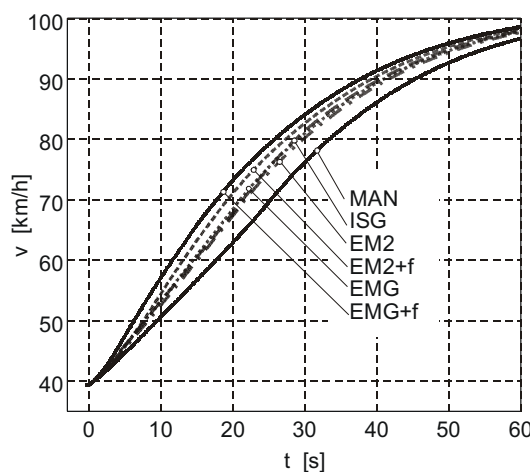
Za opisan primer obremenitve je značilno, da elektromotorja, pritrjena na gred turbopolnilnika, izboljšata dinamiko motorja predsem pri višjih vrtljajih motorja, kar je dokaj neobičajno. Omenjen pojav je posledica zelo hitrega odziva motorja in turbopolnilnika. Največja razlika v RCD, CD in moči motorja ter posledično v pospešku vozila med motorjem z EMG in drugimi različicami se pojavi šele pri $2,5\text{s}$, ko se motor že vrta s 1800 min^{-1} . Zato, v primerjavi s pospeševanjem v peti prestavi, motor z ISG razvija večjo hitrost od motorja z EMG razmeroma daljši čas, v primerjavi z motorjem z EM2 pa v celotni fazi pospeševanja. Največje vrtljaje ter hitrost $39,5$

achieved after 3.7 s at 2100 rpm, giving a much higher value than 1570 rpm when accelerating in fifth gear. This is a consequence of the very short time required for engine acceleration, which results in a large turbocharger lag due to the inertia of the turbocharger and the finite capacity of the inlet and exhaust manifolds. The influence of the ISG is larger during fast accelerations of the engine, since the ratio of ISG power to engine power is higher due to the lower CD . From the RCD curve for the engines with the EM2 and EM2+f (Fig 4-RCD) it is obvious that the EM2 is unable to raise the boost pressure above a value allowing the injection of an added fuel quantity, even more, the CD and also the RCD of the engines with the EM2 is only slightly higher than that of the baseline MAN engine. The engine with the EM2 reaches $RCD=1$ as late as 3.4 seconds at 2050 rpm. This is the consequence of turbocharger dynamics. The EM improves the turbocharger dynamics only if the ratio of the sum of the turbine, the EM, and compressor torque to the common mass moment of inertia is larger than the ratio of the sum of the turbine and the compressor torque to the mass moment of inertia of the baseline turbocharger ([1] to [3]). Mass flow through the engine increases rapidly, due to the high engine acceleration, resulting in fast turbocharger acceleration. The dynamics of the turbocharger with the EM2 is therefore only slightly better than that of the baseline one, when accelerating in third gear. When performing the same acceleration in second gear, the duration of which is shorter, the dynamics of the turbocharger with the EM2 and the baseline one are the same, while at still faster acceleration in first gear the dynamics of the baseline turbocharger is better. Neither the EM2 nor the EMG enables the injection of an added fuel quantity (Fig.4-RCD). Better EMG characteristics result in better turbocharger dynamics; consequently, more fuel can be injected (Fig.4-RCD) and faster vehicle acceleration is achieved (Fig.4-v) in comparison with the engine to the EM2. The example described reveals the need for an EM with a very high torque to mass moment of inertia ratio at a relatively high torque output when assisting turbochargers during fast engine acceleration.

It is characteristic of the case presented that an electrically assisted turbocharger improves engine dynamics, especially at high engine speed, which is rather unusual. This phenomenon is evident from Fig. 4-RCD, since the largest difference in the RCD and therefore in the CD , the engine power and the vehicle acceleration between both engines with the EMG and other engines is observed at approximately 2.5 seconds, when the engine is running at 1800 rpm. The speed of the vehicle equipped with the engine with the ISG is therefore higher than that of the engine with the EMG for a relatively longer time compared with the acceleration in the fifth gear, and throughout

km/h (sl. 4-v) doseže motor z ISG 6,4%, EM2 3,3% ter EMG 12% hitreje kakor osnovni motor MAN. Za polovico razlike v hitrosti (26 km/h) pa potrebujejo v enakem vrstnem redu 9,4%, 3% ter 12% manj časa. Poraba električne energije je v enakem vrstnem redu znašala 24,1 kJ (0,16 Ah), 4,7 kJ (0,031 Ah) ter 5,55 kJ (0,037 Ah).

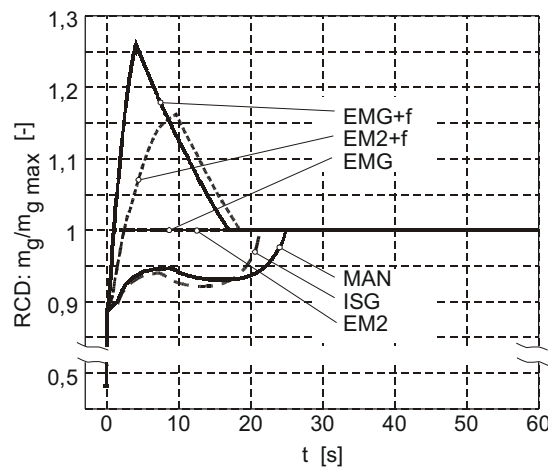
Na sliki 5 je prikazano pospeševanje vozila (motorja od 800 min^{-1}) v 6. prestavi v klanec s strmino 1° , ki predstavlja primer izrazito počasnega pospeševanja. Zaradi omejene kapacitete akumulatorjev je bil čas vklopa električnih podpornih naprav navzgor omejen s 30s, kar velja za ISG, saj so se EM, pritrjeni na gred turbopolnilnika, ki delujejo do 85000 min^{-1} , izklopili že prej. Krivulja RCD (sl. 5) za motor MAN ne pade pod začetno vrednost 89%, kar je posledica počasnega večanja vrtljajev motorja, največjo ciklično dobavo goriva pa doseže že pri 1420 min^{-1} . Zaradi vožnje v klanec je moč, ki je potrebna za premikanje vozila, večja, kar pomeni, da je razlika v moči motorja in moči bremena, ki je ustrezna pospešku, manjša, posledica česar je večja razlika v hitrosti motorja MAN in preostalih različic na polovici razlike v hitrosti. Zaradi počasnega pospeševanja je pospeševanje različice motorjev z EM2 in EMG skoraj enako, kar izhaja iz majhne razlike v CD in RCD. Motor z ISG razvije po 21s ($RCD=1$) večjo moč od motorjev z EM2 in EMG, kar je razvidno iz pospeška. Zaradi počasnega pospeševanja je v tem primeru vpliv dodatne količine goriva opazen tudi v primeru EM2+f, saj omogoča vbrizgavanje znatne dodatne količine goriva, vendar pa je ta v primeru EMG, zaradi večjega navora EM, pritrjenega na gred turbopolnilnika, kakor velik navor na enoto vztrajnostnega momenta, saj se počasno pospeševanje v limiti približa stacionarnemu delovanju.



Sl. 5. Pospeševanje od 800 min^{-1} v šesti prestavi na klancu s strmino 1°
Fig. 5. Vehicle acceleration from 800 rpm in sixth gear on a road inclined at 1°

whole acceleration when compared to the engines with EM2. The maximum engine speed 39.5 km/h (Fig. 4-v) is reached with the engine with the ISG 6.4%, the EM2 3.3%, and the EMG 12%, faster than with the MAN engine, whereas 1600 rpm (26 km/h) is reached 9.4%, 3% and 12% faster than with the MAN engine. The electric energy consumption was 24.1 kJ (0.16 Ah), 4.7 kJ (0.031 Ah) and 5.55 kJ (0.037 Ah) of electric energy or electric charge at 42 V, respectively.

Fig. 5 shows the vehicle acceleration in sixth gear on a road inclined at 1° , with all other conditions identical to those explained in Fig. 3. It is an example of slow engine acceleration. The operating time of the electrical assisting systems was limited to 30 seconds, due to limited accumulator capacity and cooling ability (regarding only the ISG in the particular case, since the EM attached to the turbocharger shaft operating up to 85000 rpm , switched off earlier). The MAN RCD curve (Fig. 5-RCD) does not fall below its initial value of 89% due to slow engine acceleration, resulting in a smaller boost-pressure lag behind the engine speed. Full fueling of the MAN engine is therefore reached at 1420 rpm . The difference between the engine power and the load power is smaller when driving uphill, resulting in slower vehicle acceleration and therefore larger velocity differences between the MAN engine and other engines during the first phase of acceleration. The velocity difference for the vehicles equipped with engines with the EM2 and EMG is smaller than that presented in former cases because the slower engine acceleration enables the injection of a significant added fuel quantity, even with the use of the EM2+f (Fig. 5-v and RCD). Slow engine acceleration places higher demands on EM torque output than on high torque to mass moment of the inertia ratio, since in the limiting case it approaches stationary-state operation.



V tem primeru obremenitve motor ne doseže 2400 min^{-1} , zato je primerjava narejena pri hitrosti 79 km/h , kar ustreza 1600 min^{-1} . Motor z ISG potrebuje 14%, EM2 11%, EM2+f 18,5%, EMG 13,3% ter EMG+f 23,5% manj časa za doseg 79 km/h kot osnovna različica MAN. Poraba električne energije je v enakem vrstnem redu znašala 252 kJ (1,67 Ah), 45,4 kJ (0,3 Ah), 41,8 kJ (0,28 Ah), 58,6 kJ (0,39 Ah) ter 50 kJ (0,33 Ah).

4 SKLEP

Iz prikazanih rezultatov je razvidno, da je že z dosedanjimi električnimi podpornimi napravami mogoče izboljšati odzivnost motorja na ravni cesti za 20%, kar pa, kakor je nakazano, še ni zgornja meja. Pri vožnji v klanec je izboljšanje odzivnosti lahko bistveno večje od te vrednosti. Prikazani primeri nakazujejo, da uporaba električnih podpornih naprav omogoča izboljšanje dinamične karakteristike motorja, ali pa, pri enakih zahtevah po dinamiki motorja, uporabo menjalnikov z manj prestavami ali uporabo motorjev z manjšo delovno prostornino. Slednja primera lahko zmajšata proizvodne stroške, zadnji pa tudi porabo goriva.

ISG je uspešen predvsem v začetni fazi pospeševanja, saj je njegov dodatni navor na voljo brez zakasnitve ter v področju največje ciklične dobave goriva, kjer je moč motorja mogoče povečati le še z neposrednim dovajanjem energije na gred motorja. Za izboljšanje dinamične karakteristike motorja je primeren ISG, ki razvija čim večji navor v širokem delovnem področju, vendar je treba najti primerni kompromis med močjo in porabo električne energije. ISG je najprimernejša električna podpora naprava v primeru nenadnega povečanja moči bremena, vendar je v podrejenem položaju proti elektromotorju, pritrjenemu na gred turbopolnilnika, glede razmerja porabljenih električne energije za enako izboljšanje dinamične karakteristike motorja pri daljšem delovanju.

Elektromotor, pritrjen na gred turbopolnilnika je primernejši od ISG za uporabo v vozilih, saj so tipični časi delovanja električnih podpornih naprav daljši od nekaj sekund. EM, pritrjen na gred turbopolnilnika, ponuja boljše razmerje med izbošanjem dinamične karakteristike motorja in porabo električne energije kakor tudi večji potencial za izboljšanje dinamične karakteristike, saj je dodatna moč ISG običajno manjša od povečanja moči motorja zaradi dodatnega vbrizganega goriva. Z večanjem specifične moči motorja se veča izboljšanje dinamične karakteristike motorja zaradi uporabe EM, pritrjenega na gred turbopolnilnika, v primerjavi z uporabo ISG. Za dvig stacionarnega srednjega efektivnega tlaka je primeren elektromotor, ki razvija velik navor. Za izboljšanje dinamične karakteristike motorjev, namenjenih za hitro pospeševanje, pa so primerni EM z velikim navorom na enoto vztrajnostnega momenta, ki pa hkrati razvijajo razmeroma velik navor, ki omogoča hiter dvig tlaka in s tem dočavo znatne količine dodatnega goriva.

All engines do not reach 2400 rpm under these operating conditions, so a comparison was made only at 1600 rpm, corresponding to 79 km/h. The engine with the ISG requires 14%, the EM2 11%, the EM2+f 18.5%, the EMG 13.3% and the EMG+f 23.5% less time than the MAN engine to achieve 1600 rpm. The electrical assisting system's energy consumption was 252 kJ (1.67 Ah), 45.4 kJ (0.3 Ah), 41.8 kJ (0.28 Ah), 58.6 kJ (0.39 Ah) and 50 kJ (0.33 Ah) of electrical energy or electric charge at 42 V, respectively.

4 CONCLUSION

It is evident from the results that present electrically assisted systems improve the turbocharged engine dynamics by up to 20% when driving on a flat road, and even more when driving uphill. All the cases presented indicate that the use of electrically assisted systems enable better vehicle dynamics, on the one hand, or allow the introduction of gearboxes with fewer gears, or the use of smaller displacement engines for the same engine dynamics, on the other. Both of the latter cases reduce production costs, while the last case could lead to a reduction in fuel consumption.

The ISG is effective, especially in the first phase of load increase, since it increases engine power without any delay, and after reaching full fueling, since thereafter engine power could only be increased with a direct power supply. A compromise considering engine applications should be made between the ISG power output, the operational time, and the electrical energy consumption. The ISG is the best electrically assisted solution in cases of a large, instant engine load increase, whereas it does not outperform electrically assisted turbochargers in terms of electrical energy consumption with the same engine dynamics improvement when operating for longer periods.

For vehicle applications, an electrically assisted turbocharger is superior to an ISG, since the typical operational times of electrical assisting systems are longer than a few seconds, thus offering a better ratio of engine dynamics improvement to electrical energy consumption, as well as a greater potential for engine dynamics improvement, since the ISG power potential hardly competes with that of additional fueling. The higher the rating of the turbocharged engine the greater is the benefit of an electrically assisted turbocharger in comparison to the ISG. For a stationary bmep rise, an EM with a high torque output is demanded, whereas to improve the dynamics of rapidly accelerating engines an EM with a high torque to mass moment of inertia ratio is required, thus also developing relatively high torque output to substantially increase boost pressure, enabling additional fueling.

5 OZNAČBE

5 SYMBOLS

ciklična dobava goriva	CD	kg/cikel	cyclic fuel delivery
nadtlak v polnilnem zbiralniku	dp_2	kPa	gauge pressure
razmernik zraka	λ	-	air-fuel ratio
moč	P	kW	power
relativna ciklična dobava goriva	RCD	-	relative cyclic fuel delivery
tlak v polnilnem zbiralniku	p_2	kPa	boost pressure
čas	t	s	time
hitrost vozila	v	km/h	vehicle velocity

6 LITERATURA

6 REFERENCES

- [1] Katrašnik, T. et al (2003) Improvement of the dynamic characteristic of an automotive engine by a turbocharger assisted by an electric motor, *ASME J. Eng. Gas Turbine Power*, 125, 590-595.
- [2] Katrašnik, T. (2001) Analysis of transient process in a turbocharged Diesel engine, Master Sc. Thesis No. M/1177, Dep. Mech. Engineering, University of Ljubljana, Slovenia.
- [3] Katrašnik, T. et al (2001) Improvement of the dynamic characteristic of an automotive engine by a turbocharger assisted by an electric motor, *Proceedings of the 2001 Fall Technical Conference of the ASME Internal Combustion Engine Division: Argonne*, Illinois, September 23-26.
- [4] Hoecker, P. et al (2001) Booster key component of a new BorgWarnerTurbo systems charging system for passenger cars, *Internationales Wiener MotorenSymposium*, Wien, Band 2, 333-352.
- [5] Medica, V. (1988) Simulation of turbocharged Diesel engine driving electrical generator under dynamic working conditions, Dr. Sc. Thesis, University of Rijeka, Croatia.
- [6] Winterbone, D. E. et al (1977) Transient response of turbocharged Diesel engines, *SAE Technical Paper* 770122

Naslova avtorjev: mag. Tomaž Katrašnik

prof.dr. Ferdinand Trenc
dr. Samuel Rodman Oprešnik
dr. Frančišek Bizjan
Univerza v Ljubljani
Fakulteta za strojništvo
Aškerčeva 6
1000 Ljubljana
tomaz.katrasnik@fs.uni-lj.si

prof.dr. Vladimir Medica
Sveučilište u Rijeci
Tehnički fakultet
Vukovarska 58
51000 Rijeka, Hrvatska
medica@riteh.hr

Authors' Addresses: Mag. Tomaž Katrašnik

Prof.Dr. Ferdinand Trenc
Dr. Samuel Rodman Oprešnik
Dr. Frančišek Bizjan
University of Ljubljana
Faculty of Mechanical Eng.
Aškerčeva 6
1000 Ljubljana, Slovenia
tomaz.katrasnik@fs.uni-lj.si

Prof.Dr. Vladimir Medica
Faculty of Engineering
University of Rijeka
Vukovarska 58
51000 Rijeka, Croatia
medica@riteh.hr

Prejeto: 15.10.2003
Received: 15.10.2003

Sprejeto: 8.4.2004
Accepted: 8.4.2004

Odprto za diskusijo: 1 leto
Open for discussion: 1 year

Osebne vesti

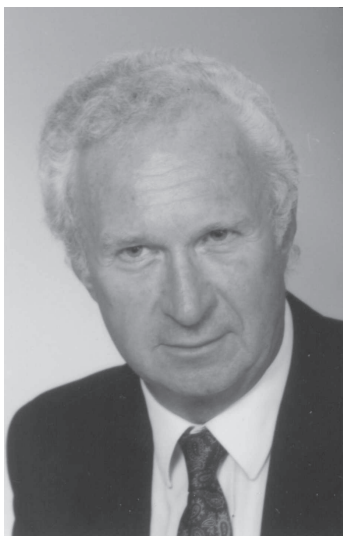
Personal Events

70 let zaslужnega profesorja dr. Adolfa Šostarja s Fakultete za strojništvo Univerze v Mariboru

Dne 26. novembra 1959 je bil v Ljudski skupščini Slovenije sprejet zakon o ustanovitvi Višje tehniške šole v Mariboru. S tem so bili dani pogoji za usposabljanje mladih, novih inženirjev strojništva, tekstilstva in drugih tehničnih znanj. Prav tako pa so bile ustvarjene možnosti za sposobne mlade inženirje iz gospodarstva, da se vključijo v novo izobraževalno središče. Profesor Adolf Šostar je bil povabljen k sodelovanju že leta 1962 in bil izvoljen za honorarnega asistenta pri profesorju Evgenu Mareku za predmete Mehanska tehnologija, Priprava proizvodnje in Tehnološke meritve.

Že v času svojega študija si je profesor Šostar pridobil izkušnje in prepotrebno praktično znanje na praksah po različnih evropskih tovarnah, kot so Steyer Daimler Puch v Gradcu, Krupp Stahlbau Rheinhausen, Tovarna avtomobilov Maribor, Philipp v Eindhoven in v Götaurkenu v Göteborgu na Švedskem. Po diplomi na Fakulteti za strojništvo v Ljubljani se je leta 1959 zaposlil v Tovarni avtomobilov Maribor v sektorju tehnološke priprave proizvodnje in delal kot konstrukter orodja, pozneje pa kot vodja skupine za osvajanje in preizkušanje proizvodnje. Leta 1966 se je zaposlil na tedanji Višji tehniški šoli v Mariboru kot predavatelj višje šole. V letu 1971 je postal znanstveni sodelavec Inštituta za proizvodno strojništvo na Tehniški univerzi v Gradcu, kjer je leta 1975 doktoriral. Istega leta je postal predstojnik Oddelka za strojništvo na tedanji Visoki tehniški šoli. Od leta 1979 do 1983 je bil dekan Visoke tehniške šole v Mariboru, v letih 1984/85 prorektor Univerze v Mariboru in od leta 1995 do 2001 dekan na novoustanovljeni Fakulteti za strojništvo v Mariboru.

V svoji pedagoško-raziskovalni karieri mu je uspelo skupaj s profesorjem dr. Šmarčanom opremiti Tehnološki laboratorij in Laboratorij za tehnološke meritve. S tem je postavljal osnovo za uspešno delo s študenti in raziskovalno delo mladih asistentov in mladih raziskovalcev. Pod njegovim vodstvom je diplomiralo, magistriralo in doktoriralo veliko število kandidatov. Profesor Šostar je zelo rad delal s študenti.



Svoje izkušnje je prenašal v postopke izobraževanja in raziskovanja. Tako so študentje dodiplomskega in poddiplomskega študija spoznavali nove usmeritve in jih upoštevali pri svojih diplomah, magisterijih in doktoratih. Vedno je poudarjal, da bistvo v tehniškem izobraževanju lahko dosežemo le z avtonomnimi postopki razmišljanja. S podajanjem tradicionalnega znanja prodira bistveno za prihodnost le redko v ospredje.

Fakulteta za strojništvo v Mariboru je pod vodstvom profesorja Šostarja postala ena vodilnih fakultet Univerze v Mariboru na področju znanstveno-raziskovalnega

dela, izvajanja projektov za gospodarstvo, znanstvenih objav in kadrovske prenove. Zato med nekdanjimi in sedanjimi sodelavci uživa velik ugled zaradi svojega ustvarjalnega prispevka k razvoju fakultete in visokega šolstva v Mariboru. **Na podlagi izjemnih in pomembnih dosežkov profesorja dr. Adolfa Šostarja na področjih visokošolskega izobraževanja, znanstveno-raziskovalne dejavnosti na Univerzi v Mariboru in drugod ter za prenos znanja razvoju gospodarstva in strokovnih združenj mu je Univerza v Mariboru na predlog Fakultete za strojništvo v letu 2001 podelila naziv zaslžni profesor.**

Profesor Šostar je Mariborčan z dušo v pravem pomenu besede, ki mu ni vseeno, kako se ravna z našim gospodarskim in tehničnim prostorom. V svojem življenju je doživeljal vse gospodarske vzpone in padce v Mariboru. Kot dečka so ga zanimali Puchovi avtomobili in motorji, ki so bili pomemben del gospodarske in tehnične zgodovine severovzhodne Slovenije. Da ne bo ta zgodovina prepričena času pozabe, se je pred kratkim lotil zelo pomembne naloge - zapisati zgodovino strojništva v Mariboru od njegovih začetkov do današnjih dni.

Ob njegovem visokem jubileju mu želimo še veliko ustvarjalnih, življenjsko polnih let.

Dekan Fakultete za strojništvo,
Univerze v Mariboru
prof. dr. Andrej Polajnar

Doktorati, magisteriji, diplome

DOKTORATI

Na Fakulteti za strojništvo Univerze v Ljubljani je z uspehom zagovarjal svojo doktorsko disertacijo:

dne 11. februarja 2004: mag. Samo Zupan, z naslovom: "Model nosilnosti vrtljive kotalne zvezе v realnih obratovalnih pogojih".

Na Fakulteti za strojništvo Univerze v Mariboru je z uspehom zagovarjala svojo doktorsko disertacijo:

dne 6. februarja 2004: mag. Marina Novak, z naslovom: "Inteligentni računalniški sistem za pomoč pri optimirjanju konstrukcij".

S tem sta navedena kandidata dosegla akademsko stopnjo doktorja znanosti.

MAGISTERIJI

Na Fakulteti za strojništvo Univerze v Ljubljani je z uspehom zagovarjal svoje magistrsko delo:

dne 9. februarja 2004: Vili Malnarič, z naslovom: "Modeliranje Coffin-Manson-Morrovih krivulj zdržljivosti izdelkov z nevronskimi mrežami".

Na Fakulteti za strojništvo Univerze v Mariboru je z uspehom zagovarjal svoje magistrsko delo:

dne 19. februarja 2004: Jurij Urh, z naslovom: "Nihanja mehanskih sistemov s

spremenljivo strukturo in določanje kaotičnih območij".

S tem sta navedena kandidata dosegla akademsko stopnjo magistra znanosti.

DIPLOMIRALISO

Na Fakulteti za strojništvo Univerze v Mariboru sta pridobila naziv univerzitetni diplomirani inženir strojništva:

dne 26. februarja 2004: Dušan GROSEK, Miha LEBENIČNIK.

*

Na Fakulteti za strojništvo Univerze v Ljubljani so pridobili naziv diplomirani inženir strojništva:

dne 12. februarja 2004: Marjan BRENČIČ, Primož KRANJC, Ivo KREČA, Darko KUŠEJ, Marko MIKLAVČIČ, Miha ŽNIDARŠIČ;

dne 13. februarja 2004: Franc MIRTEK, Blaž PLAVČAK, Branimir PLETERSKI, Stanko TRPIN, Radoš ZORKO, Rafael ZUPAN.

Na Fakulteti za strojništvo Univerze v Mariboru so pridobili naziv diplomirani inženir strojništva:

dne 26. februarja 2004: Drago BABIČ, Roman JUS, Aleksander LEDINEK.

Navodila avtorjem

Instructions for Authors

Članki morajo vsebovati:

- naslov, povzetek, besedilo članka in podnaslove slik v slovenskem in angleškem jeziku,
- dvojezične preglednice in slike (diagrami, risbe ali fotografije),
- seznam literature in
- podatke o avtorjih.

Strojniški vestnik izhaja od leta 1992 v dveh jezikih, tj. v slovenščini in angleščini, zato je obvezen prevod v angleščino. Obe besedili morata biti strokovno in jezikovno med seboj usklajeni. Članki naj bodo kratki in naj obsegajo približno 8 tipkanih strani. Izjemoma so strokovni članki, na željo avtorja, lahko tudi samo v slovenščini, vsebovati pa morajo angleški povzetek.

Vsebina članka

Članek naj bo napisan v naslednji obliki:

- Naslov, ki primerno opisuje vsebino članka.
- Povzetek, ki naj bo skrajšana oblika članka in naj ne presega 250 besed. Povzetek mora vsebovati osnove, jedro in cilje raziskave, uporabljeno metodologijo dela, povzetek rezultatov in osnovne sklepe.
- Uvod, v katerem naj bo pregled novejšega stanja in zadostne informacije za razumevanje ter pregled rezultatov dela, predstavljenih v članku.
- Teorija.
- Eksperimentalni del, ki naj vsebuje podatke o postavitev preskusa in metode, uporabljene pri pridobitvi rezultatov.
- Rezultati, ki naj bodo jasno prikazani, po potrebi v obliki slik in preglednic.
- Razprava, v kateri naj bodo prikazane povezave in pospološtive, uporabljene za pridobitev rezultatov. Prikazana naj bo tudi pomembnost rezultatov in primerjava s poprej objavljenimi deli. (Zaradi narave posameznih raziskav so lahko rezultati in razprava, za jasnost in preprostejše bralčevu razumevanje, združeni v eno poglavje.)
- Sklepi, v katerih naj bo prikazan en ali več sklepov, ki izhajajo iz rezultatov in razprave.
- Literatura, ki mora biti v besedilu oštevilčena zaporedno in označena z oglatimi oklepaji [1] ter na koncu članka zbrana v seznamu literature. Vse opombe naj bodo označene z uporabo dvignjene številke¹.

Oblika članka

Besedilo naj bo pisano na listih formata A4, z dvojnim presledkom med vrstami in s 3 cm širokim robom, da je dovolj prostora za popravke lektorjev. Najbolje je, da pripravite besedilo v urejevalniku Microsoft Word. Hkrati dostavite odtis članka na papirju, vključno z vsemi slikami in preglednicami ter identično kopijo v elektronski obliki.

Prosimo, da ne uporabljate urejevalnika LaTeX, saj program, s katerim pripravljamo Strojniški vestnik, ne uporablja njegovega formata. V urejevalniku LaTeX oblikujte grafe, preglednice in enačbe in jih stiskajte na kakovosten laserskem tiskalniku, da jih bomo lahko presneli.

Enačbe naj bodo v besedilu postavljene v ločene vrstice in na desnem robu označene s tekočo številko v okroglih oklepajih

Enote in okrajšave

V besedilu, preglednicah in slikah uporabljajte le standardne označbe in okrajšave SI. Simbole fizikalnih veličin v besedilu pišite poševno (kurzivno), (npr. *v*, *T*, *n* itn.). Simbole enot, ki sestojijo iz črk, pa pokončno (npr. ms^{-1} , K, min, mm itn.).

Vse okrajšave naj bodo, ko se prvič pojavijo, napisane v celoti v slovenskem jeziku, npr. časovno spremenljiva geometrija (CSG).

Papers submitted for publication should comprise:

- Title, Abstract, Main Body of Text and Figure Captions in Slovene and English,
- Bilingual Tables and Figures (graphs, drawings or photographs),
- List of references and
- Information about the authors.

Since 1992, the Journal of Mechanical Engineering has been published bilingually, in Slovenian and English. The two texts must be compatible both in terms of technical content and language. Papers should be as short as possible and should on average comprise 8 typed pages. In exceptional cases, at the request of the authors, speciality papers may be written only in Slovene, but must include an English abstract.

The format of the paper

The paper should be written in the following format:

- A Title, which adequately describes the content of the paper.
- An Abstract, which should be viewed as a miniversion of the paper and should not exceed 250 words. The Abstract should state the principal objectives and the scope of the investigation, the methodology employed, summarize the results and state the principal conclusions.
- An Introduction, which should provide a review of recent literature and sufficient background information to allow the results of the paper to be understood and evaluated.
- A Theory
- An Experimental section, which should provide details of the experimental set-up and the methods used for obtaining the results.
- A Results section, which should clearly and concisely present the data using figures and tables where appropriate.
- A Discussion section, which should describe the relationships and generalisations shown by the results and discuss the significance of the results making comparisons with previously published work. (Because of the nature of some studies it may be appropriate to combine the Results and Discussion sections into a single section to improve the clarity and make it easier for the reader.)
- Conclusions, which should present one or more conclusions that have been drawn from the results and subsequent discussion.
- References, which must be numbered consecutively in the text using square brackets [1] and collected together in a reference list at the end of the paper. Any footnotes should be indicated by the use of a superscript¹.

The layout of the text

Texts should be written in A4 format, with double spacing and margins of 3 cm to provide editors with space to write in their corrections. Microsoft Word for Windows is the preferred format for submission. One hard copy, including all figures, tables and illustrations and an identical electronic version of the manuscript must be submitted simultaneously.

Please do not use a LaTeX text editor, since this is not compatible with the publishing procedure of the Journal of Mechanical Engineering. Graphs, tables and equations in LaTeX may be supplied in good quality hard-copy format, so that they can be copied for inclusion in the Journal.

Equations should be on a separate line in the main body of the text and marked on the right-hand side of the page with numbers in round brackets.

Units and abbreviations

Only standard SI symbols and abbreviations should be used in the text, tables and figures. Symbols for physical quantities in the text should be written in Italic (e.g. *v*, *T*, *n*, etc.). Symbols for units that consist of letters should be in plain text (e.g. ms^{-1} , K, min, mm, etc.).

All abbreviations should be spelt out in full on first appearance, e.g., variable time geometry (VTG).

Slike

Slike morajo biti zaporedno oštevilčene in označene, v besedilu in podnaslovu, kot sl. 1, sl. 2 itn. Posnete naj bodo v kateremkoli od razširjenih formatov, npr. BMP, JPG, GIF. Za pripravo diagramov in risb priporočamo CDR format (CorelDraw), saj so slike v njem vektorske in jih lahko pri končni obdelavi preprosto povečujemo ali pomanjšujemo.

Pri označevanju osi v diagramih, kadar je le mogoče, uporabite označbe veličin (npr. t , v , m itn.), da ni potrebno dvojezično označevanje. V diagramih z več krivuljami, mora biti vsaka krivulja označena. Pomen oznake mora biti pojasnjен v podnapisu slike.

Vse označbe na slikah morajo biti dvojezične.

Za vse slike po fotografiskih posnetkih je treba priložiti izvirne fotografije ali kakovostno narejen posnetek. V izjemnih primerih so lahko slike tudi barvne.

Preglednice

Preglednice morajo biti zaporedno oštevilčene in označene, v besedilu in podnaslovu, kot preglednica 1, preglednica 2 itn. V preglednicah ne uporabljajte izpisanih imen veličin, ampak samo ustrezne simbole, da se izognemo dvojezični podvojitvi imen. K fizikalnim veličinam, npr. t (pisano poševno), pripisite enote (pisano pokončno) v novo vrsto brez oklepajev.

Vsi podnaslovi preglednic morajo biti dvojezični.

Seznam literature

Vsa literatura mora biti navedena v seznamu na koncu članka v prikazani obliki po vrsti za revije, zbornike in knjige:

- [1] Tarng, Y.S., Y.S. Wang (1994) A new adaptive controller for constant turning force. *Int J Adv Manuf Technol* 9(1994) London, pp. 211-216.
- [2] Čuš, F., J. Balić (1996) Rationale Gestaltung der organisatorischen Abläufe im Werkzeugwesen. *Proceedings of International Conference on Computer Integration Manufacturing*, Zakopane, 14.-17. maj 1996.
- [3] Oertli, P.C. (1977) Praktische Wirtschaftskybernetik. *Carl Hanser Verlag*, München.

Podatki o avtorjih

Članku priložite tudi podatke o avtorjih: imena, nazive, popolne poštne naslove, številke telefona in faks ter naslove elektronske pošte.

Sprejem člankov in avtorske pravice

Uredništvo Strojniškega vestnika si pridržuje pravico do odločanja o sprejemu članka za objavo, strokovno oceno recenzentov in morebitnem predlogu za krajšanje ali izpopolnitve ter terminološke in jezikovne korekturje.

Avtor mora predložiti pisno izjavo, da je besedilo njegovo izvirno delo in ni bilo v dani obliki še nikjer objavljeno. Z objavo preidejo avtorske pravice na Strojniški vestnik. Pri morebitnih kasnejših objavah mora biti SV naveden kot vir.

Rokopisi člankov ostanejo v arhivu SV.

Vsa nadaljnja pojasnila daje:

Uredništvo
STROJNISKEGA VESTNIKA
p.p. 197
1001 Ljubljana
Telefon: (01) 4771-757
Telefaks: (01) 2518-567
E-mail: strojniski.vestnik@fs.uni-lj.si

Figures

Figures must be cited in consecutive numerical order in the text and referred to in both the text and the caption as Fig. 1, Fig. 2, etc. Figures may be saved in any common format, e.g. BMP, GIF, JPG. However, the use of CDR format (CorelDraw) is recommended for graphs and line drawings, since vector images can be easily reduced or enlarged during final processing of the paper.

When labelling axes, physical quantities, e.g. t , v , m , etc. should be used whenever possible to minimise the need to label the axes in two languages. Multi-curve graphs should have individual curves marked with a symbol, the meaning of the symbol should be explained in the figure caption.

All figure captions must be bilingual.

Good quality black-and-white photographs or scanned images should be supplied for illustrations. In certain circumstances, colour figures may be considered.

Tables

Tables must be cited in consecutive numerical order in the text and referred to in both the text and the caption as Table 1, Table 2, etc. The use of names for quantities in tables should be avoided if possible: corresponding symbols are preferred to minimise the need to use both Slovenian and English names. In addition to the physical quantity, e.g. t (in Italic), units (normal text), should be added in new line without brackets.

All table captions must be bilingual.

The list of references

References should be collected at the end of the paper in the following styles for journals, proceedings and books, respectively:

- [1] Tarng, Y.S., Y.S. Wang (1994) A new adaptive controller for constant turning force. *Int J Adv Manuf Technol* 9(1994) London, pp. 211-216.
- [2] Čuš, F., J. Balić (1996) Rationale Gestaltung der organisatorischen Abläufe im Werkzeugwesen. *Proceedings of International Conference on Computer Integration Manufacturing*, Zakopane, 14.-17. maj 1996.
- [3] Oertli, P.C. (1977) Praktische Wirtschaftskybernetik. *Carl Hanser Verlag*, München.

Author information

The following information about the authors should be enclosed with the paper: names, complete postal addresses, telephone and fax numbers and E-mail addresses.

Acceptance of papers and copyright

The Editorial Committee of the Journal of Mechanical Engineering reserves the right to decide whether a paper is acceptable for publication, obtain professional reviews for submitted papers, and if necessary, require changes to the content, length or language.

Authors must also enclose a written statement that the paper is original unpublished work, and not under consideration for publication elsewhere. On publication, copyright for the paper shall pass to the Journal of Mechanical Engineering. The JME must be stated as a source in all later publications.

Papers will be kept in the archives of the JME.

You can obtain further information from:

Editorial Board of the
JOURNAL OF MECHANICAL ENGINEERING
P.O.Box 197
1001 Ljubljana, Slovenia
Telephone: +386 (0)1 4771-757
Fax: +386 (0)1 2518-567
E-mail: strojniski.vestnik@fs.uni-lj.si